ELSEVIER

Analogue modelling of continental extension: a review focused on the relations between the patterns of deformation and the presence of magma

Giacomo Corti[a], Marco Bonini[b], Sandro Conticelli[c], Fabrizio Innocenti[a], Piero Manetti[d,*], Dimitrios Sokoutis[e]

[a] Dipartimento di Scienze della Terra, Università degli Studi di Pisa, via S. Maria, 53, 56126 Pisa, Italy
[b] C.N.R.—Istituto di Geoscienze e Georisorse, sezione di Firenze, via G. La Pira, 4, 50121 Firenze, Italy
[c] Dipartimento di Scienze della Terra, Università degli Studi di Firenze, via G. La Pira, 4, 50121 Firenze, Italy
[d] Geochimica Isotopica—C.N.R.—Istituto di Geoscienze e Georisorse, via G. Moruzzi, 1, 56124 Pisa, Italy
[e] Netherlands Center for Integrated Earth Sciences, Faculty of Earth and Life Sciences, Vrije Universiteit Amsterdam, De Boelelaan 1085, 1081 HV, Amsterdam, The Netherlands

Abstract

Continental extension may occur in two main different modes, narrow and wide rifting, which mainly differ in the width of the deformed region. A third mechanism, the core complex, has been considered either a distinct mode of extension or a local anomaly within wide rifts. In terms of causative processes, continental rifting may be explained by both active or passive mechanisms, which also differ in the volume of magmatic products and in the rheological properties and stratification of the extending lithosphere. Both numerical and analogue models have investigated the main parameters controlling the extension of a rheologically layered lithosphere. In particular, analogue models have highlighted that the style of deformation is mainly controlled by the competition between the total resistance of the lithosphere and the gravitational forces; this competition, in turn, is mainly controlled by boundary conditions, such as the applied strain rate and the rheological characteristics of the extending lithosphere.

Magmatic bodies eventually present within the continental lithosphere may significantly affect the process of extension. Both the thermal and mechanical effects related to the presence of magma strongly weaken the lithosphere and localise strain; this effect may have important implications for the mode of continental extension. At a crustal scale, magmatic intrusions may affect significantly the local fault pattern also favouring the development of core complex structures.

Results of analogue models, performed taking into account the presence of an initially underplated magma and reproducing various continental extensional settings, suggest a close interaction between deformation and magma emplacement during extension. Particularly, magmatic underplating influences deformation localising strain in correspondence to the low-viscosity body, while on the other hand, rift kinematics and associated deformation has a major control on the pattern of magma emplacement. In particular:

(1) During orthogonal rifting, magma is passively squeezed from an axial position towards the footwall of the major boundary faults; emplacement occurs in a lateral position in correspondence to lower crust domes. This process accounts for the close

---

* Corresponding author.
E-mail address: manetti@unifi.it (P. Manetti).

association between magmatism and the development of core complex structures, as well as for the occurrence of off-axis volcanoes in continental rifts.

(2) During oblique rifting, deformation causes magma to emplace within the main rift depression, giving rise to intrusions with oblique and en echelon patterns. In nature, these patterns are found in continental rifts and also in some oceanic ridges.

(3) Polyphase first orthogonal–second oblique rifting models suggest lateral squeezing and off-axis emplacement in the first phase and oblique en echelon intrusions in the successive oblique rifting phase. This evolution matches the magmatic and tectonic history of the Main Ethiopian Rift.

(4) Development of transfer zones between offset rift segments has a great influence on both magma migration and deformation. Particularly, magma accumulates in correspondence to the transfer zone, with a main flow pattern that is perpendicular to the extension direction. This pattern may explain the concentration of magmatism at transfer zones in continental rifts.

Overall, analysis of centrifuge models and their comparison with nature suggest that deformation and magma emplacement in the continental crust are intimately related, and their interactions constitute a key factor in deciphering the evolution of both continental and oceanic rifts.

1. Introduction

Continental extension represents one the most important geodynamical processes affecting the lithosphere–asthenosphere system. As a consequence, during the last decades, many geophysical, geological and petrological data have been acquired in order to understand the causes and the mechanics of the processes through which continental breakup occurs. More recently, models derived from analysis of field data have been integrated with numerical and analogue experimental modelling, which have been proven to represent powerful tools to get insights into the evolution of continental rift systems. Particularly, these techniques provided the basic modes for the extension of a multilayered brittle–ductile lithosphere, highlighting the role played by several parameters (e.g., lithosphere rheology and thermal conditions, mechanical instability, strain rate, rift kinematics and causative stresses) in controlling the structural patterns resulting from the deformation process. However, both numerical and analogue techniques have paid little attention on the influence on extension played by the presence of melt bodies that often emplace at the base or within an extending continental crust. In this (review) paper, we focus on the relations between evolution of crustal-scale structures and magma layers during continental extension. We review analogue experiments incorporating a magma-simulating fluid to get insights into the complex relations between structural evolution and the magmatic processes matching or accompanying continental extension.

In the following sections, we introduce the different modes of continental extension and the parameters controlling the style of deformation, focusing on the effect caused by the presence of magmatic bodies within the extending lithosphere. We then review analogue models investigating continental extension processes: we draw particular attention on the mechanics of continental rifting and the mode of extension, the structural pattern resulting from orthogonal, oblique and polyphase extension and the fault pattern within transfer zones. Successively, we review the results of experiments reproducing various geometries of continental extension and taking into account the presence of a magma initially underplated below the Moho. We use the results of modelling to discuss the relations between rift kinematics, induced deformation and magma emplacement, also comparing the outlined processes to some exemplifying natural examples. We also draw attention on the influence of magma on the mode of continental extension and speculate on the implications of experimental results for the volcanological evolution of regions undergoing extension.

2. Continental extension and the influence of magmatism

Stretching of the continental lithosphere has been classically considered to develop in response to regional stress field (passive rifting) or thermal upwelling of the asthenosphere (active rifting; Neumann and Ramberg, 1978; Sengör and Burke, 1978; Baker and Morgan, 1981; Morgan and Baker, 1983; Turcotte and Emermen, 1983; Keen, 1985; Christensen, 1992; Ruppel, 1995; Lesne et al., 1998; Ziegler and Cloetingh, 2003). An ascending mantle plume causing lithosphere thinning and isostatic crustal doming is considered the driving mechanism for active rifting (Fig. 1a). In this model, tensional stresses at the base of the lithosphere are generated by the ascending convecting material (Turcotte and Emermen, 1983); the lithosphere is thermally thinned by heating and adsorption into the asthenosphere, in addition to necking in response to extension, and hence, the volume of asthenosphere rising into the lithosphere exceeds the volume of lithosphere displaced laterally by extension (e.g., Olsen and Morgan, 1995). The active rifting mechanism is able to account for some of the main problems related to rifting such as: (1) the progression from uplift to volcanism to extension which has been claimed for several continental rifts (e.g., Burke and Dewey, 1973; Sengör and Burke, 1978; Braile et al., 1995); (2) the development of rifting in zone of net compression; and (3) the associations of narrow rifts with long-wavelength topographic swells and flood basalts provinces. Indeed, rift systems such as the East African Rift System often generate within broadly elevated regions (plateaux), and their development is often preceded by eruption of large volumes of fissural basaltic lava flows (continental flood basalt provinces), which are typically associated with a regional extensional stress field but normally not with the major tectonic rift depressions. These characteristics are coherent with the thermal and/or dynamic consequences of mantle plumes acting at (or near) the base of the lithosphere (e.g., Crough, 1983).

Conversely, diapiric asthenosphere rising through the lithosphere represents a second-order mechanism in purely passive rifting where the extensional stresses act in response to a regional stress field, usually as-
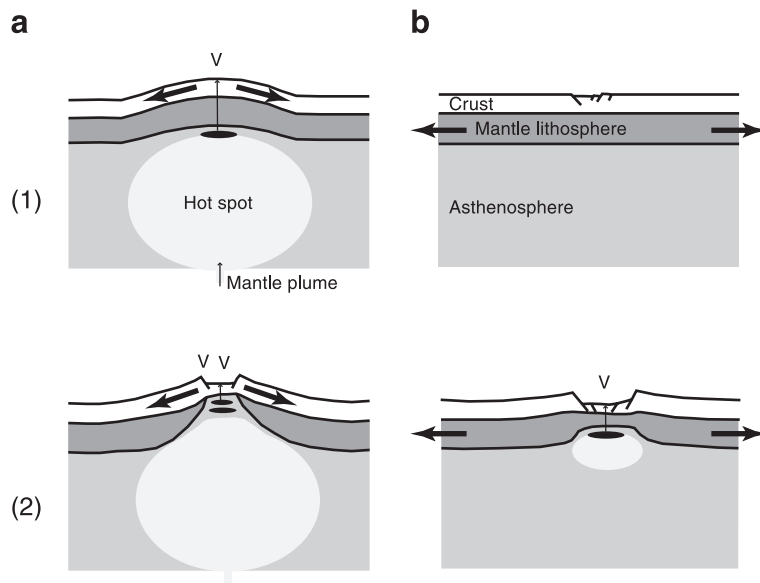

Fig. 1. Schematic diagrams showing the active (a) vs. passive (b) hypotheses for the initiation of continental rifting. (1) Initial stage and (2) subsequent stage of evolution. (a) The ascent and emplacement of a hot, low-density body in the sublithospheric mantle (hot spot) is a primary cause for extension in the active mechanism. This mechanism accounts for prerift uplift and volcanism (V). (b) In the passive mechanism, extension is driven by a tensional regional stress field, usually assumed to originate from remote plate boundary forces. In this case, generation of a hot, low-density region in the asthenosphere is a consequence of extension; magmatic underplating (black areas) and volcanism occurs only when the rifting process is well developed (after Bott, 1995).

sumed to originate from remote plate boundary forces (Fig. 1b). In this process, lithosphere is thinned only in response to extension, and the passive asthenospheric upwelling gives rise to many secondary processes such as decompressional melting, crustal/lithospheric magma underplating, eruption of continental flood basalts, the onset of secondary convection and the development of large lateral thermal gradients between extended and unextended regions (see Ruppel, 1995 for references).

Many natural rifts share features that are typically addressed to the passive or active models. Thus, these two end-member processes are likely to contribute to rifting, though the importance of a single mechanism can prevail in different continental rifts or can vary during the rift evolution (e.g., Morgan and Baker, 1983; Bott, 1992; Wilson, 1993; Ruppel, 1995; Huismans et al., 2001; Merle and Michon, 2001; Michon and Merle, 2001). For example, many rifts appear to be characterised by an evolutionary cycle from an initial passive phase through to a later active phase (e.g., Wilson, 1993; Merle and Michon, 2001; Michon and Merle, 2001; Ziegler and Cloetingh, 2003). Numerical models by Huismans et al. (2001) support these observation as they show that passive stretching destabilises the lower lithosphere and leads to an active phase characterised by small-scale convective upwelling of the asthenosphere. This change from plate-mode passive extension to diapiric-mode active extension is expected to take place in the late synrift and/or postrift evolution of extensional regions (Huismans et al., 2001). It has also been highlighted that the active rifting mechanism is not able to produce significant crustal extension unless it is associated with favourable plate kinematics (i.e., with also a passive rifting component; e.g., Mulugeta, 1985; see Section 3.4). Furthermore, rapid rotations of the near-surface stress field have been documented in many extensional areas (e.g., in the East African Rift System; Strecker et al., 1990; Bosworth et al., 1992; Ring et al., 1992; Bonini et al., 1997). Since it is unlikely that large-scale mantle circulation patterns can fluctuate at such rapid rates, drag at the base of the lithosphere may not be the dominant force controlling the orientation of the stress field. Thus, intraplate forces (i.e., passive rifting components) are expected to significantly contribute to configuring the continental crustal stress

regime (e.g., Bosworth et al., 1992). Finally, the evolution of active and passive rift systems is different mainly during the initial stages of crustal thinning, whereas the evolution of both active and passive modes converges when the asthenosphere rises underneath the rift, triggering partial melting in the mantle and generating the emplacement of magma bodies within the crust (see Morley, 1994, 1999a,b).

2.1. Modes of continental extension

From a structural point of view, continental extension has been efficaciously described in terms of (1) narrow rifting, (2) wide rifting and (3) core complex modes (e.g., England, 1983; Buck, 1991; Fig. 2a and b).

2.1.1. Narrow rifting

Examples of narrow (or discrete) rifts include the East African Rift System, the Rio Grande Rift, the Baikal Rift, the northern Red Sea, the West Antarctic rift and the European Cenozoic Rift System (Artemjev and Artyushkov, 1971; Illies and Greiner, 1978; Bonatti, 1985; Morgan et al., 1986; Rosendahl, 1987; Steckler et al., 1988; Behrendt et al., 1991; Ziegler, 1995; Prodehl et al., 1997). These rifts are characterised by a concentrated crustal and mantle lithospheric extension that gives rise to narrow regions (generally up to 100–150 km wide) of intense normal faulting (Buck, 1991; Fig. 2a). Following this localised extension, narrow rifts are characterised by large lateral gradients in crustal thickness and topography (Fig. 2a). Within the deformed regions, the continental crust is thinned, whereas a relative thickening of the crust may be observed at the rift shoulders, interpreted to result from magmatic intrusions or lower crust flow (e.g., Zeyen et al., 1996; Burov and Cloetingh, 1997; Prodehl et al., 1997; Ziegler and Cloetingh, 2003). The localised lithospheric thinning in narrow rifts has an expression also in the elevated heat flow within rift depressions compared to the adjacent rift shoulders or cratonic blocks (e.g., Bonatti, 1985; Ruppel, 1995 and references therein). This local anomaly in the heat flow, together with seismic evidences, suggest the presence of a hot (possibly asthenospheric) upper mantle beneath the rift (e.g., Prodehl et al., 1997). The width of the hot upper mantle zone follows, at
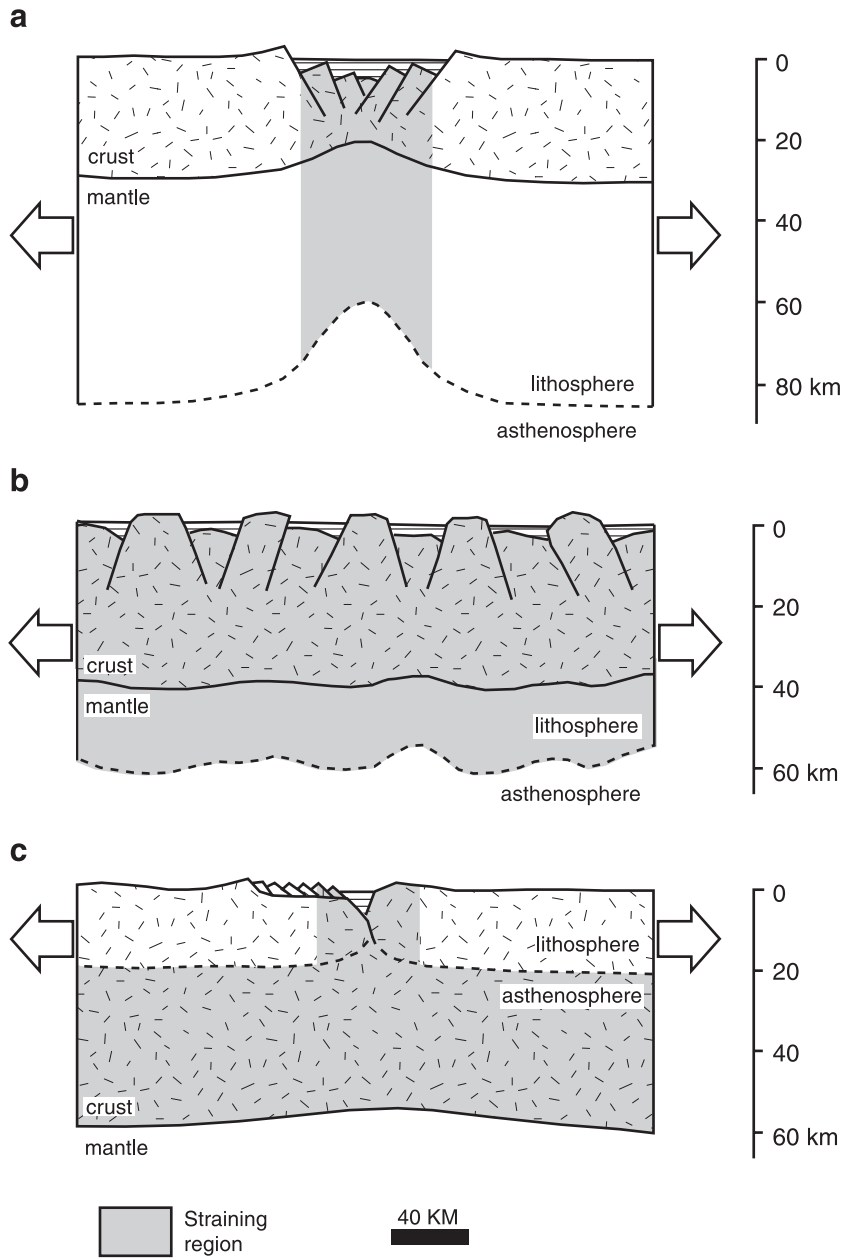
Fig. 2. Different modes of continental extensional tectonics. (a) Narrow rift mode; (b) wide rift mode; (c) core complex mode. See text for further explanations (after Buck, 1991).

depth, the width of the surface expression of the rifting process (Achauer et al., 1994; Braile et al., 1995; Prodehl et al., 1997). Notably, interpreted crustal and uppermost mantle velocity structure in the Kenya Rift

displays a high degree of symmetry (e.g., Braile et al., 1995).

The overall structure of intracontinental discrete rifts is characterised by an along-axis segmentation

in a series of single grabens, mainly characterised by an asymmetric morphology, bordered by high-angle normal faults (e.g., Rosendahl, 1987; Ebinger, 1989a). These normal faults also delimit rift shoulders characterised by local uplifts (rift flank uplifts), which have been explained in terms of lateral heat transport, dynamic effects (spatial variation of the extension rate), flexural forces, small-scale convection or underplating (see Burov and Cloetingh, 1997 and references therein). Along the main rift, single basins, normally displaying alternating polarities, are arranged en echelon and linked by transfer or accommodation zones (e.g., Rosendahl, 1987). Transfer zones, characterised by a significant component of strike– and oblique–slip deformation, accommodate significant along-axis variations in subsidence of grabens and elevation of uplifted flanks (e.g., Rosendahl, 1987; Faulds and Varga, 1998; Morley, 1999c). Normally, estimates of crustal extension in narrow rifts converge towards low values (bulk extension < 30%).

2.1.2. Wide rifting

Wide rifts (or highly extended terranes or diffuse rifts; see Buck, 1991; Olsen and Morgan, 1995; Ruppel, 1995), such as the Basin and Range Province of western North America, the Aegean and the Tibet (e.g., Armijo et al., 1986; Hamilton, 1987; Jackson, 1994), result from an uniform crustal and lithospheric mantle thinning over a width greater than the lithospheric thickness (Fig. 2b). This distributed deformation gives rise to a typical surface expression characterised by a large number of separated basins extending over a region up to 1000 km wide. Generally, wide rifts are characterised by high extensional strain which, however, is not uniformly distributed over the extended region. As an example, in the Basin and Range, crustal extension of 50–100% (e.g., Hamilton and Myers, 1966; Wernicke et al., 1982; Zoback et al., 1981; Wernicke, 1992) is partitioned into areas characterised by extension up to 100–400% and regions with values < 10% (e.g., Miller et al., 1983; Gans, 1987). Despite these strong variations in the magnitude of stretching, the Basin and Range Province is associated with small lateral gradients in topography and a rather uniform thickness of the crust over large areas (Fig. 2b). The actual crustal thickness (30–35 km) can be reconciled with the estimates of bulk extension, considering an initial overthickened crust

(with thickness up to 50 km) and addition of material through intrusion of magma from the mantle (underplating) coupled with regional lower crust ductile flow (e.g., Gans, 1987). Magmatic underplating, which has been interpreted to represent a major process in the Basin and Range Province (e.g., Gans, 1987; Hauser et al., 1987; Parsons, 1995; MacCready et al., 1997), contributes to smooth the Moho undulations created during extension, thus allowing to maintain a rather flat Moho topography in wide rifts (e.g., Hauser et al., 1987).

2.1.3. Core complex mode of extension

Buck (1991) described a third mode of extension, the core complex mode (Fig. 2c). In core complex structures, described in the Basin and Range, Aegean area and D'Entrecasteaux Islands, high-grade metamorphic rocks originating in the middle–lower crust are exposed at the surface, exhumed by low-angle normal faults, uplift and erosion (e.g., Coney, 1980; Crittenden et al., 1980; Lister and Davis, 1989; Gautier et al., 1990, 1999; Hill et al., 1992, 1995; Sokoutis et al., 1993; Brun and Van Den Driessche, 1994; Brun et al., 1994; Chéry, 2001). The exposed high-grade rocks are typically separated by a detachment, carrying low-grade rocks, warped upwards into antiformal structures below which the crust is normally as thick as the surrounding less-extended terranes.

Core complexes are normally associated with wide rifts (e.g., in the Basin and Range and Aegean), and this close correspondence has been interpreted as related to successive rifting phases characterised by different styles of extension (e.g., Sokoutis et al., 1993; Parsons, 1995; see below), as also supported by numerical models (see Section 2.2). However, such a close association led Brun (1999) to consider core complex structures as local anomalies within wide rifts and not a distinct mode of continental extension (see Section 3.3).

Typically, core complexes have been explained in terms of a post-orogenic collapse of a previously thickened lithosphere (e.g., Coney, 1980; Crittenden et al., 1980; Lister and Davis, 1989; King and Ellis, 1990; Lister and Baldwin, 1993; Brun et al., 1994). In such a process, the thermal relaxation of the thickened crust, characterised by a brittle/ductile thickness ratio in the order of 1:3, determines a localised extension in the upper crust (over an area < 100

km wide) coupled with a diffused thinning of a very fluid lower crust (Fig. 2c). As extension thins the brittle crust, isostasy causes a lateral flow of a fluid-like lower crust from the surrounding regions, which contributes to keep the topographic gradients small and a rather flat Moho (e.g., Block and Royden, 1990). In domal regions, the lower crust flow may occur in an opposite sense to that of the extending upper crust also causing a relative local thickening of the lower crust (e.g., MacCready et al., 1997). Extension and exhumation of deep rocks may be contemporaneous or follow lithospheric shortening as a result of gravitational re-equilibration of over-thickened crust (e.g., Teyssier and Vaderhaeghe, 2001; Ziegler and Cloetingh, 2003 and references therein). Additionally, recently core complex-like structures have been recognised in other different extensional settings, such as the East African Rift System (e.g., Talbot and Ghebreab, 1997; Morley, 1999d; Ghebreab and Talbot, 2000), the Tertiary Thailand rift basins (e.g., Morley et al., 2001 and references therein) and in the oceanic crust (Blackman et al., 1998; Ranero and Reston, 1999).

The abovementioned different modes of continental extension may represent different stages in a spectrum of lithospheric extension, e.g., the beginning of continental extension may result in the formation of single grabens affecting only the higher levels of the crust; these grabens may evolve into a rift system affecting the whole lithosphere; in turn, for increasing extension (up to 100% extension), the rift system may evolve into wide rifts, and this process may end with the formation of passive margins and a new ocean basin (e.g., Olsen and Morgan, 1995; Fig. 3). However, some observations suggest that, at least in some cases, this simple evolutionary sequence is not able to account for the structural difference between the different modes of extension. For example, it has been highlighted that the Basin and Range Province evolved in two separated rifting stages, an initial stage of localised high extension in isolated metamorphic core complexes (core complex mode of extension) and a later stage of high-angle distributed block faulting (wide rift stage; see Parsons, 1995 for a review). Furthermore, some narrow rifts have been interpreted to have evolved into passive margins without passing through the wide rift stage; in addition, along-strike variations in volcanic and structural style of passive margins have been observed (e.g., Bassi et al., 1993). Thus, although a continuum between the abovementioned end members is expected to exist, these different structural features may be linked to different modes of extension related to the potential of the lithosphere to localise or distribute strain during progressive extension. The parameters that have been considered to control the distribution or localisation of deformation during extension have been investigated through numerical (see the following section) and analogue (see Sections 3–5) models.

2.2. Parameters controlling the modes of continental extension

Both numerical and analogue models have been used to study the main parameters controlling the structural style of extension. In this section, we briefly introduce the main numerical works addressed to investigate the mode of continental extension; analogue models will be introduced and discussed in detail in Section 4.

Numerical models have investigated the parameters that control deformation of a lithosphere undergoing extension, such as: (1) the strain rate (e.g., England, 1983; Sawyer, 1985; Houseman and England, 1986; Kuznir and Park, 1987; Sonder and England, 1989); (2) the initial conditions (mainly initial thermal profiles and crustal thickness; Buck, 1991; Hopper and Buck, 1996); and (3) the mechanical instability caused by extension of rheologically layered lithosphere (e.g., Fletcher and Hallet, 1983; Richard and Froidevaux, 1986; Zuber and Parmentier, 1986; Braun and Beaumont, 1987; Zuber et al., 1986; Bassi, 1991, 1995; Christensen, 1992; Martinod and Davy, 1992; Bassi et al., 1993 among the others).

(1) The role of the strain rate is intimately related to the heat diffusion during extension. England (1983) first suggested that during continental thinning, diffusion of heat will result in cooling of any lithospheric layer as it is brought close to the surface, leading to an increase in the total strength of the lithosphere. Because extension always concentrates in the weakest area of the lithosphere, such processes have a strong influence on the spatial distribution of deformation (Kuznir and Park, 1987; Sonder and England, 1989). Indeed, weak regions, after a certain amount of thinning, may cool
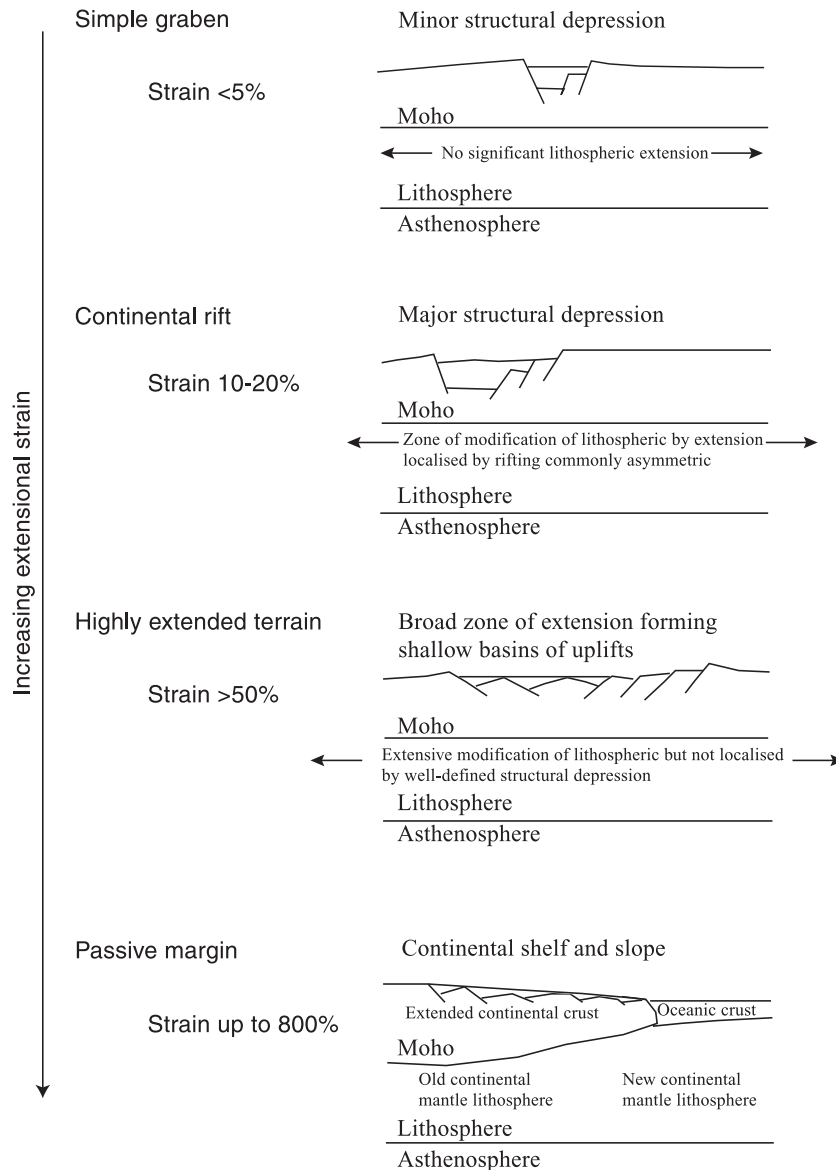
Fig. 3. Main structural styles of continental extension as a function of the increasing extensional strain (after Olsen and Morgan, 1995).

and increase their strength, eventually becoming stronger than the adjacent area and triggering a shifting of deformation into this weaker region. In this view, the parameter that controls the migration of deformation is the strain rate (Kuznir and Park, 1987): at slow strain rates, cooling dominates and deformation moves laterally, giving rise to wide rifts, whereas for high strain rates, deformation concentrates in a region leading to the development of narrow rifts.

(2) Buck (1991) reached a different conclusion, pointing out that changes in buoyancy forces (caused by the change of the density-depth distribution as the lithosphere and crust thin) represent the dominant parameter controlling the style of continental exten-

sion (see also Hopper and Buck, 1996). The calculations showed that initial crustal thickness and thermal conditions control the changes in buoyancy forces and hence, the mode of continental extension: narrow rifts will form if the lithosphere is initially cold, whereas wide rifts will form if the lithosphere is warmer. Wide rifts can also form in case of very weak crustal rheologies because of a horizontal offset between the loci of extension in the upper crust and upper mantle (shear decoupling; Hopper and Buck, 1996). For very thick crusts and high Moho temperatures, flow in the lower crust becomes important, leading to the development of core complexes. In this case, the upper crust is extended locally, but the lower crust flow has the effect of thinning the crust over a wide region; this flow can be rapid enough to maintain the topography of the Moho and the surface flat. With increasing extension, the core complex mode is expected to evolve in a wide rift and then into a narrow rift that eventually may lead to the formation of a new oceanic basin (Buck, 1991). Similar evolution from core complex to wide rift mode has been described in the Basin and Range (e.g., Parsons, 1995) and the north Aegean (Sokoutis et al., 1993).

(3) Many authors have highlighted that an important control on the extensional process is exerted by the level of mechanical instability, represented by the tendency for any initial weakness to be amplified or smoothed during extension (e.g., Fletcher and Hallet, 1983; Richard and Froidevaux, 1986; Zuber and Parmentier, 1986; Zuber et al., 1986; Braun and Beaumont, 1987; Bassi, 1991, 1995; Christensen, 1992; Martinod and Davy, 1992; Bassi et al., 1993). Thus, mechanical instability controls the process of necking, a dramatic concentration of deformation during extension of a ductile material in a zone of initial imperfection. Bassi (1991) pointed out that rheology has major effect in controlling the level of mechanical instability: the more nonlinear is the rheology, the more unstable is the material under tension, and thus, plastic deformation (favoured by colder geotherm and/or "stronger" minerals) is expected to lead to a rapid and narrow necking, whereas a power-law rheology (characteristic of warmer temperatures and/or "weaker" minerals) will result in wider rifts (Bassi, 1991, 1995; Bassi et al., 1993). When this mechanical instability is taken into account, the effect of synrift cooling is,

on one hand, to strengthen the lithosphere, favouring wide rifting, on the other, to favour a plastic behaviour, and hence, a localisation of the extension. The calculations by Bassi (1995) suggest that initial conditions, and in particular, the presence of plastic layers in the lithosphere, play an important role in determining a particular mode of extension. When plastic layers are initially present in the mantle or are generated by to the combined effect of thinning and cooling, the rate of extension appears to have little effect on the rifting pattern, and deformation migration is not observed, thus leading to a narrow rifting. On the contrary, when the upper mantle is weak and viscous, the cooling-induced strengthening and hence the strain rate influence significantly the rift geometry: in this case, as predicted by Kuznir and Park (1987), a widening of the rift occurs for low strain rates.

Beside these key elements (cooling of the lithosphere during extension, changes in buoyancy forces and mechanical instability) that contribute to imposing the mode of extension, it is highlighted that other important parameters, such as the presence of important volumes of hot magma intruded into a thinned crust, seem to have a strong control on the deformation pattern during continental extension (e.g., White and McKenzie, 1989). Magmatic activity is indeed commonly associated with extensional tectonics, and it is often observed that magmatism precedes the rift development (e.g., Baker et al., 1972; Ramberg and Morgan, 1984; Morgan et al., 1986). In these circumstances, at least in some rifts, mechanical instability due to the presence of a low-viscosity melt layer and the thermal weakening of the lithosphere due to magmatic processes may strongly control the rifting process. In particular, localised thermal inhomogeneities may produce a melt-induced strain localisation, favouring the development of narrow rifts in correspondence to the anomalously weak areas (e.g., Lynch and Morgan, 1987; Chèry et al., 1989; Callot et al., 2001, 2002).

2.3. Influence of magmatism on tectonic evolution

Emplacement of magmatic bodies within the continental lithosphere represents a major process through which modifications of the initial physical properties of the system may occur during extension.

The introduction of large volumes of melt in the continental lithosphere modifies its thermal and mechanical properties, resulting in an interplay between magmatism and tectonics which plays a role of major importance in controlling the structural evolution of the rift system (e.g., Lynch and Morgan, 1987; Chèry et al., 1989; Tommasi et al., 1994; Brown and Solar, 1998; Geoffroy, 1998, 2001; Morley, 1999a,b; Simpson, 1999; Callot et al., 2001, 2002; Ebinger and Casey, 2001). Indeed, modification of the thermal field and consequently of the rheological properties of the crust strongly weaken the lithosphere, enhancing deformation and strain localisation (e.g., Lynch and Morgan, 1987; Chèry et al., 1989; Geoffroy, 1998; Morley, 1999a). This process is further increased by the mechanical effect related to the introduction of molten magmatic bodies within the lithosphere: even a small amount of melt in solid rocks drastically reduces their strength (Arzi, 1978), thus introducing a strong rheological heterogeneity that further tends to localise deformation. This process has been also recognised in compressional environments (e.g., Hollister and Crawford, 1986; Tommasi et al., 1994; Neves et al., 1996) and may lead to a feedback interaction between magmatism and deformation (Brown and Solar, 1998).

In the view of the continental extension modes, the widening or narrowing of the deformed area is also influenced by the geometry of magma bodies underplating the base of the crust (e.g., Lynch and Morgan, 1987; Chèry et al., 1989; Benes and Davy, 1996; Morley, 1999a; Callot et al., 2001, 2002). In this case, the rheological profile of a stable lithosphere is locally perturbed, particularly the lateral continuity of the brittle upper mantle may be interrupted by the presence of a ductile, partially molten body. Since the upper brittle mantle has the greatest strength in the stable lithosphere (see Section 3.1), this local perturbation generates a strong lateral difference in lithospheric strength that may result in a strong strain localisation above the magma body (Callot et al., 2001, 2002; see Section 4.1). This process has been inferred to control the development and the width of the volcanic continental margins, which are usually narrower than non-volcanic margins (White and McKenzie, 1989; White, 1992; Callot et al., 2001, 2002; Section 4.1).

At a crustal scale, the presence of magmatic bodies may control the structural style and the fault pattern of narrow rifts (e.g., Morley, 1999a). It has been observed that during the progressive extension of the continental crust, the area affected by major magma intrusions may become narrower, also determining a narrowing of the weakened crustal portion. This process may lead to a shift of deformation from major boundary faults to minor fault swarms concentrated in narrow regions within the rift depression (e.g., Mohr, 1987; Morley, 1994, 1999a,b; Ebinger and Casey, 2001). Additionally, magmatic bodies intruding the upper crust may locally influence the fault pattern in various ways (e.g., Morley, 1999a,b), such as the initiation of low-angle normal faults. In particular, Parsons and Thompson (1993) suggested that magmatism causes a significant heterogeneity in the stress regime that can drive the formation of low-angle faults. Inflation of overpressured magma in the middle–upper crust may create local compressional stresses, causing the maximum principal stress direction to rotate from a vertical orientation near the surface to horizontal approaching the intrusion. Furthermore, the magma-induced heating may allow the lower crust to flow, creating a basal shear stress between the flowing and the stable crust with a consequent reorientation of the principal stress axes (Yin, 1989). In both cases, the process of faulting is influenced in a way that causes a variation in the normal faults dip from the angles of $45-70°$ predicted by the Andersonian theory to sensibly lower values of $<30-45°$ (see also Morley, 1999a). Furthermore, the addition of new magmatic material within the crust may potentially adsorb extension, thus significantly affecting the stress regime of extending regions (e.g., Parsons and Thompson, 1991, 1993). In particular, in areas affected by diffuse magmatism, emplacement and inflation of magmatic dykes perpendicular to the minimum principal stress (σ_3) in the elastic crust may aseismically accommodate large extensional strain, preventing the development of normal faults (e.g., in the Snake River Plain in the Basin and Range Province; Parsons et al., 1998).

Finally, several works highlight the coincidence of magmatic processes at transfer zones: examples include the East African Rift System (Rosendahl, 1987; Ebinger, 1989a,b; Ebinger et al., 1989; Hayward and Ebinger, 1996), the Rio Grande Rift (Chapin, 1989; Chapin and Chater, 1994), the Gulf

of California (Axen, 1995) and the Basin and Range Province (Faulds and Varga, 1998 and references therein). In most cases, magmatism predates extension, suggesting that crustal magmatism, which in turn may be controlled by deep-seated processes such as the emplacement of magma by distinct diapirs, may control the axial structural and mechanical segmentation of continental rifts (e.g., Ruppel, 1995; Faulds and Varga, 1998). Thus, emplacement of magmatic bodies within the extending crust may favour the development, and in some cases dictate the position, of transfer zones. In particular, both partially molten plutons and crystallized batholiths are expected to be less likely to rupture than favorably oriented preexisting structures in the country rocks, thus interrupting the lateral propagation of normal fault systems (e.g., Faulds and Varga, 1998; Morley, 1999a). Additionally, brittle deformation may give way to distributed ductile deformation in the vicinity of active magmatic centres due to the presence of partially molten material or significantly warmer crust (Faulds and Varga, 1998).

2.3.1. Magmatism and core complex formation

The development of core complex structures almost never occurs without accompanying magmatism. Several authors have highlighted the close association in space and time between magmatism and metamorphic core complexes (e.g., Coney, 1980; Crittenden et al., 1980; Gans, 1987, 1997; Gans et al., 1989; Glazner and Bartley, 1984; Ward, 1991; Axen et al., 1993; Lister and Baldwin, 1993; Hill et al., 1995; Gans and Bohrson, 1998), with igneous rocks mainly intruding the lower plate of major low-angle normal faults (see Parsons, 1995 and references therein). These associations has suggested a mechanical link between these two processes.

According to models of core complex formations (see previous Section 2), this mode of extension is favoured when the lower crust is characterised by a very low viscosity allowing its easy flow. Magmatic underplating of the continental crust is one important mechanism allowing the transfer of heat to shallower crustal levels and thus, sensibly decreasing the viscosity of the lower crust (e.g., Parsons and Thompson, 1993; MacCready et al., 1997). In these conditions, the ductile flow causes a relative thickening and outcropping of the lower crust at dome

regions to compensate the voids created by extension in the upper crust (see Brune and Ellis, 1997; Section 3.3).

Influence of magmatism on the deformation process has been also discussed by Gans et al. (1989), which highlighted that thermal weakening due to magmatic intrusions may localise and enhance extensional strain. Additionally, Lister and Baldwin (1993) and Hill et al. (1995) proposed a model in which plutonic activity represents the main process triggering metamorphic core complex formation. In fact, underplating of mafic material below the Moho causes the production of acidic magmas (by partial melting or fractional crystallisation) that rise buoyantly from lower crustal levels to mid-crustal levels. This raise causes a twofold effect: on one side, it determines the thickening of the middle crust and a relative uplift of the metamorphic domes; on the other side, it causes a heat transfer to shallower crustal levels that triggers and localises deformation in normal shear zones that, in turn, facilitates the exhumation of lower plate rocks. As noted above, in these conditions, the process of core complex formation is further favoured by the high mobility of the thermally softened lower crust, which allows it to enhance the isostatic rebound of the normal fault footwall (Parsons and Thompson, 1993).

3. Lithospheric and crustal-scale analogue modelling of continental extension: a review

Analogue models have been widely used to analyse the deformation resulting from extension of continental lithosphere, integrating the investigation carried out through numerical models. Indeed, whereas numerical models are able to simulate the strong temperature dependence of rock rheology but not complex fault patterns in the upper brittle layers, analogue models can properly reproduce the fault development in an extending lithosphere, but are unable to properly take into account the complex rheological variations induced by temperature changes (see Brun, 1999).

In the following sections, we discuss the strength profiles that characterise an extending lithosphere. Then, we review the previous crustal and lithospheric-scale analogue experiments of continental extension performed in both the terrestrial gravity

field (normal-gravity experiments) and in enhanced gravity field by means of centrifuge apparatus (e.g., Ramberg, 1981; Koyi, 1997; Brun, 1999). Particularly, we discuss models reproducing rift evolution without considering the influence of magmatic bodies on deformation that will be analysed in detail in Section 4.

3.1. Lithosphere rheology and strength profiles

Strength profiles have been widely used to represent the rheological characteristics and the coupling degree among the brittle and ductile layers composing the lithospheric multilayer (e.g., Kirby, 1983; Carter and Tsenn, 1987; Kirby and Kronenberg, 1987; Ranalli and Murphy, 1987; Ranalli, 1995 among the others). The simplified strength profiles of the continental lithosphere can be approximated by an alternation of a different number of layers that deform according to two different end-member mechanisms: brittle failure and ductile creep. Brittle failure typically occurs for low temperatures and high strain rates, whereas ductile creep is expected for high temperatures and low strain rates. Starting from the frictional shear failure criterion (for brittle behaviour) and the power-law creep equation (for ductile behaviour; see Appendix A for calculations), strength profiles of the lithosphere can be properly calculated.

Generally, some characteristic strength profiles represent the different thermal gradients of the continental lithosphere (e.g., Davy and Cobbold, 1991; Fig. 4). A young continental stable lithosphere, characterised by low temperature gradients, is normally approximated by four brittle/ductile layers resting upon a highly ductile asthenosphere (Fig. 4a). In this case, the continental crust consists of an upper brittle layer and a ductile lower crust (e.g., Faugère and Brun, 1984; Davy, 1986; Davy and Cobbold, 1991). Similarly, the lithospheric mantle is characterised by an upper brittle layer and a lower ductile layer (Davy, 1986; Allemand et al., 1989; Allemand and Brun, 1991; Davy and Cobbold, 1991, Brun et al., 1994; Brun and Beslier, 1996; Brun, 1999). Assuming such a rheological layering, two strength peaks separated by the low-strength lower crust can be identified below the Moho and at the base of the upper crust, respectively. More recently, Maggi et al. (2000a,b) questioned this classical view of a weak lower crust sandwiched between a very strong upper crust and upper mantle. In particular, these authors proposed that, at least in some areas, the upper mantle could be very weak, even weaker than the overlying lower crust, and no brittle behaviour is suggested for this layer.

Old lithospheres characterised by a low thermal gradients can result in a different rheological layering composed of two layers only: an upper brittle layer, including the whole crust and the brittle uppermost part of the mantle, and an underlying ductile layer, comprising the ductile part of the lithospheric mantle (e.g., Brun, 1999; Mart and Dauteuil, 2000; Fig. 4b).
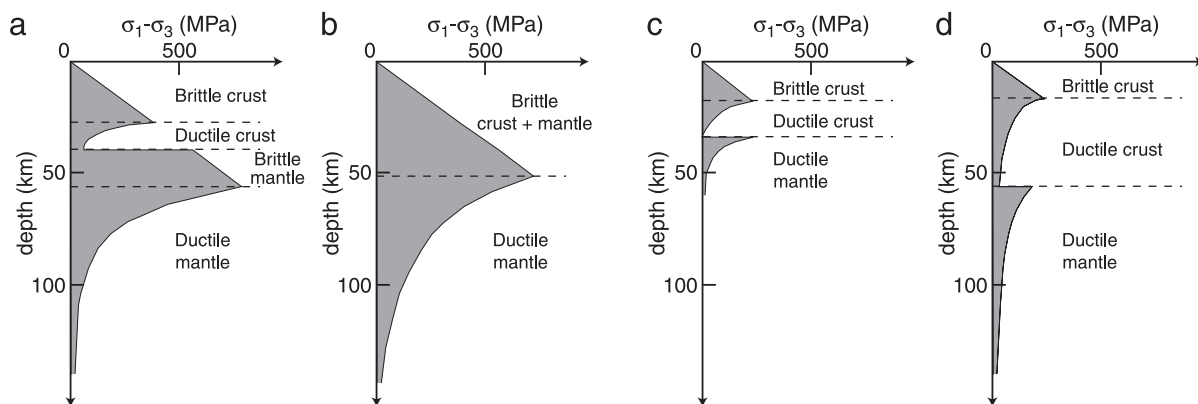

Fig. 4. Examples of strength profiles for a young stable four-layer lithosphere (a), an old stable two-layer lithosphere (b), a thinned three-layer lithosphere (c) and a thickened three-layer lithosphere (d). (a), (b) and (d) are modified from Brun (1999); (c) is modified from Fadaie and Ranalli (1990).

Because rock rheology is strongly controlled by the thermal conditions, thicknesses of the brittle and ductile layers, as well as the existence of a brittle layer within the upper part of the mantle, depend on the temperature gradient of the lithosphere. For intermediate to high temperature gradients, the lithosphere can be represented by three or even two layers, respectively. In the case of a three-layer lithosphere, the brittle–ductile crust and the ductile lithospheric mantle rest upon the asthenosphere, whereas in the case of a two-layer lithosphere, the two crustal layers rest directly upon the low-viscosity asthenosphere (Davy, 1986; Davy and Cobbold, 1991; Benes and Davy, 1996; Fig. 4c). Similar rheological conditions with a two- or three-layer lithosphere may characterise thickened lithospheres, such as in areas where extension follows the cessation of crustal thickening (see core complex mode of extension). In such conditions, provided that the time after the thickening is high enough to allow thermal relaxation to weaken the crust and the underlying mantle (e.g., about 20 Ma; Bartley and Glazner, 1985; Sonder et al., 1987), the strength of the sub-Moho mantle is greatly reduced, giving a dominant strength peak in the middle crust at the base of the upper brittle crust (Brun et al., 1994; Brun, 1999; Fig. 4d).

These different rheological stratifications of the lithosphere may represent different stages of rifting evolution, from continental breakup to oceanic seafloor spreading (e.g., Prodehl et al., 1997). In particular, the strong variations in crustal thickness generated during the process of continental extension may be viewed as a function of rift development stage: the further the rifting process has progressed, the thinner is the crust (e.g., Girdler, 1983; Prodehl et al., 1997; Fig. 5). The process of continental breakup starts in a four-layer lithosphere; with increasing extension, a strong thinning of the continental crust occurs, and the sub-Moho strength peak is progressively reduced until it vanishes. Lithospheric thickness is strongly reduced up to about 20 km, with the crust resting directly above the asthenosphere; further extension leads to the transition to a true oceanic seafloor spreading. During such a process, the upper mantle below the crust tend to be replaced by an anomalous mantle (characterised by low seismic velocities), which may contain up to 5% of melt (e.g., Prodehl et al., 1997). This partially molten and low-viscosity ($\eta < 10^{21}$ Pa s) layer can be considered to behave as the asthenosphere (e.g., Buck, 1991).

According to Prodehl et al. (1997), this rheological evolution is characteristic of passive rifting. In case of the rise of a mantle plume causing an active rifting component the associated thermal perturbation is expected to modify the initial rheological stratification of the lithosphere, locally reducing or suppressing the sub-Moho strength peak and possibly causing early magmatic underplating (e.g., Morley, 1994, 1999b; Callot et al., 2001, 2002; Fig. 1). In these cases, the four-layer lithosphere model may be replaced by a two- or three-layer profile from the early stages of stretching (Callot et al., 2001, 2002; see also Section 4.1 and Fig. 14). This, in turn, may favour a more rapid and concentrated deformation, leading to continental breakup.

3.2. Centrifuge models and the passive vs. active mechanism

Previous experimental centrifuge models have been performed to investigate the dynamics of rift systems development (e.g., Ramberg, 1963, 1971, 1981; Mulugeta, 1985; Mulugeta and Ghebreab, 2001). Many of these models were based on geophysical data supporting that many continental rifts are underlying by a low-viscosity and low-density mantle that is thought to play a major role in the rifting process. Starting from these assumptions, centrifuge models simulated the formation of continental rift valley systems by means of a diapiric uprise of subcrustal viscous material whose spreading generated tension and rifting in the overlying crust (Ramberg, 1971). These models allowed the main characteristics of continental rift systems to be reproduced. Such characteristics include morphology, mainly expressed by wedge block subsidence and shoulder upwarping, listric geometry of the major boundary faults and (in plan view) anastomising arrangements of fractures and faults. Rift valley dynamics and the causative processes for extension (i.e., passive vs. active rifting mechanisms) have been investigated by Mulugeta (1985), who performed two different series of models: a bending type, in which the crust was laterally confined, and a spreading type, in which the crust was allowed to move laterally. This setup was
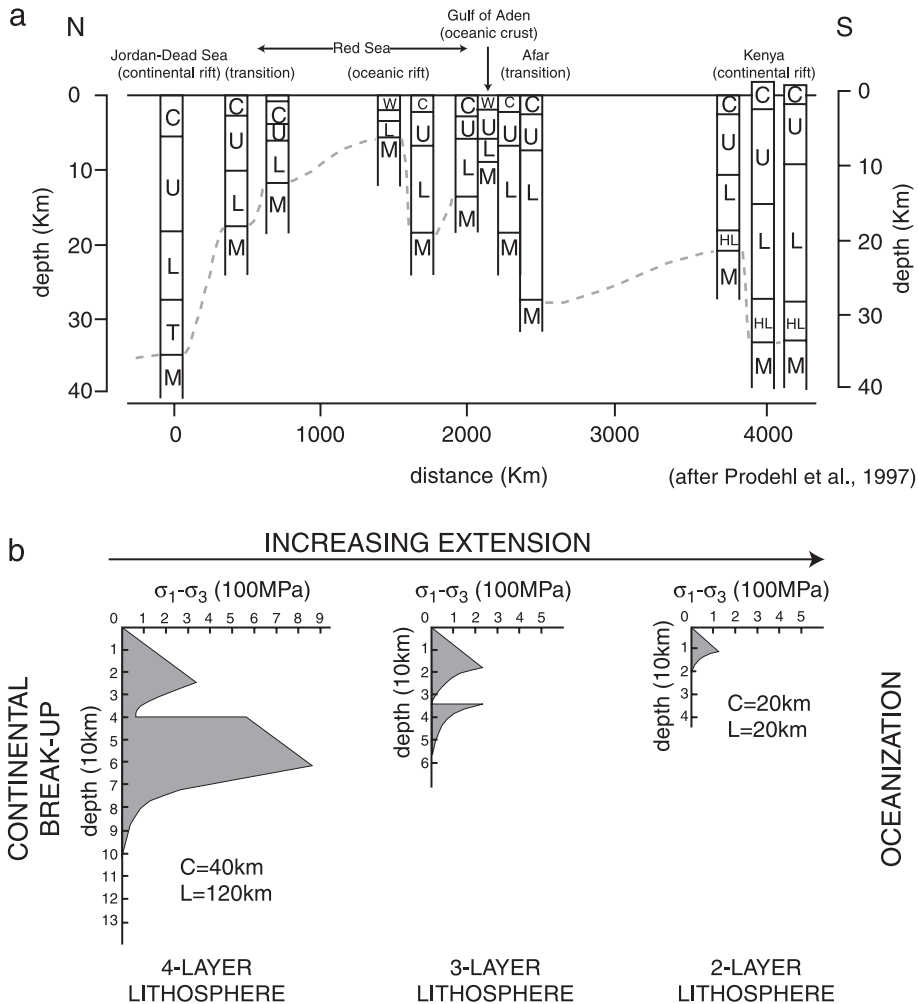
Fig. 5. Spatial and temporal rifting evolution in the Afro-Arabian rift system. (a) Evolutionary sequence illustrating the crustal rheological variation from the Jordan–Dead Sea transform system through the Red Sea, Gulf of Aden and Afar triangle to the southern end of Kenya Rift (modified after Prodehl et al., 1997). W: water; C: cover rocks; U: upper crust; L: lower crust; HL: high-velocity lower crust; T: crust–mantle transition rocks; M: Moho. (b) Interpreted variations in strength profiles during the transition from a stable four-layer lithosphere to a thinned (and heated) two-layer lithosphere preceding oceanization (rheological profiles from the East African Rift System. C: crustal thickness; L: lithospheric thickness compiled after Fadaie and Ranalli, 1990).

designed to investigate if the bending without lateral extension of the crust (i.e., the active rifting process alone) was sufficient to generate the structures of continental rift valleys. Mulugeta's (1985) results reveal that even if the tensional stresses provided by the upwelling and laterally spreading of a diapiric anomalous upper mantle body were large enough to fracture the crust in tension, the boundary conditions during the bending type models (i.e., laterally con-

fined crust) inhibited the rift valley formation. In particular, the amplitude of uplift of the model crust above the dome could account for no more than 3% of the extensional strain. This observation suggest that the bending process (and thus, the active rifting alone) as a mechanism of rifting is unrealistic, since it is not able to account for the common features and the measured values of extension in continental rift systems (>10%, e.g., Buck, 1991; Ruppel, 1995).

Conversely, models which allowed the lateral extension of the crust (i.e., crust which was laterally free to move) reproduced the main characteristics of continental rift systems, such as a well-developed graben (Fig. 6).

The geometry of brittle–ductile extension and the mechanics of normal faulting in relation to steady or episodic rifting of the continental lithosphere have been investigated in centrifuge models by Mulugeta and Ghebreab (2001). These authors considered both a constant displacement rate at the lateral boundaries (steady extension) and heterogeneous stretching in which periods of sideward displacement at a constant rate alternate with no displacement (episodic extension). Results suggest the dynamics of the rifting process has a major influence on the geometry of the resulting structures. In the case of constant, progressive rifting, extension is accommodated by rapid subsidence and flexure of the brittle crust, with formation of a central rift zone characterised by a complex array of domino-style faults and bounded

marginal grabens. On the contrary, episodic stretching of the lithosphere supports formation of spaced grabens and horsts, with less-pronounced subsidence. This pattern is produced by a counterflow of ductile material from the margins to the central rift zone, which is a dynamic consequence of heterogeneous stretching. Indeed, during extension, an isostatic imbalance is generated in the rheologically stratified model lithosphere due to thinning of the central zone; buoyancy forces try to restore the so-created difference in pressure by promoting ductile flow and thus redistributing material. During steady extension, forces that drive extension are higher than buoyancy forces generated by the differential pressure between the rift depression and the rift margins; this drive an outward flow of ductile material that promote thinning and subsidence of the central rift zone. In contrast, during pauses of extension, there is a counterflow of ductile materials from the regions of higher topography towards the rift depression; this flow tries to remove the differential pressure between the rift margins and the rift depression and to restore isostatic equilibrium.

3.3. Normal-gravity models and the modes of continental extension

Many analogue experiments performed in terrestrial gravity field were addressed to investigate the structural evolution and the main parameters controlling the mechanics of continental extensional tectonics (Faugère and Brun, 1984; Brun et al., 1985, 1994; Vendeville et al., 1987; Allemand et al., 1989; Allemand and Brun, 1991; Beslier, 1991; Brun and Tron, 1993; Benes and Davy, 1996; Brun and Beslier, 1996; Brune and Ellis, 1997; Gartrell, 1997, 2001; Brun, 1999; Michon and Merle, 2000; Callot et al., 2001, 2002). Results of analogue experiments have proven that the style of continental extension is mainly controlled by the competition between the total resistance of the analogue lithosphere and the gravitational forces which causes spreading of the model lithosphere over the asthenosphere (Benes and Davy, 1996). These two parameters control the transition between narrow and wide mode of continental extension.

Narrow rifts form when the total resistance of the lithosphere dominates over the gravitational forces,
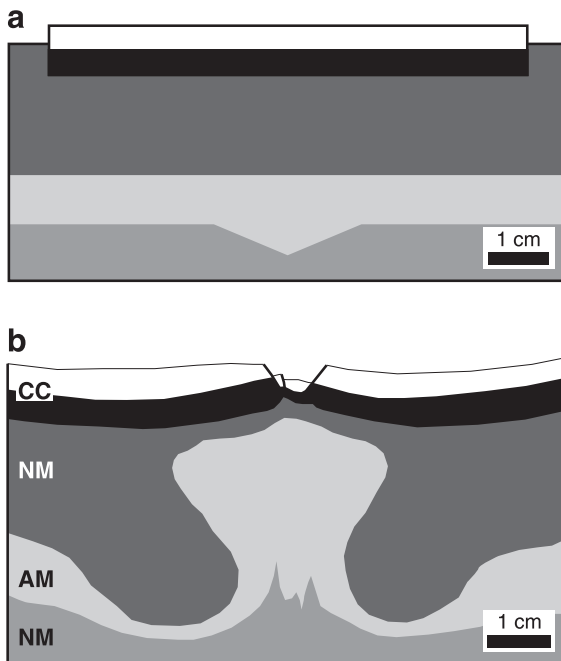

Fig. 6. Initial arrangement (a) and final profile (b) of a centrifuge rifting model showing the diapiric uprise of subcrustal viscous material generating extension in the overlying crust (redrawn after Mulugeta, 1985). CC: crust, AM: anomalous mantle, NM: normal mantle.
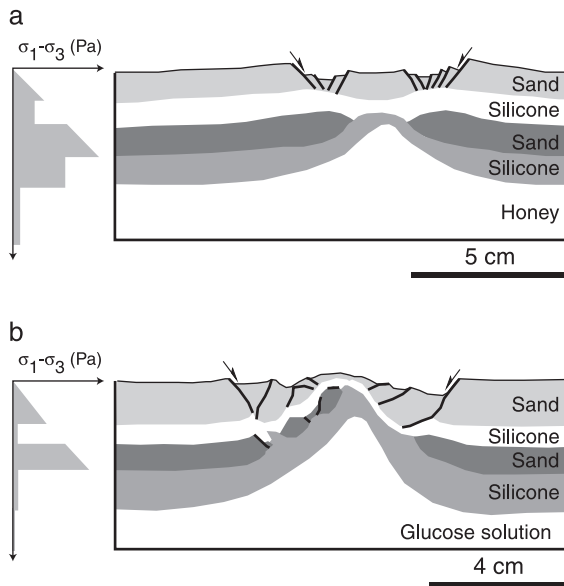
Fig. 7. Necking of the brittle upper mantle in four-layer analogue models. (a) Modified after Allemand et al. (1989) and (b) modified after Brun and Beslier (1996).

allowing a localisation of deformation at a lithospheric scale. This can occur in relation to the process of necking of a very strong brittle upper mantle in case of a four-layer lithosphere (e.g., Allemand et al., 1989; Fig. 7) or to a high brittle/ductile crust thickness ratio (Benes and Davy, 1996; Table 1; Fig. 8A). During the narrow rifting process, deformation is concentrated within a narrow area over the model surface, giving rise to rift structures whose initial width is, to a first order, a direct function of the brittle upper crust thickness (e.g., Allemand and Brun, 1991). Commonly, the grabens border faults join at the brittle–ductile interface, suggesting that the thickness of the brittle layer (T), the width of the deformed zone (W) and the fault dip (β) may be linked by a linear relationship in the form (Allemand and Brun, 1991; see also Mauduit and Dauteuil, 1996):

$$W = \frac{2T}{tg\beta}. \tag{1}$$

Since the strength peak in the uppermost mantle, under low-temperature conditions, offers the greatest resistance to extension, the process of necking of the brittle upper mantle during stretching of a four-layer

lithosphere represents a major process in controlling the evolution of deformation (e.g., Allemand et al., 1989; Beslier, 1991; Brun and Beslier, 1996; Brun, 1999; Michon and Merle, 2000; Callot et al., 2001, 2002; Fig. 7). In turn, the necking process is influenced by the applied strain which controls the coupling between brittle and ductile layers (e.g., Brun and Tron, 1993). Low strain rates result in a low brittle–ductile coupling determining the development of a single neck in the uppermost mantle that gives rise to a narrow deformed zone at a lithospheric scale. On the contrary, higher strain rates increase the brittle–ductile coupling, leading to a multiple necking (i.e., boudinage) of the brittle mantle. In this case, the upper crust extending zone may contain several rifts, depending on the geometry of the mantle ruptures and on the strain rate (Allemand et al., 1989; Beslier, 1991; Brun and Beslier, 1996; Michon and Merle, 2000). Thus, an increase in the strain rate and the brittle–ductile coupling favours a distribution of deformation over wide areas (e.g., Brun and Tron, 1993).

The wide rifting mode of extension occurs when gravity forces dominate over the resistance of the lithosphere. In case of a three- or two-layer lithosphere, this may occur because of the low resistance associated with a thin analogue brittle crust (Benes and Davy, 1996; Fig. 8B; Table 1). If this occurs, the influence of the ductile flow in the lower crust increases, resulting in a homogeneous stretching that distributes deformation over a wide area (Fig. 8B). Wax models by Brune

Table 1
Rheological characteristics of the continental lithosphere according to three modes of continental extension

Mode of extension	Hypothesised initial lithospheric stratification	Initial upper crust thickness (km)	Initial lower crust thickness	Brittle/ ductile thickness ratio
Narrow rifting	four-layer[a,b]	15–25[a,b]	10–15[a,b]	2:1–1.5:1
Wide rifting	three-layer[b]	10–30[b,c,d]	20–30[b,c,d]	≈ 1:1–1:2
Core complex	three-layer[b]	10–20[a,b]	up to 100[e]	≈ 1:2–1:3

[a] Fadaie and Ranalli (1990).
[b] Buck (1991).
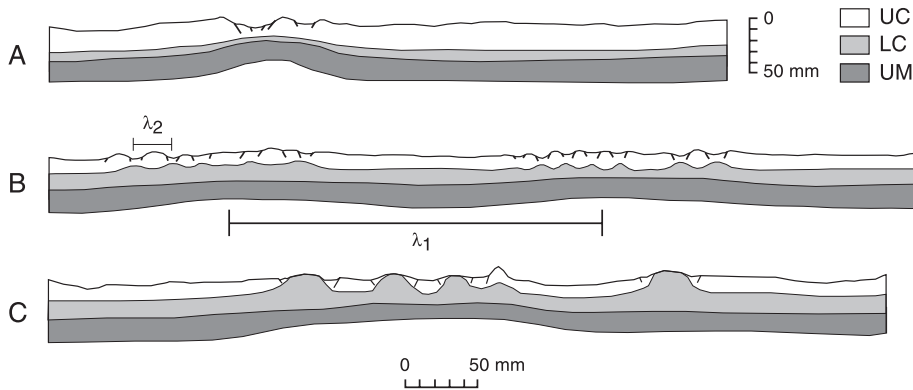[c] Benes and Davy (1996).
[d] Brun (1999).
[e] Hill et al. (1995).

Fig. 8. Different modes of extension in experiments by Benes and Davy (1996): (A) narrow rift mode; (B) wide rift mode; (C) core complex mode. λ_1 and λ_2 represent long-wavelength and short-wavelength instabilities, respectively. See text for further explanations. UC: brittle upper crust (sand); LC: ductile lower crust (silicone); UM: ductile mantle (silicone). Modified after Benes and Davy (1996).

and Ellis (1997) support the observation that the brittle/ductile thickness ratio is of paramount importance in controlling the style of extension, suggesting that old, thick and cold crust are expected to produce narrow rifts, whereas young, thinner and warmer crust should result in wide rifts. This behaviour reflects the process of strain softening at a crustal or lithospheric scale: when a thick brittle crust fails, the strength of a crustal or lithospheric column is strongly reduced, rapidly lowering the force necessary to continue extension and leading to strain softening with formation of narrow rifts. Thus, in this case, the force necessary to continue slip on a preexisting fault is less than that required to produce a new fault. Conversely, when a thin brittle crust ruptures, the force required to continue faulting is only slightly reduced and the layer-scale strain softening does not take place. In this case, an increase in extension leads to the outward growth of the deformation zone from the initial faulting area into undeformed regions, giving rise to the wide rifting mode (Benes and Davy, 1996).

Brun et al. (1994) and Brun (1999) discussed the wide rifting mode in terms of gravity-spreading-type instability that develops in previously thickened domains (Table 1). A consequence of unstable over-thickening of the continental lithosphere is that it will attempt to release the accumulated potential energy in order to return to its pre-compressional thickness. In these conditions, if the thermal relaxation is able to weaken the thickened crust, the dominantly ductile behaviour of the crust makes it

able to spread under its own weight. Experiments show the development of tilted domains (indicators of high strain rates and extension dominantly driven by gravity) and a nearly horizontal brittle–ductile interface that well accounts for the lack of crustal-scale necking and the nearly horizontal Moho often observed in wide rifts.

Core complexes represent a transitional style of continental extension that occur when an anomalously low viscosity and thick lower crust characterises the analogue asthenosphere (Fig. 8C; Table 1). Benes and Davy (1996) showed that gravity forces dominate the extension process during the first stages, leading to a diffuse deformation. For increasing extension, lower crust flows into the stretched regions, replacing the thinned brittle crust and removing the effect of the gravity forces (Fig. 8C). This restricts the migration of deformation into the undeformed regions. The importance of the presence of a viscous lower crust in determining the formation of core complexes is further supported by wax models by Brune and Ellis (1997). In their model, the key factor of core complex formation is represented by a significant thickness of the viscous layer that flows laterally to fill the spaces generated by the stretched upper brittle crust. Thus, their results support Jackson and Vendeville (1994) findings that extension, rather than density contrast, provides the driving force for triggering diapirism by generating a zone of low pressure into which diapirs of viscous material move. These models also support numerical models by Buck (1991) in that the different

modes of extension is controlled by the initial conditions, in terms of the brittle/ductile thickness ratio that reflects different heat flow, crustal age and thickness (see also Sections 2.2 and 5.1.1).

The association of core complexes with wide rifts led Brun (1999) to consider such structures as local anomalies within wide rifts and not a distinct mode of continental extension. This hypothesis is based on the results of models by Brun et al. (1994) which showed that core complexes may form within wide rifts because of the presence of local rheological heterogeneities within the ductile lower crust due to the presence of a partially molten zone (Fig. 9). Such anomalies may be able to localise stretching, leading to the development of highly extended areas in which the ductile lower crust is easily exhumed (Fig. 9). Model core complexes are characterised by local strong thinning of the brittle crust (with β values up to 2.25) which is compensated by uprising and exhumation of the ductile crust and is accommodated by low-angle detachment faults resulting from the progressive flattening of initially steeply dipping faults (Fig. 9). Benes and Davy (1996) discussed the possibility that localised thermal anomalies may influence the distribution of deformation in the crust, resulting in a strain localisation. Therefore, the transition between the wide rifting and the core complex mode seems to be partly dependent on the initial distribution of thermal anomalies within the crust.

Benes and Davy (1996) also discussed the different modes of continental extension in terms of stability of the extension process. Narrow rifting represents a stable form of extension, whereas wide rifting is an unstable form of extension, since deformation propagates outward the zone of initial faulting. Similarly to what predicted by numerical models (e.g., Zuber et al., 1986), this unstable mode of extension is characterised by the development of two types of periodic instabilities with different wavelengths. Long-wavelength instabilities correspond to periodic alternation of faulted domains separated by undeformed regions, whereas short-wavelength instabilities control the graben spacing within the deformed regions (see the λ_1 and λ_2 wavelengths in Fig. 8B). The development of these instabilities is favoured by the presence of a strong upper crust and upper mantle separated by a weak lower crust (e.g., Smith, 1977; Fletcher and Hallet, 1983; Zuber et al., 1986; Martinod and Davy, 1992). In particular, the higher the strength contrast between the brittle and ductile crust, the larger the growth rate and the wavelength of the instabilities. However, the absence of instabilities during narrow rifting suggest that there is a limit to the upper crust thickness above which the potential of the ductile crust flow to develop periodic instabilities is sup-
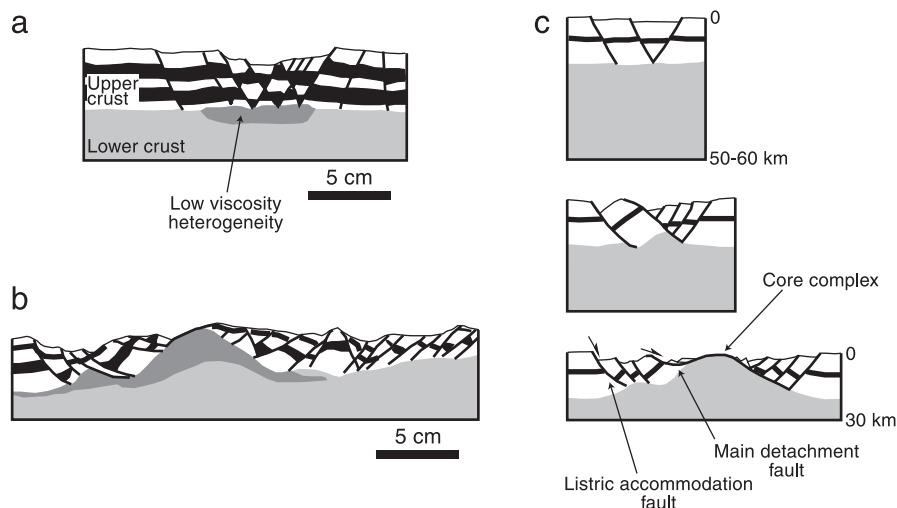

Fig. 9. Analogue models of core complexes. (a) Patterns of model deformation at early stage and (b) at the core complex stage. (c) Idealized model of core complex development deduced from model results. Modified after Brun (1999) and Brun et al. (1994).

pressed by the dominant strength of the brittle crust (Benes and Davy, 1996).

3.4. Models simulating oblique and polyphase rifting

In oblique rifting, the deformed zone trends obliquely to the stretching vector, such that both extension perpendicular to the rift trend and shear parallel to the rift axis contribute to rift formation (e.g., Withjack and Jamison, 1986; Tron and Brun, 1991). Such an oblique extension can arise because of (1) reactivation of preexisting crustal or lithospheric zone of weakness trending oblique to the stretching vector, or (2) rotation of the direction of extension through time in the so-called polyphase rifts. Reactivation of preexisting structures is probably the major process in controlling oblique rifting. The structural inheritance may be related to the presence of pervasive or discrete fabrics within the upper crust (e.g., Morley, 1999e,f and references therein). Pervasive fabric (present throughout large volumes of rocks) impose a strength anisotropy able to influence the orientation of the majority of faults in an area, whereas discrete planes or zones of weakness exert a local influence on rift faults. Other inherited strength anisotropies may be related to the presence of a weakness zone in the high-strength upper mantle layer that is expected to have a strong control on lithospheric deformation (e.g., Allemand et al., 1989); being the stretching direction not necessarily perpendicular to this zone, oblique rifting can occur (e.g., Tron and Brun, 1991). Vauchez et al. (1997) and Tommasi and Vauchez (2001) have proposed a complementary model in which the source of structural inheritance is related to the preservation, within the uppermost mantle, of a lattice-preferred orientation of olivine crystals formed during previous main tectonic phases.

Scaled analogue models have been successfully applied to the analysis of the deformation pattern resulting from oblique extension of the continental lithosphere (Withjack and Jamison, 1986; Tron and Brun, 1991; Brun and Tron, 1993; Dauteuil and Brun, 1993, 1996; McClay and White, 1995; Scott and Benes, 1996; Mart and Dauteuil, 2000; Clifton et al., 2000; Román-Berdiel et al., 2000; Clifton and Schlische, 2001; Fig. 10). At a lithospheric scale, these models have shown that in a brittle–ductile system resting on the asthenosphere and affected by oblique extension, the rift systems form through the linking of

initial oblique en echelon basins and oriented perpendicular to the direction of extension (Mart and Dauteuil, 2000). The lateral propagation of these basins merged them into a single sinuous rift characterised by a linear series of pull-apart basins separated by uplifted thresholds or transfer zones preserving the initial en echelon geometry of basins. During progressive deformation of the models, diapirs of ductile materials penetrated the floor of the internal rifts, then propagated along the axial zone (Mart and Dauteuil, 2000).

Models applied to investigate the geometrical and kinematical characteristics of oblique rifts have shown that the main parameter controlling the final surface structural pattern is the angle between the extension vector and the rift trend (i.e., angle of obliquity, α) that represents the ratio between shearing and orthogonal stretching components (e.g., Withjack and Jamison, 1986; Tron and Brun, 1991; McClay and White, 1995; Scott and Benes, 1996; Clifton et al., 2000; Román-Berdiel et al., 2000; Clifton and Schlische, 2001). The angle α controls the orientation, the dip and the kinematics of faults as well as the strain partitioning between different sets of structures. Previous models allowed to outline some general characteristic of oblique rifting, particularly, (1) en echelon fault pattern; (2) mean fault trend(s) not perpendicular to the resulting stretching vector (θ, the angle between the fault trend and the direction of extension, tend to decrease with α); (3) mean initial fault dip higher than for dip–slip normal fault; (4) frequent curved faults (along which the displacement can vary from dominant dip–slip to dominant strike–slip) for low obliquity rifting; (5) strain partitioning between distinct families of oblique–slip and strike–slip faults for high obliquity rifting (e.g., Tron and Brun, 1991; Fig. 10). Generally, the sense of shearing along single structures is the same as the one applied to the system, although opposite senses of displacement can be observed because of rotation of internal blocks (e.g., Withjack and Jamison, 1986; Tron and Brun, 1991).

Clay models by Clifton and Schlische (2001) have shown that the angle of obliquity α also controls the temporal evolution of fault populations and the maximum fault length, with important implications for earthquake hazard assessment. In particular, their experiments show that for high obliquity, rifting clusters of displacement-normal faults form parallel arrays, leading to fault growth dominated by tip
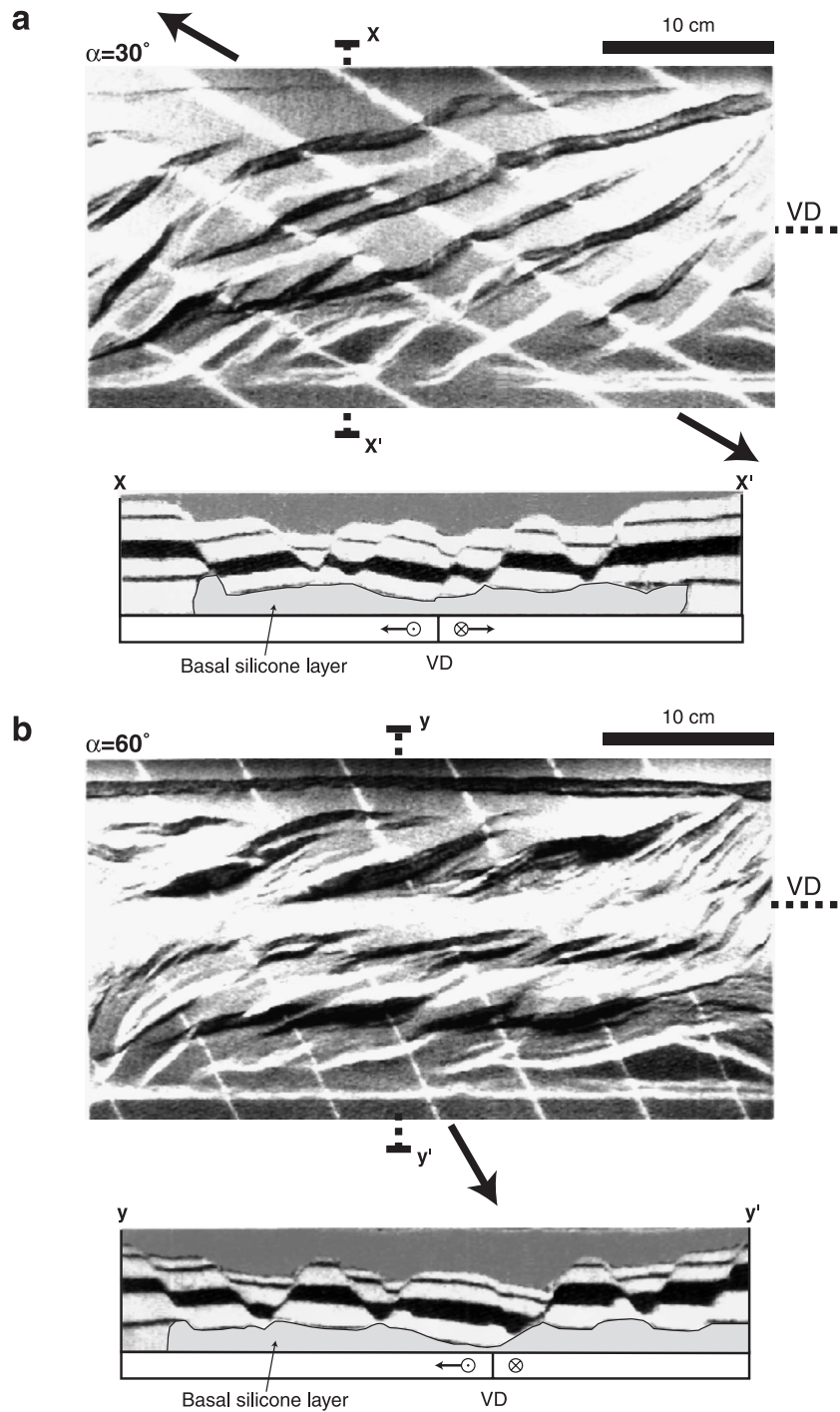
Fig. 10. Top views and cross-sections of oblique rifting models by Tron and Brun (1991). (a) Symmetric extension with $\alpha = 30°$. (b) Asymmetric extension with $\alpha = 60°$. Oblique lines on the top views are parallel to the stretching vector that is indicated by the black arrows. After Tron and Brun (1991).

propagation until a maximum length (corresponding to the rift width) is achieved. Then, rift-parallel faults form with a maximum length limited by the preexisting displacement-normal faults; with further deformation, these two sets of faults may link to form complex, branching structures. On the contrary, for low-obliquity rifting, fault growth is less restricted: faults form in clusters with an en echelon geometry such that structures may easily link and grow rapidly. The final fault trace is longer than in the case of high obliquity: the maximum attainable fault length is more than three times the width of the rift zone. Thus, assuming that potential earthquake hazard is related to fault length, the maximum potential earthquake in a mature highly oblique rift should be less than that in an orthogonal or less-oblique rift (Clifton and Schlische, 2001).

Oblique rifting can also result from a rotation of the direction of extension with respect to the rift trend during successive rifting episodes, as documented for both continental and oceanic rifts (e.g., Strecker et al., 1990; Ring et al., 1992; Dauteuil and Brun, 1993). In these polyphase or multiphase rifts, the structural pattern is normally very complex, being characterised by different sets of rift-parallel and rift-oblique faults. This structural pattern has been successfully modelled by Bonini et al. (1997) and Keep and McKlay (1997) that have investigated the structural evolution result-

ing from two non-coaxial rift events. These works highlighted that the structures produced by the first phase of extension have a significant control on the geometries of the later phase extensional faults (Fig. 11). This occurs when the rifting evolution is characterised by a first orthogonal extension phase followed by an oblique rifting episode, as well as when this sequence is reversed (Bonini et al., 1997; Fig. 11). When the progression is from orthogonal to oblique, the faults formed during the first phase force the oblique rifting-related structures to form within the preexisting graben borders. The oblique deformation of the second rifting episode is accommodated by an oblique–slip reactivation of the master faults (for low obliquity angles, $\alpha \le 45°$) and by newly formed strike and oblique–slip faults (for high obliquity angles, $\alpha > 45°$). When the progression is reversed, for $\alpha \le 45°$, oblique faults formed during the first oblique phase continue to develop during orthogonal extension and connect with each other to give sigmoidal fault blocks. For $\alpha > 45°$, new normal faults trending parallel to the rift trend develop in zones previously weakened by numerous oblique faults.

3.5. Modelling of transfer zones

Extended terranes are often partitioned into regionally extensive domains of uniformly dipping normal-
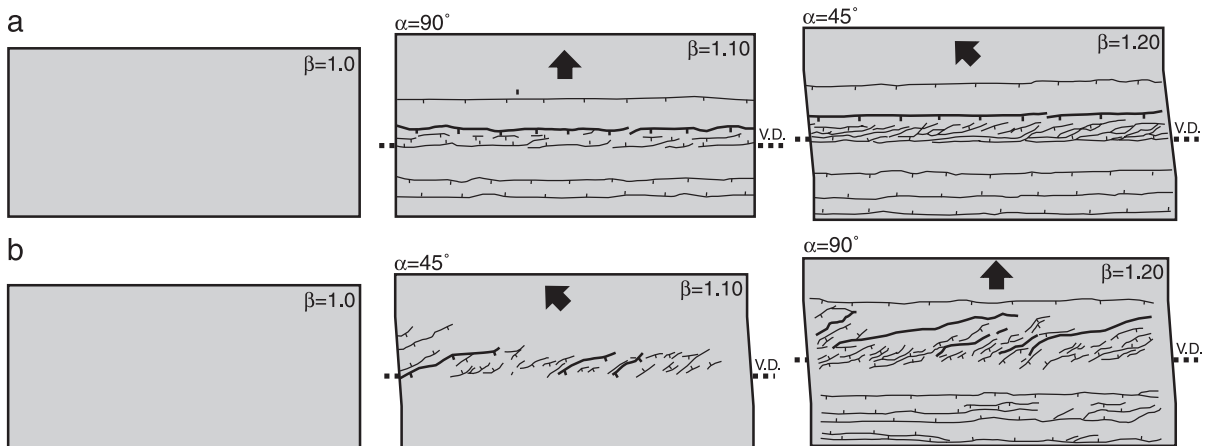

Fig. 11. Top view line drawings showing the progressive deformation in polyphase rifting experiments. (a) Models characterised by a first phase of orthogonal extension followed by a second phase of oblique rifting, with $\alpha = 45°$. (b) Models characterised by a first phase of oblique extension (with $\alpha = 45°$) followed by a second phase of orthogonal rifting. The arrows indicate the direction of extension. Modified after Bonini et al. (1997).

fault systems and attendant tilt-block domains (see Faulds and Varga, 1998 and references therein); this first-order segmentation represents one of the most important characteristic of both oceanic and continental rifts. During the development of the rift system, individual segments grow and interact, giving rise to half and full-grabens (e.g., Rosendahl, 1987; Ebinger et al., 1989; Morley et al., 1990; Nelson et al., 1992). Several studies highlighted that along-strike, marked changes in basin geometry do occur, such as half grabens with alternating asymmetries or passing into full-grabens (e.g., Morley et al., 1990; Nelson et al., 1992). Linking and mechanical interaction between different rift segments is accommodated by the presence of transfer zones, structurally complex areas in which boundary faults interact to conserve extension or extensional strain (Nelson et al., 1992). Transfer zones represent a change from a more or less two-dimensional extension (plane strain) to oblique–slip fault systems associated with three-dimensional extension (non-planar strain; Morley, 1988). As a consequence, the architecture of the areas of mechanical interactions between extensional segments are normally very complex, including discrete zones of strike– and oblique–slip faults and/or more diffuse belts of overlapping fault terminations (e.g., Rosendahl, 1987; Morley et al., 1990; Nelson et al., 1992; Faulds and Varga, 1998 and references therein). In correspondence to transfer zones, major boundary faults may curve, giving rise to arcuate structures in plan view, and a strain partitioning between different sets of faults may arise (e.g., Acocella et al., 1999a, 2000 and references therein).

Several studies showed that the interaction between individual rift segments and the structural pattern of transfer zones may be influenced by several parameters, such as the presence of inherited anisotropies, the initial configuration of the rift segments, the geometry of décollement layers as well as variations on the deformation style (e.g., along-axis variations in the extension rate; e.g., Acocella et al., 1999a, 2000 and references therein). The influence of these parameters on the architecture and the development of both transfer and transform zones in continental and oceanic domains has been investigated through clay (Courtillot et al., 1974; Elmohandes, 1981; Serra and Nelson, 1988; Fig. 12) and sand-box (Naylor et al., 1994; Mauduit and Dauteuil,

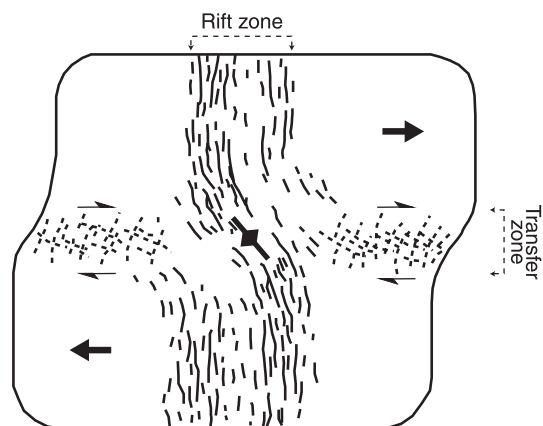

Fig. 12. Surface fault pattern in clay models of transfer zones. Modified after Serra and Nelson (1988).

1996; Acocella et al., 1999a,b, 2000; Basile and Brun, 1999; Fig. 13) analogue modelling studies. Here, we focus on the experiments reproducing transfer zones in continental rifts (Elmohandes, 1981; Serra and Nelson, 1988; Naylor et al., 1994; Acocella et al., 1999a,b, 2000; Basile and Brun, 1999). These experiments reproduced en echelon (offset) basins that during the extension process are connected by areas characterised by curved normal faults, which tend to become subparallel to the extension direction, and by anticlines with axis oblique to the direction of extension (Elmohandes, 1981; Serra and Nelson, 1988; Naylor et al., 1994; Acocella et al., 1999a,b, 2000; Figs. 12 and 13). The arcuate normal faults form as a consequence of a local variation in the extension direction within the transfer zone; because of this reorientation of the stress trajectories, the arcuate faults display a dominant dip–slip motion even if they are subparallel to the extension direction (Acocella et al., 1999a). Together with these arcuate normal faults, strike–slip structures form in the experimental transfer zone, provided that the angle between the transfer zone and the direction of extension (α) is less than $45°$ (Acocella et al., 1999a): in these conditions, a strain partitioning between the normal and strike–slip kinematics within the transfer zone arises. On the contrary, for α angles higher than $45°$ strain partitioning is not observed, and the strike–slip component in the transfer zone is accommodated entirely by oblique kinematics on arcuate faults. In the presence of preexisting basement anisotropies, the angle α between the transfer zone and the extension
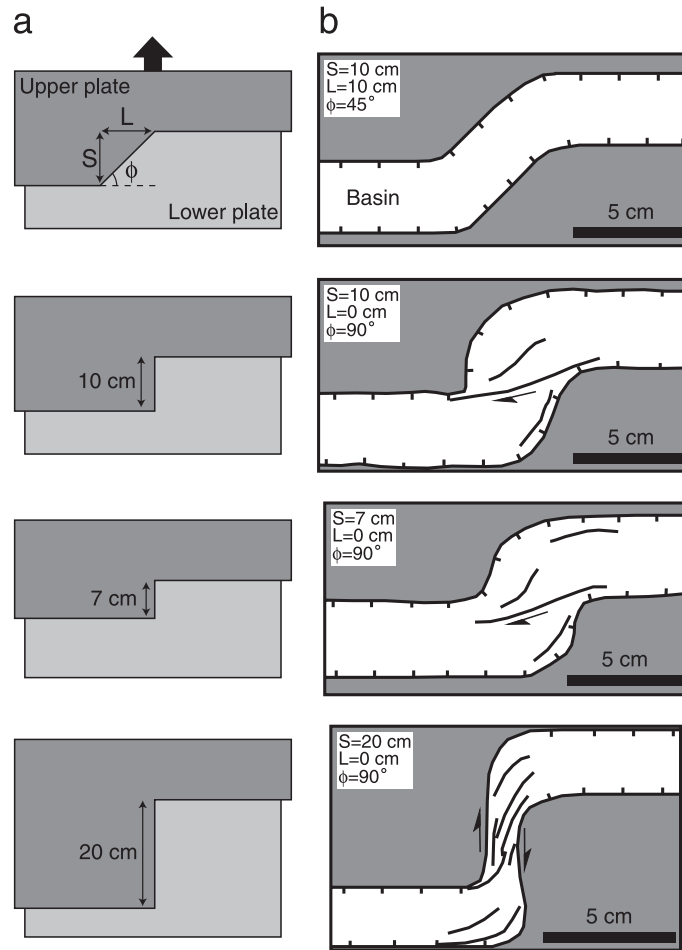
Fig. 13. Sand-box transfer zone experiments by Acocella et al. (1999a,b). (a) Experimental configurations showing the geometry of the upper and lower metal plates simulating preexisting basement anisotropies in nature. The model sand-pack is sedimented above these plates. (b) Final surface fault patterns of the different models. Modified after Acocella et al. (1999a,b).

direction is dependent on the direction of the inherited structure in the transfer zone and on the overstep between the en echelon basins (i.e., the along-axis length of the transfer zone). In particular, α decreases, increasing the angle (ϕ) between the inherited structure in the transfer zone and the extension direction and (for a fixed ϕ) increasing the overstep between the en echelon rifts (Fig. 13). Furthermore, while increasing the overstep, the extension-parallel rifts within the transfer zone tend to become narrower. These observations accord with the results of transform fault experiments by Mauduit and Dauteuil (1996) in that decreasing the angle between the transfer zone and the extension direction increases the strike–slip component of movement and hence the fault dips (thus reducing the rift width according to Eq. (1); Section 3.3).

Strain partitioning do not arise when the offset between the rift segments is given by the geometry of a décollement layer (silicone layer) at depth: in that case, the strike–slip faults do not form, and the transfer zone is characterised by the development of relay ramps (Acocella et al., 2000). On the contrary, strike–slip faults form at the interface between the two extending plates moving at different extension rates and curve to join the boundary normal faults. Note that in these experiments,

normal faults develop prior to strike–slip faults, as expected from the reduced strength in extensional regime compared with the transcurrent regime (Basile and Brun, 1999).

4. The influence of magmatic bodies in analogue models of continental extension

In Section 2.3, the influence of magmatism on tectonic evolution has been briefly discussed, highlighting that the presence of low-viscosity magmatic bodies and the related thermal softening of the country rocks are able to generate a local strong lithospheric-scale strain softening that, in turn, localises and possibly enhances deformation (e.g., Lynch and Morgan, 1987; Chèry et al., 1989; Benes and Davy, 1996; Morley, 1999a). The geometry of such rheological anomalies within the continental lithosphere might also represent an important parameter controlling the distribution of surface deformation. On the other hand, deformation is expected to have an influence on the distribution and possibly controls the plumbing systems of volcanic activity and the timing of eruptions. As corollary, tectonic environments at surface might lead magmas to reside at depth for some time rather than pouring out, favouring the occurrence of extensive evolutionary processes to modify the original compositions of primitive magmas. In the following sections, we review previous normal-gravity models on magma emplacement at various levels within the lithosphere and the influence on the deformation process. We then review the results of previous centrifuge experiments on continental extension and magma underplating and integrate them with new data to discuss the relations between deformation and magma emplacement in various extensional settings.

4.1. Normal-gravity models

Experiments by Callot et al. (2001, 2002) considered the effect of soft magma bodies at depth on the mechanical behaviour of a four-layer lithosphere during continental breakup. Their results show that the presence of a low-viscosity body (LVB) can play a major role in controlling the necking process, especially when the rheological anisotropy is located within the brittle upper mantle, thus interrupting the lateral

continuity of this strong layer (Fig. 14). Indeed, when the LVB does not cut across the brittle upper mantle, the deformation pattern is similar to the results by Brun and Beslier (1996), and lithospheric necking is accom-
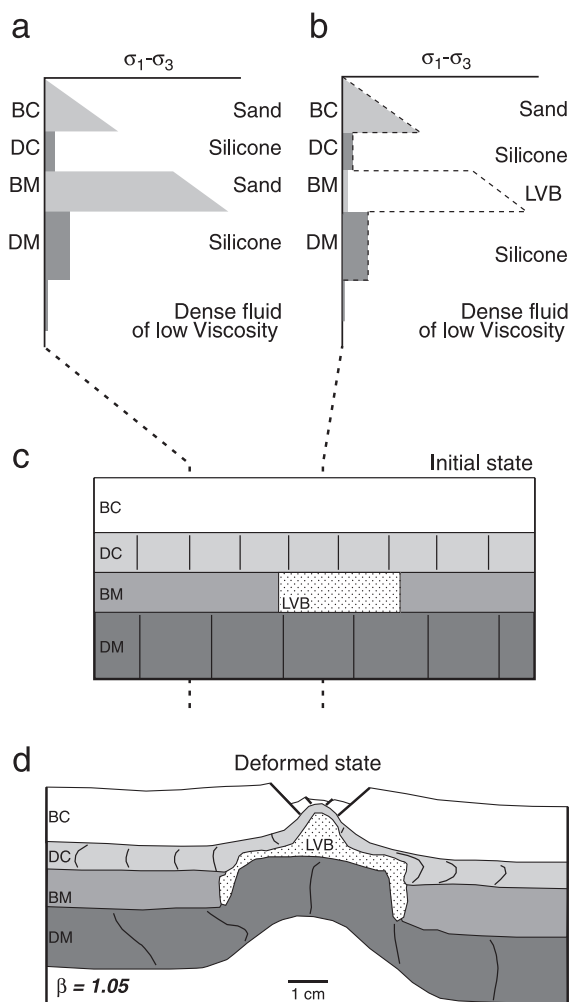

Fig. 14. Analogue models of continental extension by Callot et al. (2001) involving the influence of the presence of a low-viscosity body (LVB) on deformation. (a–b) Initial lithospheric strength profiles; (c) initial model setup; (d) final model cross-section highlighting a strong localisation of deformation in correspondence to the low-viscosity body. Note that the presence of a LVB determines the strength peak in the brittle mantle to disappear causing a strong reduction in lithospheric strength and the transition from a four-layer lithosphere (a) to a local two-layer lithosphere (b). In (b), the dashed line indicates the "normal" four-layer profile. BC: brittle crust; DC: ductile crust; BM: brittle mantle; DC: ductile mantle. Redrawn after Callot et al. (2001).

modated by boudinage over a wide zone. On the contrary, when the LVB is located within the brittle mantle, lithospheric necking occurs over a narrower zone, promoting a stronger and more localised mantle uplift resulting in the development of a single graben in the upper crust (Fig. 14). Thus, the difference in strength between the four-layer and the local two-layer lithosphere in correspondence to the soft magma body results in a strong strain localisation above the LVB (Callot et al., 2001; Fig. 14). Note that similar results in terms of a strong magma-induced strain localisation were obtained by Brun et al. (1994) in core complex models (see above Section 3.3). In the presence of more magmatic bodies within the extending lithosphere, strain localisation above these "soft spots" (i.e., low-strength zones) strongly controls rift development and the breakup process (Callot et al., 2002). During extension, the soft spots induce an along-strike segmentation of the rifted domain; rift segments initiate above the low-viscosity bodies and propagate toward adjacent segments. In the case of non-aligned viscosity heterogeneities, the distribution of the soft spots is able to control the rift orientation and segmentation more than the direction of regional extension (Callot et al., 2002).

Román-Berdiel et al. (2000) investigated the intrusion of a high-viscosity granitic magma during oblique extension of the upper crust and the influence of such localised rheological anisotropies on the structural pattern. Their results showed that granite intrusions localise strain from the first stages of deformation and influence the final fault pattern leading to the development of an oblique graben above the intrusions. In turn, deformation influences the shape of magmatic intrusions, leading (for α between $45°$ and $60°$) to magma emplacement in the footwall of major listric normal faults, in a similar fashion to the "extensional footwall growth" model by Quirk et al. (1998; see also Section 4.2.3).

4.2. Centrifuge models involving the influence of magmatic underplating

4.2.1. Analogue modelling strategy

The mechanical influence of a magmatic body at the base of the crust on the extension process has been poorly explored in analogue models. Magmatic underplating represents indeed an important process that is able to modify the thermo-mechanical properties of continental lithosphere (e.g., Furlong and Fountain, 1986; Matthews and Cheadle, 1986; Gans, 1987; Bergantz, 1989; Bohlen and Mezger, 1989; Wilshire, 1990; Fyfe, 1992; Parsons et al., 1992; White, 1992; Fig. 15). When the thermal state of the lithosphere is perturbed by the raising of the asthenosphere (both in active and passive processes), partial melting in the upper mantle is triggered, with production of different amounts of mafic magmas. Many important processes involving the magma are controlled by density: for example, buoyancy largely controls the rise of magma from a source region. Accordingly, in the analogue modelling, the difference of densities between the scaled lithosphere and the underplated magma is one of the most important factor controlling magma motion. Densities of magmas are dependent upon their chemical compositions, temperatures and pressures. Calculations using available computer programs (e.g., the program Pele; Boudreau, 1999; also available at www.eos.duke.edu) show that transitional-tholeiitic basalts commonly found in rift systems have densities of about $2750-2850$ kg m^{-3} at temperatures of 1300 °C and pressures of 10 kbar, corresponding to the depth of the subcontinental Moho (≈ 35 km). At the atmospheric pressure, the density drops to values of about $2550-2650$ kg m^{-3}. Melts of rhyolitic compositions have lower densities of about $2450-2600$ kg m^{-3} at Moho depth pressures. Therefore, the lower continental crust has a density (about $2800-2950$ kg m^{-3}) which can be
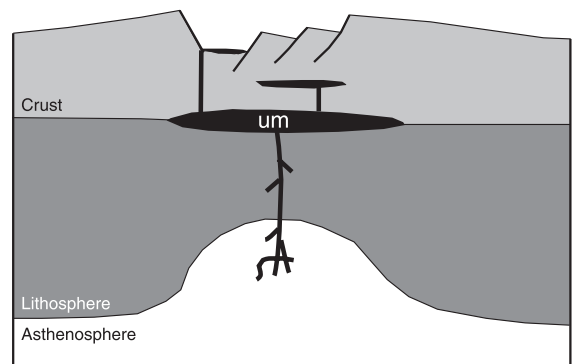

Fig. 15. Schematic diagram showing magmatic underplating of the continental crust. um: underplated magma. After Olsen and Morgan (1995).

considered slightly higher than that of magmas occurring at its base. On this basis, the experimental series simplified the rift evolution assuming an initial model setup characterised by an underplated partially molten body, slightly lighter than the overlying crust (see Appendix B). In order to reproduce rifting conditions characterised by a relatively high thermal gradient, a ductile rheology for the upper lithospheric mantle was used during the experiments.

Because in the models, deformation takes place when the magma is already emplaced below the Moho, experimental results may be a better representative of an extensional deformation in which thermal perturbations by an ascending mantle plays an important role (i.e., active rifting processes). In this case, the initial high thermal state is able to generate important volumes of magma (able to ascend and underplate) before significant extension has occurred (e.g., Morley, 1994, 1999b; Fig. 15). However, we are confident that model results may also provide clues for the dynamic relations between magma and deformation in a well-established rift generated by passive rifting process. Indeed, the evolution of active and passive rift systems is different mainly during the initial stages

of crustal thinning, whereas the evolution of both active and passive modes converges when the asthenosphere rises underneath the rift, triggering partial melting in the mantle and generating the emplacement of magma bodies within the crust (e.g., Morley, 1994, 1999b). Furthermore, we draw attention on the fact that, although the experiments are scaled to represent the continental crust, these models present a rheological profile similar to that commonly used for the oceanic crust (e.g., Mauduit and Dauteuil, 1996). On this basis, the modelling results can also give useful insights into the evolution of oceanic extensional areas (see the comparison of oblique rifting experiments with the structural and volcanic pattern in oceanic ridges in Section 5.2.2).

In the following sections, we examine four series of centrifuge experiments reproducing orthogonal (symmetric and asymmetric) extension (series Magm), oblique extension (series ObR), polyphase rifting (series PR) and the development of transfer zones in continental rifts (series NRTZ). The experimental setup of the these series is schematically illustrated in Fig. 16 and described in more detail in Appendix C.
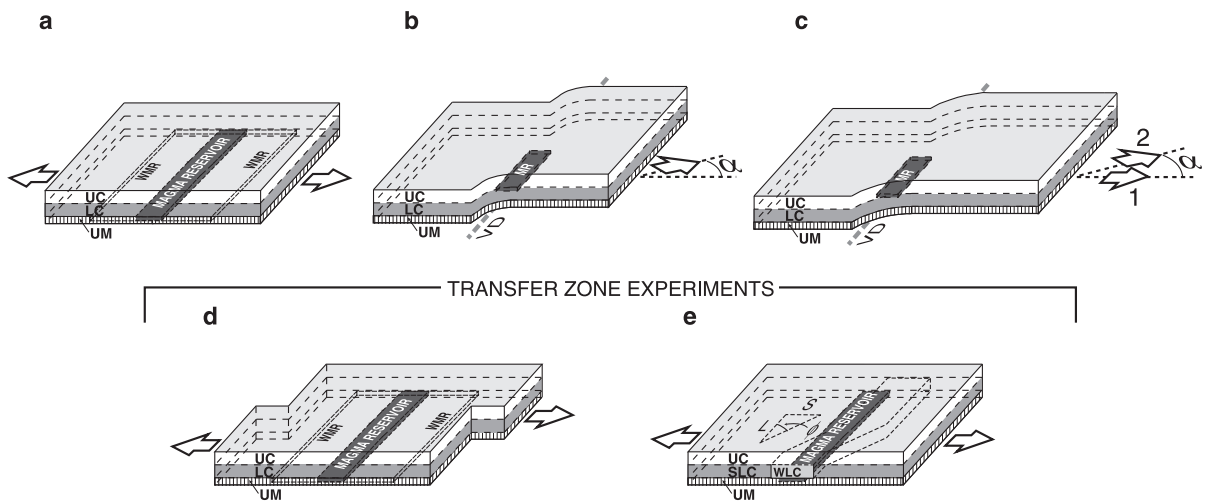

Fig. 16. Initial model setup for various settings of continental extension discussed in the text: orthogonal extension (a, series Magm), oblique extension (b, series ObR), polyphase extension (c, series PR) and transfer zone experiments (d, series TrZn; e, series NRTZ). The angle α in (b) and (c) indicates the obliquity of extension. In (e), S is the overstep, L the overlap and ϕ the angle between the weak lower crust rift segments (see Acocella et al., 1999a). In (b) and (c), the rigid moving plate boundary imposes a discrete velocity discontinuity (VD), whereas in (a), (d) and (e), the model setup does not involve a rigid VD. Numbers 1 and 2 in (c) indicate the sequence of the extensional episodes. UC: upper crust; LC: lower crust; SLC: strong lower crust; WLC: weak lower crust; UM: upper mantle; MR: magma reservoir; WMR: wide magma reservoir.

4.2.2. Simplifications and limitations involved in modelling the emplacement of magmatic bodies

Modelling of continental extension involving magmatic processes necessarily involves some limitations that are mainly related to the thermal conditions and the rheology of the natural process. Particularly, one of the main limitations is related to the impossibility to reproduce thermal variations during the extensional process in both the lithosphere and magmas. In particular, we could not account for the cooling of magma (and associated rheological variations) and the thermal weakening of the continental crust, which is expected to influence the rifting process (e.g., Morley, 1999a,b). Furthermore, we could not reproduce chemical reaction nor other particular phenomenon related to the presence of magma such as the presence of volatile, overpressured fluids and perturbation of the stress field by igneous intrusions. These thermal and physical effects are thought to influence the development of structures during rifting, particularly leading to an important intrusion-related strain localisation (see Section 2.3).

Beside the thermal effects, other important simplifications of the current models concerns the rheological characteristics of the underplated material (see also Appendix B). Indeed, the material used to simulate magma is only five orders of magnitude less viscous than the lower crust, implying that, when scaled to nature, glycerol is only able to simulate a crystal-bearing magma ($\approx 10^{15}-10^{17}$ Pa s). In particular, the low viscosity required to properly reproduce the flow of natural magmas would allow a rapid flow along narrow dykes or fractures without transmitting stresses to the adjacent rocks sufficiently to strain and rupture them (e.g., Ramberg, 1971). Thus, this feature affects the mechanism of magma transfer within the crust because of the relatively high viscosity, allowing the glycerol to rise upwards mostly in a diapiric way rather than to penetrate the crust as narrow sills or dykes (e.g., Ramberg, 1971). This means that our models, mainly accounting for only one (i.e., diapirism) of the three main mechanisms which explain magma transfer into the continental crust (e.g., dyking, pervasive transport through shear zones and diapirism; Petford et al., 2000), simplify the complex modalities of the natural process under investigation.

Additionally, we did not include in our modelling the isostatic compensation provided by the asthenosphere. This involves that in some models, the Moho is depressed below the rift floor, whereas in nature, Moho rising associated with strong thinning of the lower crust is normally imaged by seismic profiles. Furthermore, not reproducing the asthenosphere also involves that we could not account for the increased thinning of the lower crust-induced uprising of the isotherms associated with the asthenospheric updoming.

On the other hand, because our investigations were exclusively focused on the mechanical interactions between deformation and the presence of a magmatic body introducing a rheological heterogeneity at the base or within the crust, we consider the current analogue simulations as still relevant despite the above-mentioned simplifications.

4.2.3. Magma emplacement during symmetric and asymmetric extension

The models of series Magm investigated the relationships between continental extension and evolution of magmatic chambers in case of symmetric and asymmetric extension (see also Bonini et al., 2001). During the experiments, extension was controlled in order to reproduce two different sets of models characterised by high and low extension rates (Type 1 and Type 2 models, respectively; see Appendix C; Table A3.1; Fig. 16a).

Experiments showed that faulting of the brittle crust and doming of the ductile crust are the primary response of the lithosphere to extension (Fig. 17). Ductile flow in the lower crust resulted in the thinning of the ductile layer and in the development of crustal-scale domes, corresponding to a graben structure at surface. Typically, magma was laterally extruded from its central position, emplacing beside the initial reservoir in correspondence to the domes' cores (Fig. 17). The pattern of surface deformation and lower crust doming mainly depends on

(1) the applied strain rate: reflecting the different brittle–ductile coupling (e.g., Brun and Tron, 1993), high strain rates results in a deformation distributed across the whole model. On the contrary, for low strain rates, surface deformation concentrated into discrete grabens, above lower crustal ductile dome(s) (Fig. 17);

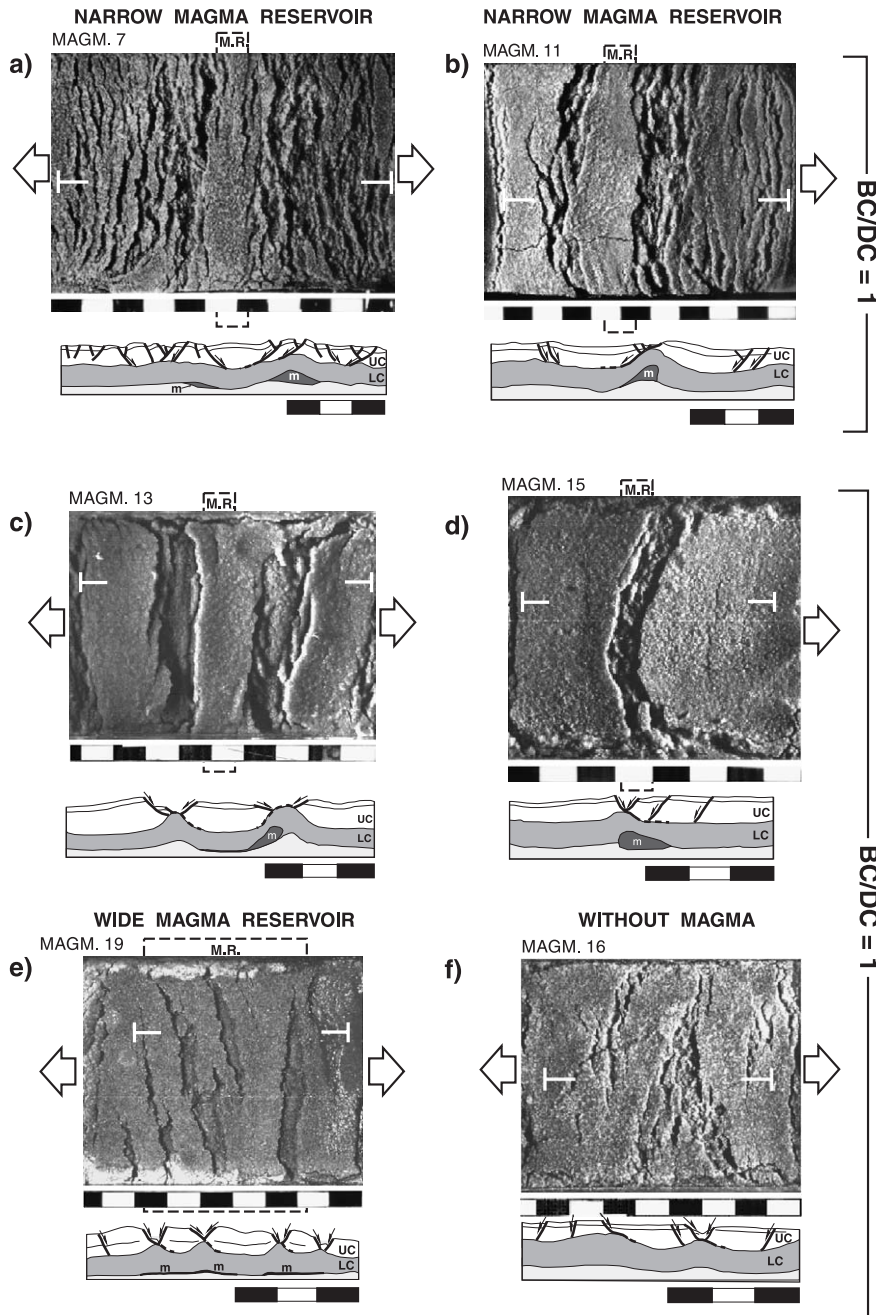(2) the geometry of extension (asymmetric vs. symmetric extension): the deformation localisa-

Fig. 17. Top view and cross-section of Type 1 (a–b) and Type 2 (c–m) models. The initial position of the magma reservoir (MR) and the symmetric or asymmetric mode of extension are indicated. The trace of the cross-section is indicated in white on the model top surface. The brittle–ductile thickness ratios refer to the initial model configurations. Note that although models are characterised by different amounts of bulk extension, deformation localised within dome regions since the first stages of extension; the amount of stretching influences the dome amplitude only. (a–f) from Bonini et al. (2001). The rulers are in centimeters.
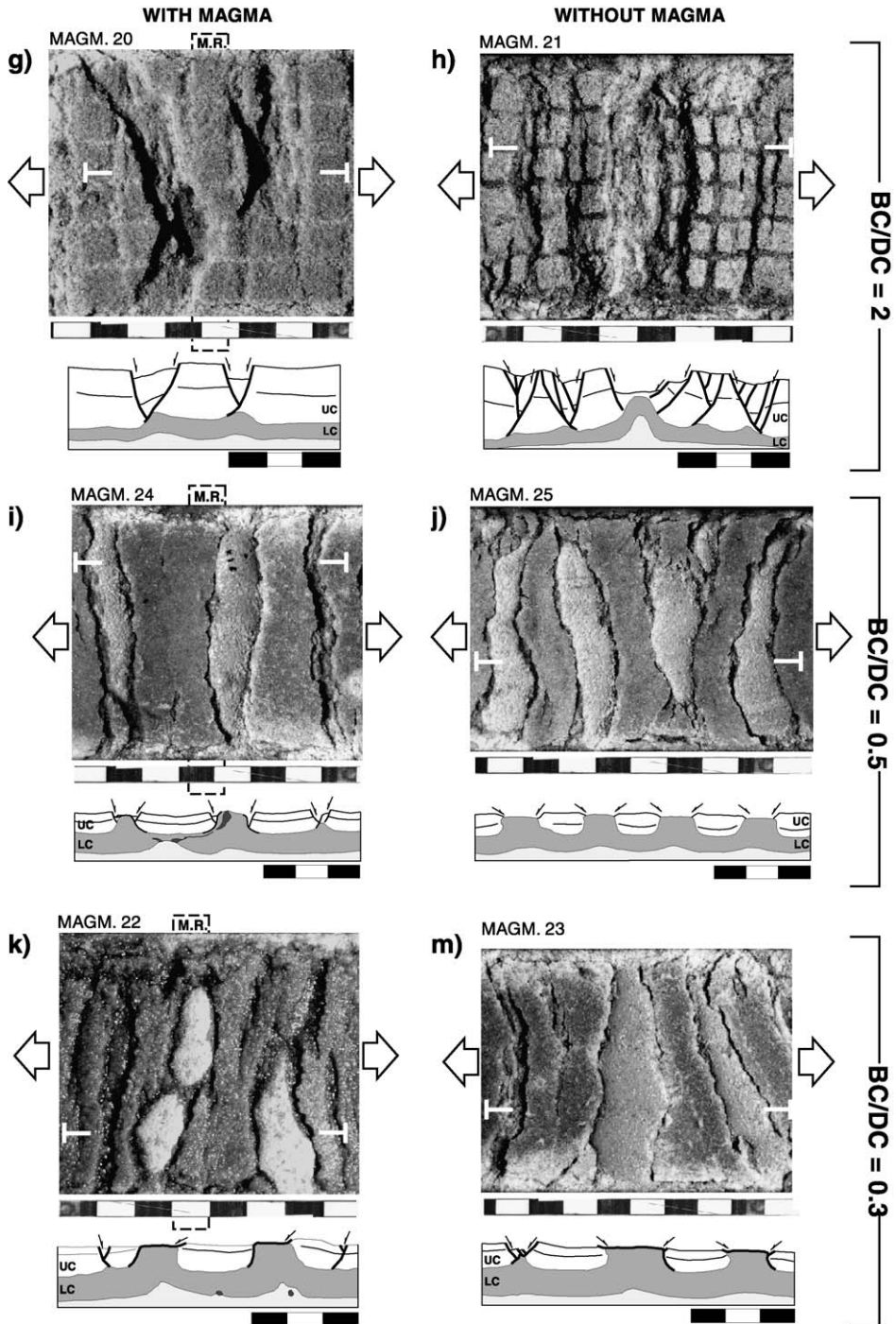
Fig. 17 (*continued*).

tion controlled by the strain rate was enhanced by the asymmetric mode of rifting;

(3) the relative thickness of brittle and ductile layers (Fig. 17g–m). High thickness of the upper crust (BC/DC = 2:1) promoted a more localised deformation in the brittle layer, coupled to a prominent and well-localised lower crust and mantle upraising (e.g., model Magm21; Fig. 17g and h). On the contrary, increasing the relative thickness of the lower crust (BC/DC = 1:2–1:3) resulted in a more diffused deformation; ductile doming played a major role in accommodating strain, and the upper crust was isolated between lower crust domes during the progressive deformation (Fig. 17i–m);

(4) the initial magma chamber geometry. Wide magma chambers (extending almost over the whole model) are able to distribute deformation, giving rise to several discrete grabens, corresponding to ductile domes at depth (Bonini et al., 2001). Con-

versely, narrow magma reservoirs localise deformation beside the chamber, favouring the development of two grabens corresponding at depth to two prominent domes.

Detailed analysis of model results suggests that the applied strain rate (see above point 1) has an important influence on the dynamic process of ductile dome development. Low strain rate (Type 2) models promote a relative thickening of ductile materials at the core regions (see the $1/\beta$ factor in Fig. 18b, where $1/\beta$ is the ratio between the final and the initial thickness of the model crust) that is also accompanied by magma intrusion of the lower crust (Fig. 18b). On the contrary, in high strain rate (Type 1) models, the ductile crust was thinned at the dome regions, but lateral squeezing of the underplated magma toward the dome(s) core (representing areas of relative low pressure) resulted in a relative thickening of viscous material (see the $1/\beta$
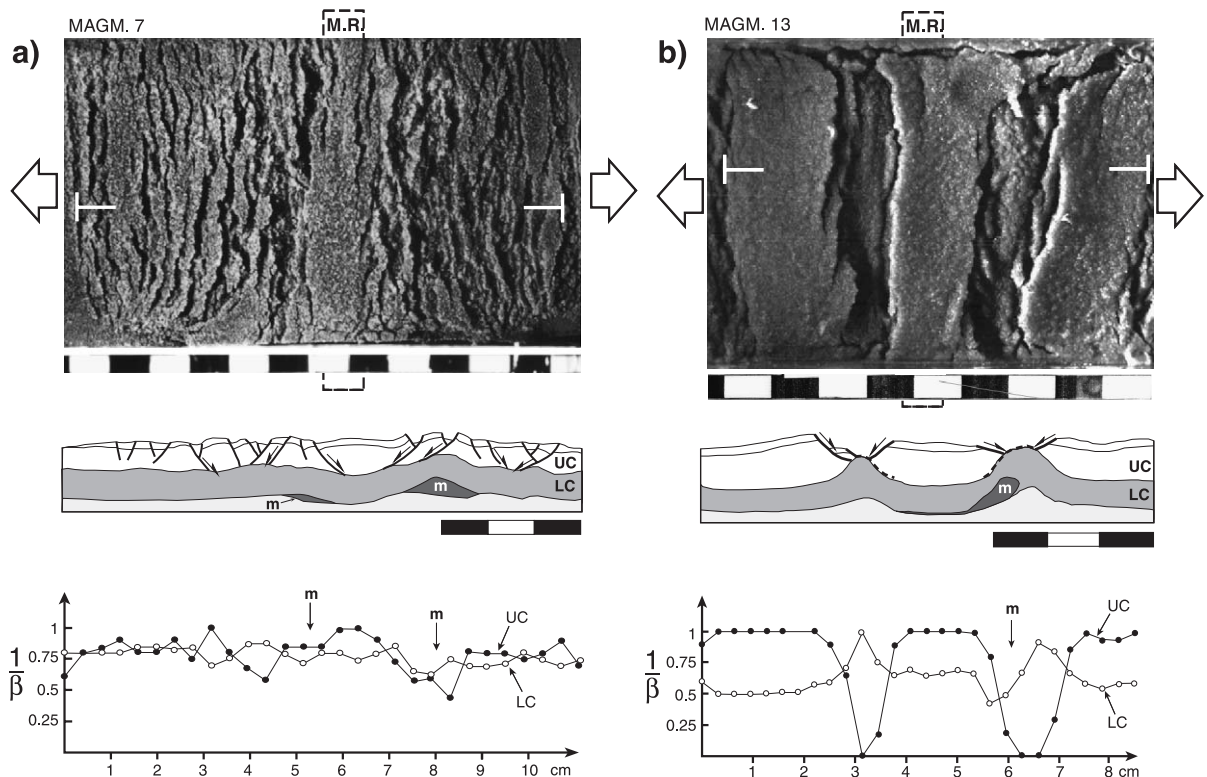

Fig. 18. Comparison of deformation style exhibited by Type 1 and Type 2 models using $1/\beta$ diagrams, showing the relative thickening or thinning of the brittle and ductile layers. See text for explanations. Symbols and abbreviations are as in Fig. 17; the rulers are in centimeters. After Bonini et al., 2001.

factor in Fig. 18a). Notably, in these models, magma always accumulated at the base of the (thinned) ductile crust (Fig. 18a).

The doming process was also controlled by the brittle/ductile crust thickness ratio and the geometry of magma at depth (above points 3 and 4), strongly influencing the development of regularly spaced domes in the lower crust and their characteristic wavelength. In model Magm19 (Fig. 17e), character-ised by a brittle/ductile thickness ratio of ≈ 1 and a wide magma chamber, regularly spaced domes resulted in a characteristic mean wavelength of ~ 16 mm (~ 32 km in nature), that is very similar to the λ_1 wavelength (of about 35 km) obtained by Benes and Davy (1996; see Section 3.3 and Fig. 8). Domes' wavelengths fit those reported for natural examples of extensional areas, like the Basin and Range Province (20–50 km with a mean value of about 30 km; e.g. Fletcher and Hallet, 1983). In models characterised by a higher thickness of the lower crust and no underplated magma (Fig. 17j and m), dome spacing was controlled by the different brittle/ductile thickness ratio resulting in a mean wavelength of ~ 23 mm for model Magm23 (BC/DC = 1:3) and ~ 32 mm for model Magm25 (BC/DC = 1:2). Narrow magma chamber models displayed instead two main domes, whose position appears to be controlled by the geometry of the initial reser-voir (e.g., Bonini et al., 2001). As a consequence, in models with low brittle/ductile crust thickness ratio (BC/DC = 1:2–1:3), a narrow magma chamber inhibits the development of regularly spaced domes (compare models Magm22 and Magm24 with cor-responding models Magm23 and Magm25; Fig. 17i–m). Notably, as reported in Benes and Davy (1996), in case of a high brittle/ductile thickness ratio, the tendency of the lower crust to develop domes is strongly reduced by the thick (and resistant) brittle layer. In model Magm 20 (Fig. 17g) two minor domes, characterised by a small amplitude, formed
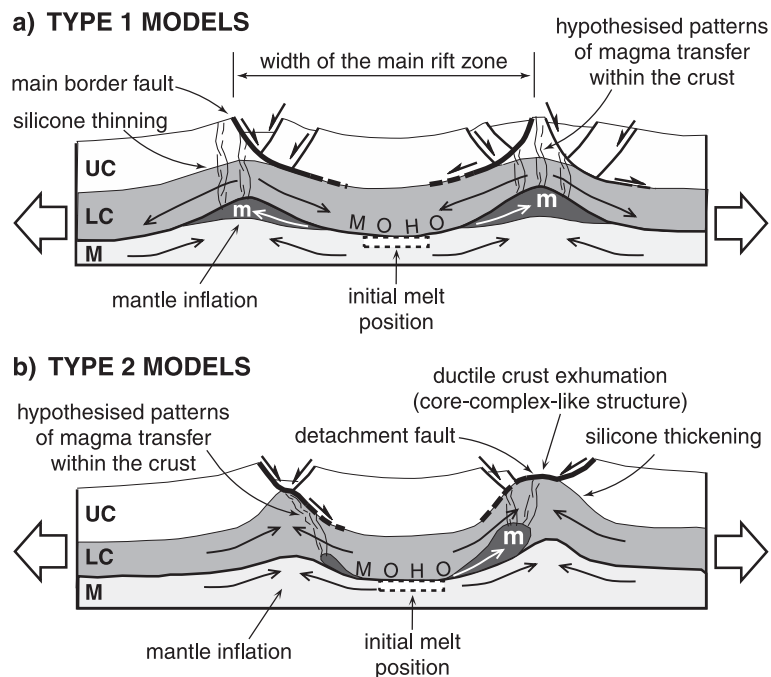

Fig. 19. Schematic diagrams showing the mechanism of lateral extension and dome formation observed in the centrifuge experiments. Arrows schematically indicate the ductile lateral flow trajectories inferred for the lower crust (LC), mantle (M) and underplated magma (m). After collection of magma at dome regions, the hypothesised patterns of magma uprising within the crust are schematically indicated. See text for details. After Bonini et al. (2001).

beside the initial reservoir, while in model Magm 21 (Fig. 17h), a major dome developed below the main central depression.

Results of orthogonal rifting experiments suggest that the main process driving the deformation models was the lateral flow of the magma and lower crust that

determined a relative thickening of viscous layers at the footwall of the major normal faults developed in the brittle crust (e.g., Buck, 1988; Figs. 19 and 20). This behaviour represents a typical response of viscous fluids, such as the ductile crust and the magma, to stretching of the continental crust: the driving forces
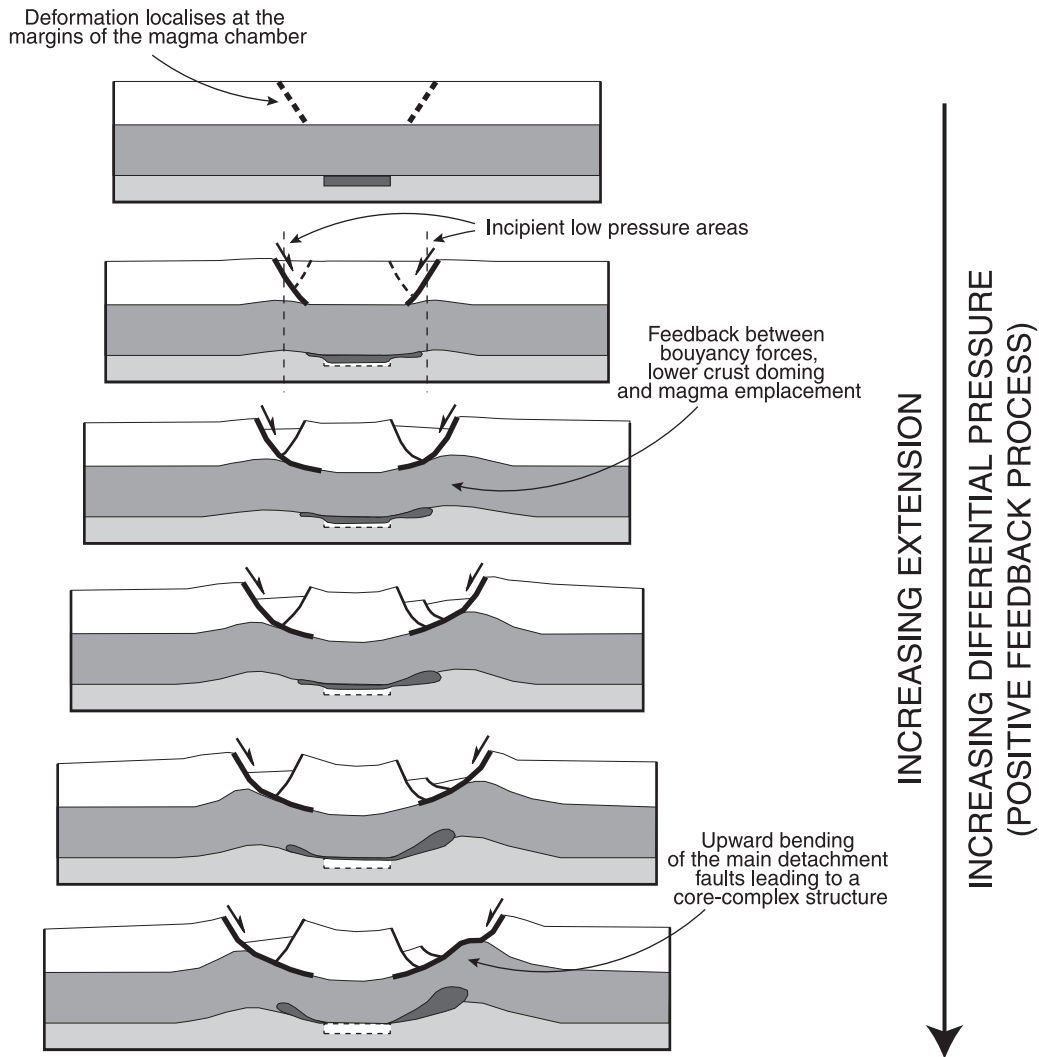

Fig. 20. Schematic cartoon showing the progressive development of core complex-like structures in models characterised by a brittle/ductile crust thickness ratio of ≈ 1:1 with a narrow magma reservoir (based on interpretation of model Magm13). At the onset of extension, deformation is localised beside the magma reservoir. With progressive extension, the crustal block above the reservoir sink and magma is laterally squeezed towards the lower crust domes. In these regions, movement on normal faults decreases the pressure acting on both the lower crust and the magma, enhancing the further collection of ductile materials at the domes. In this conditions, a feedback relation arises between buoyancy forces, lower crust doming and magma emplacement which causes further relative thickening and magma accumulation in the footwall of major normal faults. This evolution well accord with experiments by Brun et al. (1994), also in that low-angle detachment faults delimiting core complexes arise from a progressive uplift and rotation of initial planar normal faults.

for lower crustal and magma flow are the lateral pressure gradients created by a heterogeneously thinned upper crust (e.g., Block and Royden, 1990). Indeed, calculations of the pressure acting on the model at the end of deformation show low-pressure areas, located beside the initial reservoir, where ductile materials migrated, causing doming (Fig. 21). Notably, this process is similar to that observed in wax models of core complexes by Brune and Ellis (1997) and is also similar to results of sand–silicone models by Brun et al. (1994). This lateral flow of lower crust and magma driven by pressure gradients created during extension is also similar to the "reactive" diapirs model of Jackson and Vendeville (1994).

In this process (illustrated in Figs. 19 and 20), at the onset of deformation, the magma in the central narrow reservoir is laterally squeezed, and two major grabens formed at the boundaries of the magma chamber, such that deformation invariably localised beside the initial reservoir (Fig. 20). Notably, the inferred trajectories of lateral magma flow nearly parallel the extension direction. As extension proceeds, the pressure gradients created by faulting in the upper crust drive the migration of magma bodies toward the footwall of the major normal faults. This mechanism may be considered similar to the "exten-

sional footwall growth" model by Quirk et al. (1998), proposing that viscous fluid, such as magma or salt, preferentially migrate and collect in the low-stress zone in the normal fault footwall. This process may involve a feedback relation between extension, buoyancy stresses, thermal softening and melt accumulation, causing the further collection of large volumes of magma into the footwall. Further extension may lead to an upward bending of the main detachment fault, the outcrop of the lower crust and the development of core complex-like structures in case of a three-layer lithosphere (see Fig. 20 and Section 5.2). These results may be also applied to narrow continental rifts, where lateral flow of both lower crust and magma may induce the development of ductile domes below the border faults footwall, possibly enhancing flank uplift (e.g., Burov and Cloetingh, 1997). Very large amounts of bulk extension ($\beta > 2$) may increase doming in the lower crust, giving rise to core complex-like structures, such as those described in the Afar region (Talbot and Ghebreab, 1997; Ghebreab and Talbot, 2000). Notably, this process may provide a possible explanation for the accumulation of magma below the rift shoulders and the development of flank or off-axis volcanoes (see Section 5.2.1.1). Models suggest that magma uprising
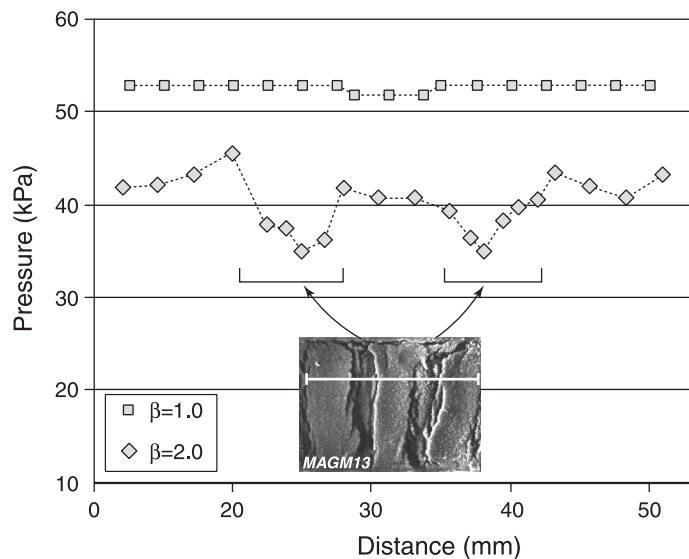

Fig. 21. Calculations of the pressure acting on the orthogonal rifting model Magm13 at the end of deformation. The white line on the model top view indicates the transect along which the pressure has been evaluated. Note the low-pressure areas corresponding to domes of ductile material in a lateral position with respect to the initial magma reservoir.

does not play an active role in dome development, as domes formed even in the absence of magma or when the magma was denser than the overlying crust

(Bonini et al., 2001). Thus, these results support the findings of Jackson and Vendeville (1994) and the results of Brune and Ellis (1997), in that extension
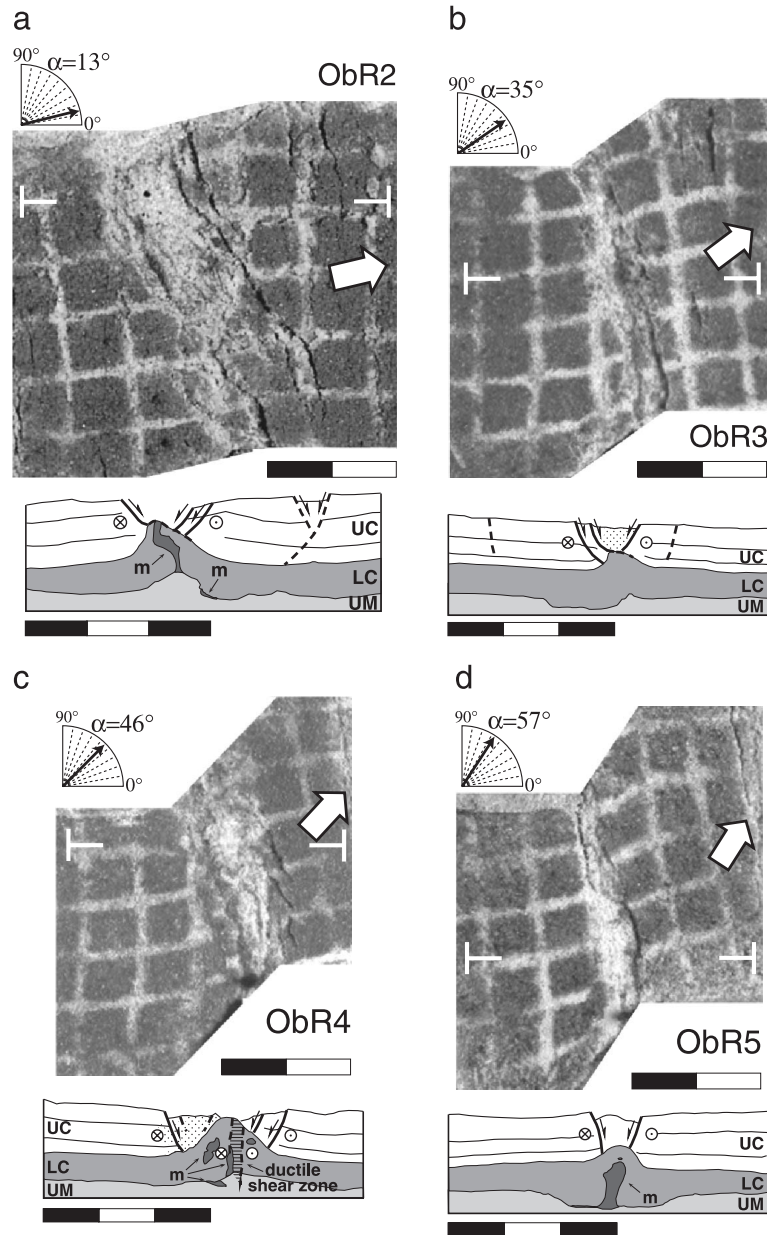

Fig. 22. Top view and cross-sections of oblique rifting models. The trace of the cross-section is indicated in white on the model top surface. In (e), model ObR9 (α = 0°, i.e., orthogonal extension), the central part of the model, bordered by normal fault systems with associated ductile doming, is interpreted as representing the main rift zone. Arrows on model top view point to the displacement vector direction; stippled patterns in cross-sections indicate magma intrusions in the model upper crust; m: magma; other symbols as in Fig. 17. The rulers are in centimeters. Modified after Corti et al. (2001).
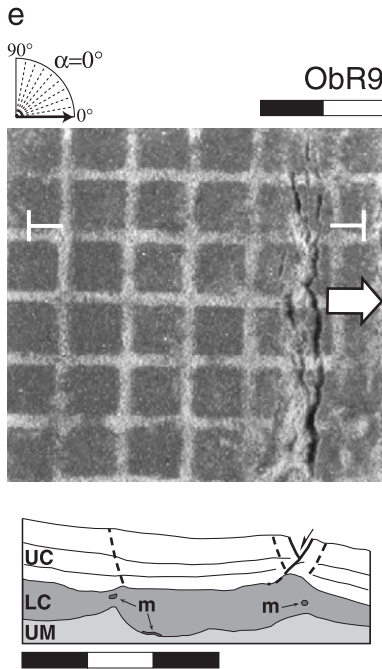
e

Fig. 22 (*continued*).

process, rather than density instability, controls emplacement of viscous diapirs.

4.2.4. Magma emplacement during oblique rifting

The experiments of the series ObR were designed to explore the effects of magma underplating the continental crust on the structural pattern resulting from oblique rifting, as well as the relationships between structural evolution and magma emplacement in the continental crust (Corti et al., 2001). In these experiments, extension was controlled in order to reproduce different angles of obliquity (from 0° to about 60°; see Table A3.2) with respect to a central velocity discontinuity (VD; see Appendix C; Fig. 16b). This VD that coincided with the axis of the underplated magma may represent an inherited structural trend in the uppermost lithospheric mantle (e.g., Tommasi and Vauchez, 2001; Fig. 16).

Experiments of the series ObR confirmed that the main characteristics of oblique rifting are represented by a deformation pattern characterised by en echelon fault patterns, with mean trends oblique to the extension vector, and strain partitioning between different sets of faults (e.g., Tron and Brun, 1991; see Section

3.4). Oblique extension resulted indeed in the development normal to oblique−slip en echelon faults bounding crustal-scale grabens which formed in the central area of the models (Corti et al., 2001; Fig. 22). Ductile domes typically corresponded at depth to these grabens.

Similarly to previous models, the angle of obliquity (α) controlling the ratio between the shearing and the orthogonal stretching components of deformation (e.g., Withjack and Jamison, 1986; Tron and Brun, 1991; Clifton et al., 2000; see also Section 3.4), strongly influenced the structural pattern of the models. For α ≤ 35°, deformation was diffused over a wide region, being partitioned between oblique−slip faults in the central area above the VD and dip−slip normal faults outside this area (Corti et al., 2001; Fig. 22a and b). Dip−slip faults were parallel to the VD, while oblique−slip faults were oblique to both the VD and the extension vector (Fig. 22a and b). Conversely, for α ≥ 45°, deformation was more concentrated, and no normal faults were observed outside the area above the central VD (Fig. 22c and d). Narrow grabens developed in the central region of the model, and the extensional strain was partitioned between normal to oblique−slip-bounding faults and external strike−slip faults (Fig. 22c and d). Both sets of faults were oblique to the VD and to the stretching vector. Notably, in accord with sand−silicone models by Tron and Brun (1991), the major change in surface fault pattern (and hence, in strain partitioning) occurred for obliquity angles in the range of 35−45° [note that in clay models by Withjack and Jamison (1986) and Clifton et al. (2000), this transition occurred for angles of about 45°−60°; see Corti et al., 2001].

Beside the angle of obliquity, the presence of the underplated magma had a major control on surface deformation. This latter, in turn, influenced the patterns of magma emplacement, thus highlighting an interplay between deformation and the presence of an underplated magma during oblique rifting (see also Román-Berdiel et al., 2000). On one side, the occurrence of magma at depth localised strain in the overlying crust, thus controlling the surface fault pattern; on the other side, deformation caused magma to emplace within the lower crust domes with an oblique and, in some cases, en echelon pattern (Corti et al., 2001). For low obliquity
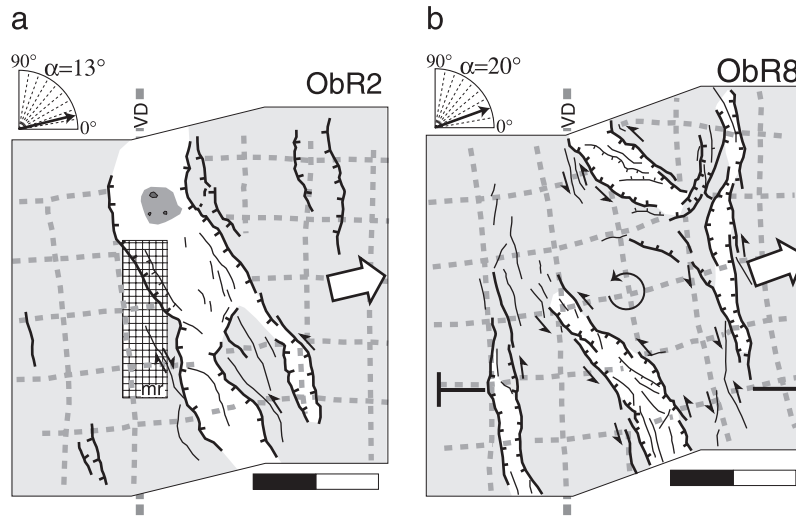
Fig. 23. Comparison of low-obliquity rifting models performed with (a) or without (b) underplated magma. Symbols as in Fig. 22. Modified after Corti et al. (2001).

angles, the presence of magma strongly controlled the surface fault pattern, leading to a strain localisation above the initial melt reservoir that repre-

sents a low-strength layer in the central part of the model (Fig. 23). These results are similar to analogue models by Román-Berdiel et al. (2000; see
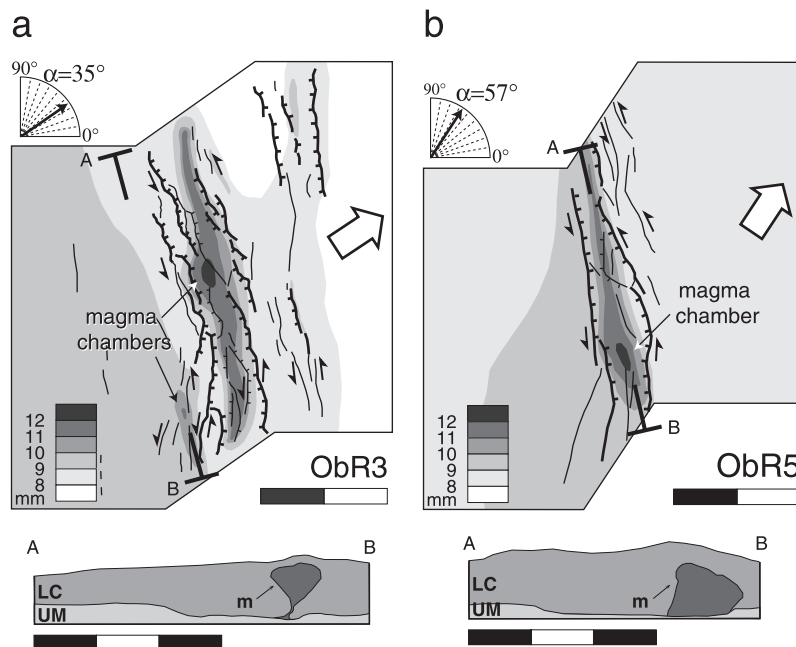

Fig. 24. 3D internal structure of models ObR3 and ObR5. In the models, the elevation of the top of the lower crust is reported, highlighting a marked ductile doming. The location of magma emplacement is indicated. Modified after Corti et al. (2001).

Section 4.1). The effect of this localisation is that deformation was mostly accommodated by central oblique–slip faults, thus reducing the strain partitioning and partly inhibiting the development of external normal faults. On the contrary, for $\alpha \geq 45°$, the presence of magma at depth had a low influence on the structural pattern, with a final fault distribution that was substantially similar in the two types of models.

On the other hand, deformation influenced magma emplacement, forcing intrusions to occur within the lower crust domes with a pattern that was mainly controlled by the rift kinematics (Fig. 24). In orthogonal rifting models, similarly to models of series Magm, magma emplacement occurred in the ductile domes which formed beside the initial magma reservoir, with a pattern that was parallel to the central VD (and orthogonal to the stretching vector; Fig. 22e). On the contrary, during oblique rifting, the combination of shearing and doming in the lower crust favoured an oblique,

and in some cases en echelon, magma emplacement pattern (e.g., model ObR3), which occurred above the initial magma reservoir and within the main rift zone (Fig. 24). In this case, pressure gradients forced the ductile material to flow toward the central part of the model (above the initial reservoir) where pressures were lower than the rift flanks (Fig. 25, compare with Fig. 21). Notably, the emplacement of magma at cores of lower crust domes resulted in a dome amplification that, in some cases, led to an absolute thickening of ductile materials below the main deformed zone (Fig. 26). Development of shear zones in the lower crust, accommodating the strike–slip component of displacement, determined the development of sheeted intrusions characterised by a high length/width ratio.

4.2.5. Magma emplacement during polyphase rifting

Deformation resulting from a polyphase extension has been investigated by the series PR experiments,
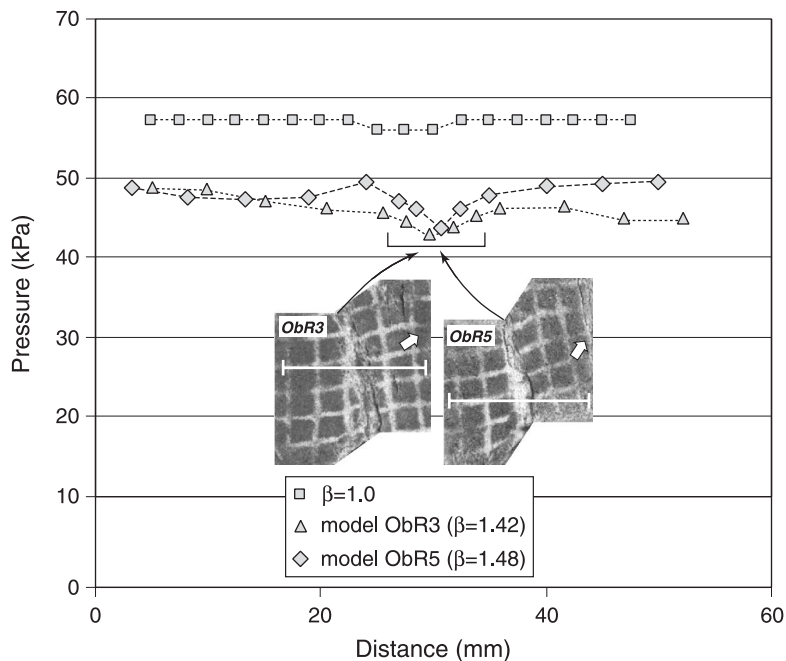

Fig. 25. Calculations of the pressure acting on oblique rifting models. The white lines on the model top views indicate the transect along which the pressure has been evaluated. Note the low-pressure areas corresponding to domes of ductile material in central part of the model, in correspondence to the initial magma reservoir.
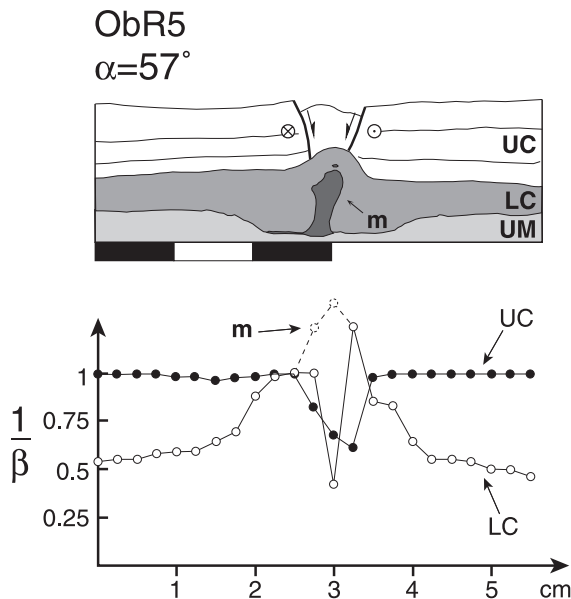
Fig. 26. $1/\beta$ values across model ObR5. Note the absolute thickening of the lower crust below the central graben as denoted by $1/\beta > 1$. Dashed line represents thickness of both lower crust and magma. The rulers are in centimeters. After Corti et al., 2001.

simulating a first phase of orthogonal rifting followed by a second phase of oblique rifting that considered both high and low obliquity angles (Corti et al., submitted to the *Journal of African Earth Sciences*, referred hereafter as Corti et al., submitted for publication; Appendix C; Table A3.3; see Fig. 16c for definition of the angle α).

In the first orthogonal rifting phase, extension resulted in the development of major VD-parallel normal faults that invariably formed above the moving half of the model. Similarly to previous experimental works (Bonini et al., 1997; Keep and McKlay, 1997; see Section 3.4), these orthogonal rifting-related structures strongly controlled the structural evolution during the second oblique stage, particularly forcing the successive faults to form within the preexisting graben borders (Fig. 27). During the oblique rifting phase, for low angle of obliquity ($\alpha \approx 15°$), the strike–slip component of the displacement was mainly accommodated by an oblique–slip reactivation of the preexisting normal faults (Fig. 27a). For a higher obliquity angle ($\alpha \approx 45°$), discrete en echelon strike–slip faults formed

within the main depression to accommodate the increased transcurrent component of movement along the rift axis (Fig. 27b). Thus, similarly to Bonini et al. (1997), the final fault pattern of the models was characterised by rift-parallel major border faults, delimiting a central rift depression containing oblique faults generated during the second stage of model deformation (Fig. 27).

In a similar fashion to models of the series ObR, analysis of lower crustal doming and magma emplacement in PR models suggest a strong interaction between deformation and the presence (and the re-mobilisation) of the underplated low-viscosity body. Particularly, two lower crustal dome trends (with associated magma chambers) were identified in the models: a major rift-parallel set beneath the border faults and a secondary, but well-defined, set that was typically confined within the rift depression following the trend of strike–slip faults (Fig. 28b). This second set of domes was characterised by an oblique pattern (to the rift margins) and an en echelon arrangement (Fig. 28b). Following this pattern of ductile doming, emplacement of magma occurred both below the rift shoulders (where the main accumulations were observed) and in correspondence to the central en echelon domes (e.g., model PR2; Fig. 28).

These results point to a first-order role played by the rift kinematics in controlling the pattern of magma intrusions: the two distinct structural positions of magma emplacement may indeed reflect the influence of the two successive rifting stages. Particularly, we suggest that as in the series Magm, during the orthogonal rifting phase, magma is squeezed laterally from the initial central position, migrating and accumulating at the footwall of major normal faults (off-axis emplacement; Fig. 29). On the other hand, as in the series ObR, magma emplacement during the successive oblique rifting phase is strongly influenced by the development of en echelon oblique faults and ductile domes, resulting in magma intrusions that typically occur within the main rift depression, with a trend oblique to the rift axis as well as to that of the initial reservoir and, in some cases, exhibiting an en echelon arrangement (Fig. 29).

4.2.6. Experiments on magmatism at transfer zones

Experiments of the series TrZn investigated the relations between deformation and the emplacement
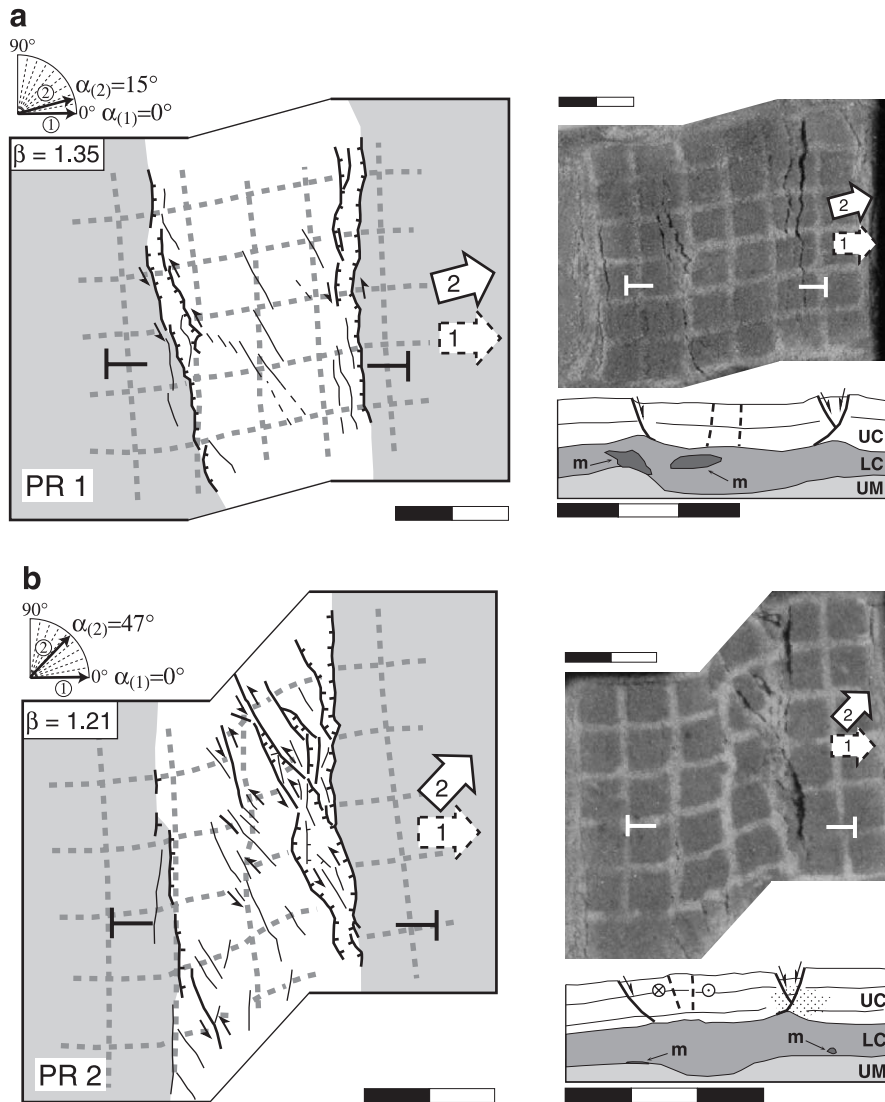
(after Corti et al., submitted)

Fig. 27. Final top view line drawings, top views and cross-sections of models PR1 and PR2. Symbols as in Figs. 17 and 22. Arrows indicate the extension direction during the two different phases. The rulers are in centimeters.

of magma within a developing transfer zone (Corti et al., 2002; Table A3.4; Fig. 16d). These models highlighted a very close interaction between deformation and magma transfer and emplacement during the development of a crustal-scale transfer zone: particularly, the magma distribution at depth effectively controls the strain distribution in the overlying crust, and strain distribution, in turn, controls magma

uprising and emplacement. This has been tested by comparing models characterised by different geometries of the initial magma reservoir (see Appendix C.1.3).

The experiments show that an initial wide magma reservoir, corresponding to an areally extensive underplating of magma, allowed the deformation to distribute across almost the whole model surface (Fig. 30a).
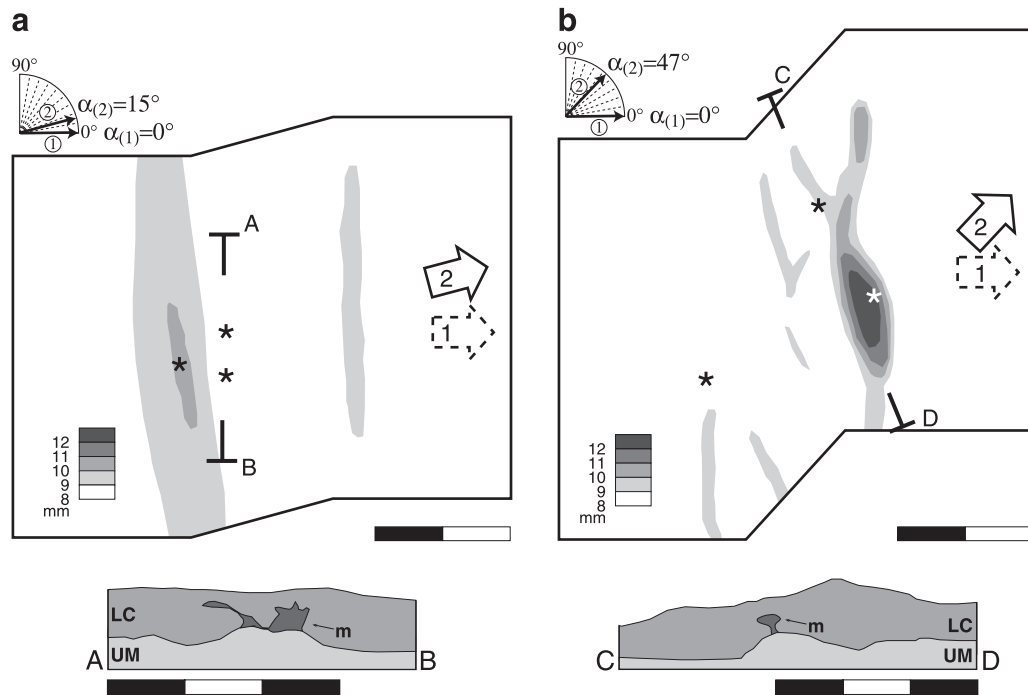
Fig. 28. 3D analysis of models PR1 (a) and PR2 (b) showing ductile doming and magma emplacement. Stars indicate the position of magma chambers. Symbols as in Figs. 17 and 22. The rulers are in centimeters.

This structural pattern corresponded at depth to a limited magma upwelling that produced local magma chambers in the lower crust beneath the faulted upper crust (Fig. 30b).

Conversely, a narrow magma reservoir was able to localise deformation into the overlying crust, giving rise to discrete transfer faults and depressions corresponding to pull-apart-like structures in the central part of the model (Fig. 30c). As seen for the previous orthogonal and oblique rifting models (see Sections 4.2.3 and 4.2.4), the development of the pull-apart structures in the upper crust decreased the pressure acting on the lower crust, favouring ductile doming and lateral magma transfer and accumulation. Particularly, magma tended to migrate in a direction orthogonal to the extension vector towards the central part of the model and collecting in correspondence to the transfer zone where a major magma chamber developed (Figs. 30d and 31). Notably, in the areas characterised by magma accumulation, the thermal softening of the country rocks may favour further deformation (e.g., Morley,

1999a,b), possibly leading to a positive feedback interaction between tectonics and magmatism (Corti et al., 2002), which has also been recognised in transpressional settings (e.g., Brown and Solar, 1998) as well as during post-orogenic collapse (McCaffrey et al., 1999).

Experiments of series NRTZ investigated the effect of inherited zones of weakness in the lower crust of narrow continental rifts on transfer zones development and magma migration and emplacement (Table A3.5; Fig. 16e). The model setup for this series has been designed starting from the observation that, in nature, rifts systematically reactivate ancient structures, and the geometry of these preexisting fabrics strongly influences the architecture of extensional structures, particularly, the fault pattern at transfer zones (e.g., Acocella et al., 1999a and references therein). To account for the presence of such anisotropies and to study their influence on deformation, we reproduced a rheological heterogeneity within the lower crust characterised by a lower viscosity (hence, a lower resistance) than surround-
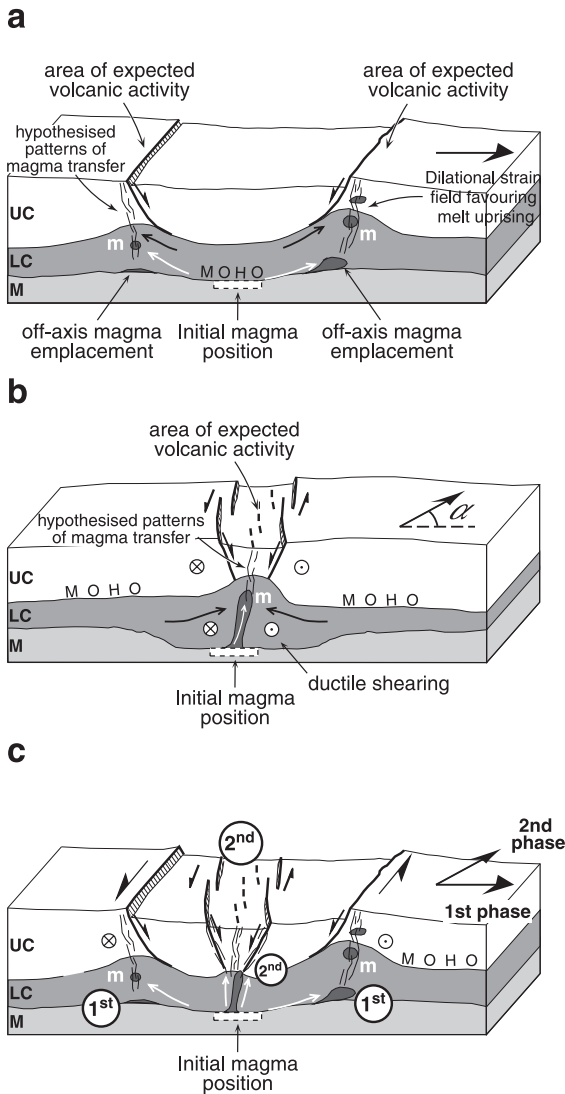
Fig. 29. Schematic cartoon showing the mechanism of magma emplacement during orthogonal or oblique rifting based on the modelling results. (a) Lateral squeezing and off-axis emplacement during orthogonal rifting. (b) Oblique magma emplacement along shear zones during oblique rifting (for α ∼ 45°). (c) Combined effect of a first phase of orthogonal rifting and a second phase of oblique rifting (polyphase rifting). Note the different patterns of magma emplacement and the resulting different spatial distribution of magmatic products resulting from the two successive rifting phases. Small arrows schematically indicate the lateral flow trajectories inferred for the lower crust and the underplated magma. The hypothesised patterns of magma uprising within the crust are schematically indicated.

ing regions (weak lower crust, WLC). This setup can be considered analogous to inherited weak zones within the lower crust, such as the Pan-African orogenic belts bounding the stable cratonic areas (e.g., Ebinger, 1989a; Morley, 1999f). It may also be considered as representative of an advanced rifting stage characterised by a localised thermal anomaly (such as those occurring in narrow rifts) that gives rise to a local heterogeneity in the lower crust rheology.

Since the rheological anisotropy localised strain in the brittle crust, we investigated different rift-segment interactions by varying the geometry of the WLC (Fig. 16d). Particularly, following Acocella et al. (1999a,b), we changed the overlap between the WLC offset segments to reproduce different angles (ϕ) between the direction of the rheological discontinuity in the transfer zone and the rift trend (see also Appendix C; Table A3.5; Fig. 16e).

Results of this experimental series highlight that model deformation was typically accommodated by development of narrow grabens that closely followed the rheological interface between the WLC and the ''strong'' lower crust. In all models, a detailed analysis of the model cross-sections reveals that these narrow grabens bounded a major topographic depressed area, corresponding at depth to a marked thinning of the WLC (see Figs. 32 and 33). Similarly to previous analogue works (Acocella et al., 1999a), the surface fault pattern and the arrangement of rift segments were primarily controlled by the geometry of the weak zone in the lower crust (in particular, the angle ϕ; see also Section 3.5; Fig. 32). For low ϕ values (e.g., model NRTZ7, $\phi = 25°$; Figs. 32a and 33a), a single rift depression characterised the central part of the model, whereas for high ϕ values (model NRTZ5, $\phi = 90°$; Figs. 32c and 33b), the surface deformation was characterised by two offset rift segments. For intermediate ϕ values (model NRTZ6, $\phi = 45°$; Fig. 32b), the surface fault pattern was more complex, and deformation was accommodated by a larger number of fault sets, with faults' throw and grabens' width less pronounced than in model NRTZ5 (compare final top views of Fig. 32b and c). The transfer zone connecting the offset rift segments were characterised by oblique fault segments, with opposite trend to that of the weak lower crust step (Fig. 32);
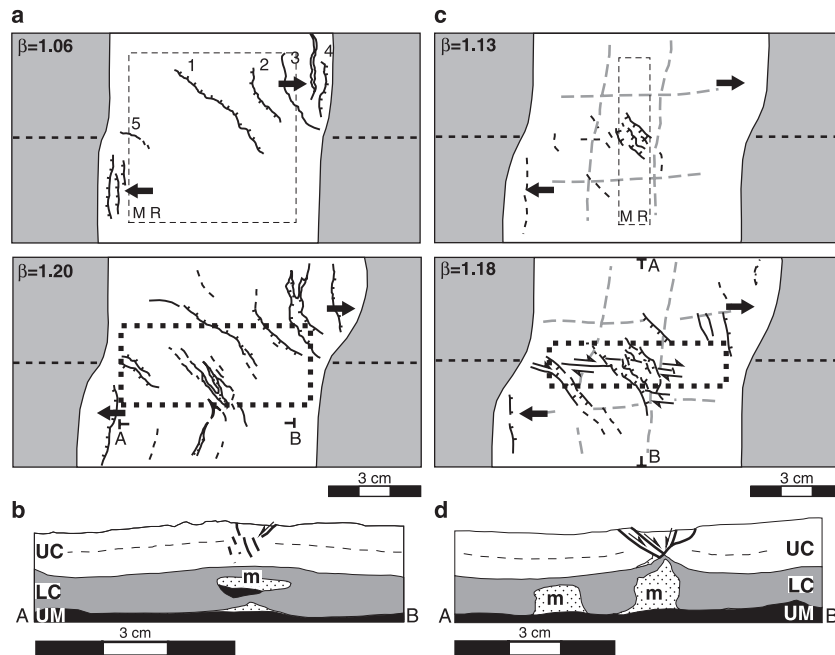
Fig. 30. Cartoon showing the sequential deformation and cross-section of models TrZn2 (a–b) and TrZn3 (c–d). The initial position of the magma reservoir is indicated. Numbers indicate the progressive development of faults. UC: upper crust (sand); LC: lower crust (sand–silicone mixture); UM: upper mantle (high-density sand–silicone mixture); m: magma (glycerol); MR: initial magma reservoir. Grey dashed lines represent the passive grid markers. Dashed rectangular boxes indicate the inferred location of the transfer zones. After Corti et al. (2002).

curvature of normal faults has been observed in previous models of transfer zones and has been interpreted in terms of a rotation in the stress field (e.g., Acocella et al., 1999a).

Similar to experiments discussed in the previous sections, evolution of models NRTZ is characterised by an interaction between deformation and magma emplacement. On one side, the influence of magma on the structural pattern is clearly illustrated by the comparison of the final surface fault patterns of models NRTZ6 (with magma) and NRTZ1 (without magma; Fig. 34). This comparison shows a marked localisation of deformation in the presence of an underplated magma. Particularly, in model NRTZ1 (Fig. 34b), the transfer zone is composed of a major fault set linking the two alternated grabens and forming a rather low angle to the extension direction ($\approx 37°$). Conversely, in the model NRTZ6, the correspondent oblique set is unable to connect with the grabens because it was forced to follow the

trend of the underplated magma, thus resulting in a fault pattern displaying a higher angle to the direction of extension ($\approx 67°$; Fig. 34b). Additionally, the grabens developing beside the initial magma reservoir were considerably much more developed in length than the correspondent grabens in the model NRTZ1, presumably reflecting the effect of the lateral squeezing of magma in a process which is similar to that characterising the series Magm experiments.

On the other side, the structural pattern (that is, in turn, controlled by the angle ϕ) strongly influences the modality of magma transfer and accumulation. In particular, two end-member patterns of magma emplacement were recognised depending on the WLC geometry (Fig. 35). In model NRTZ8 (characterised by $\phi = 0°$ and no transfer zone development), magma was laterally transferred toward the main depression margins, resulting in rift-parallel accumulations below the normal fault
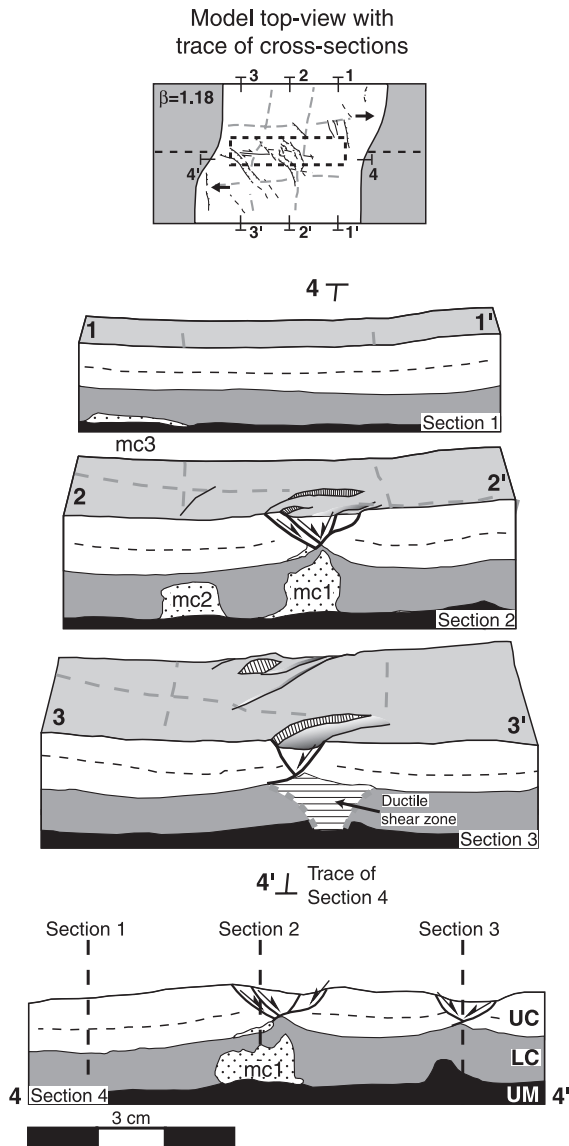
Model top-view with
trace of cross-sections

Fig. 31. Transversal and longitudinal cross-sections highlighting the 3D internal structure of model TrZn3. Traces of cross-sections are reported in a model top view. mc: magmatic chambers; other abbreviations as in Fig. 30. After Corti et al. (2002).

footwall, with a pattern that is substantially similar to those displayed by series Magm models, as well as to that of model ObR9 (Fig. 35b). Notably, in this process, subhorizontal major magma chambers were isolated below the rift depression, whereas minor volumes of magma accumulated below the

footwall of boundary faults (Fig. 35b). Conversely, in model NRTZ5 (characterised by $\phi = 90°$), almost the whole underplated magma collected at the core of a prominent lower crust dome, in correspondence to the central transfer zone connecting the two offset rift segments (Fig. 35a).

The experimental results of both series TrZn and NRTZ point to a very similar process, involving strain localisation and lateral pressure gradients, which may account for the accumulation of magma at transfer zones. In particular, we suggest that this process, leading to the observed pattern of ductile doming and magma accumulation, may evolve as follows:

(1) due to the presence of both magma and the weak lower crust, deformation in the upper crust is localised within the transfer zone, particularly above the initial reservoir;

(2) as a consequence to faulting in the upper crust, pressure acting on ductile materials decreases in the transfer zone; since the transfer zone-related faults cross-cut the rift, the so-created pressure differences acts also in a direction that is perpendicular to the extension direction;

(3) the pressure gradients drive a ductile flow towards the transfer zone, causing doming; following this process, magma is transferred laterally in a direction that is perpendicular to the extension direction (i.e., towards the central part of the model). This process may involve a positive feedback interaction: accumulation of the less-dense magma, indeed, further decrease the pressure in the transfer zone, thus possibly enhancing doming and magma emplacement.

5. Discussion and comparison with natural examples

In the previous sections, we have outlined the main parameters, derived from both numerical and analogue modelling, controlling the basic modes of continental extension. We have then focused on the importance of underplated magma and magmatic processes on continental deformation using centrifuge modelling. The current analogue experiments demonstrated that the emplacement of large magmatic bodies at various levels within the lithosphere
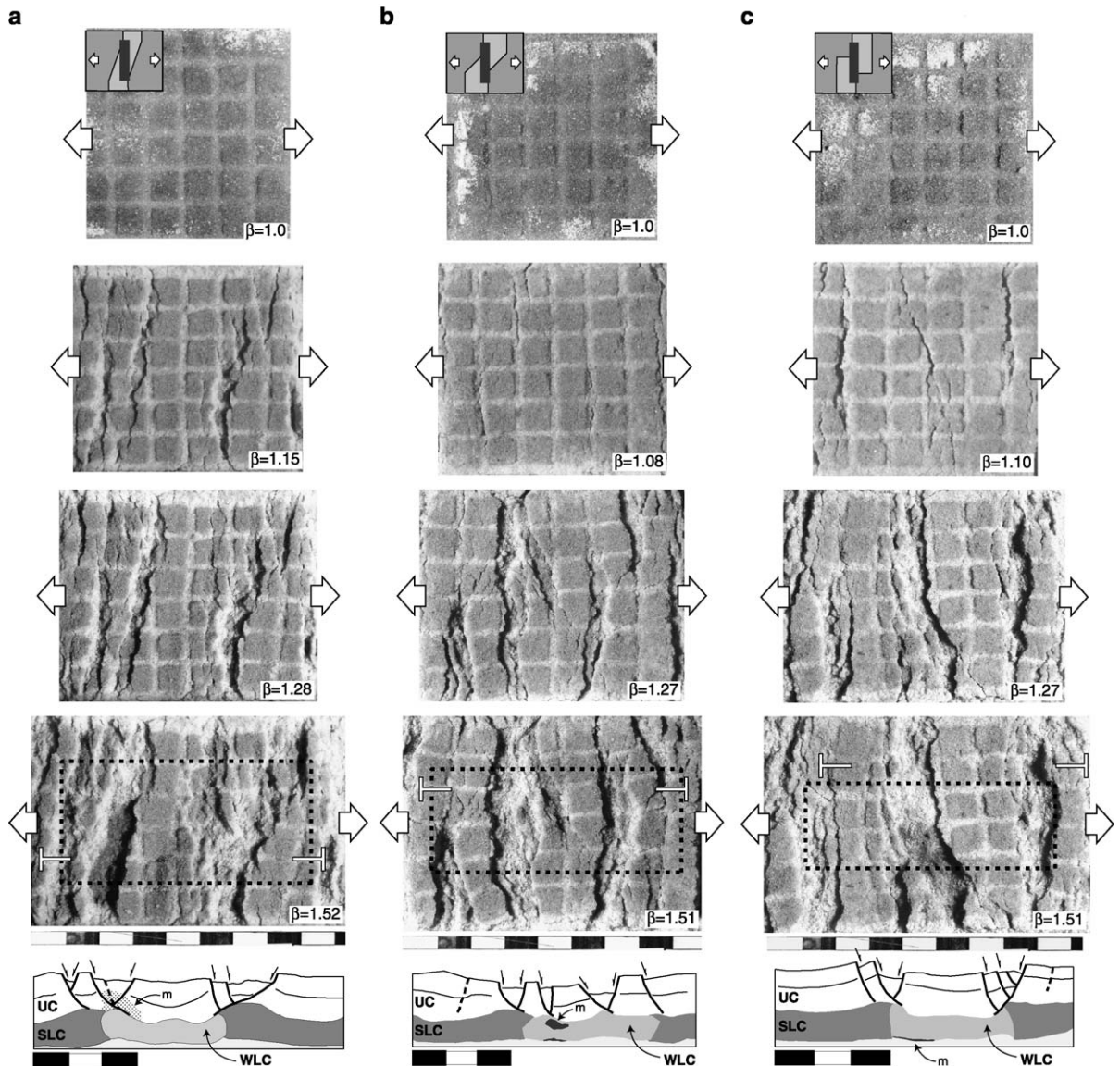
Fig. 32. Top views showing the progressive evolution of models NRTZ7 (a), NRTZ6 (b) and NRTZ5 (c). These three models were characterised by a different geometry of the weak lower crust (i.e., a different geometry of the region connecting the two offset rifts). Longitudinal cross-sections are also reported for each model. SLC: strong lower crust; WLC: weak lower crust. Other symbols as in Figs. 17 and 22. The dashed rectangular boxes represent the transfer zone between the two offset rift segments. The rules are in centimeters.

represents indeed an important parameter in controlling the tectonic evolution, which has not received considerable attention in the past.

In the following sections, we firstly integrate the results of the current modelling results with those in the literature to examine the role played by the un-

derplated magma in influencing the mode of continental extension. We then compare analogue models with natural examples of regions undergoing extension and we propose a model for the development of off-axis (or flank) volcanism in continental rifts. Finally, we present an integrated model for the tec-

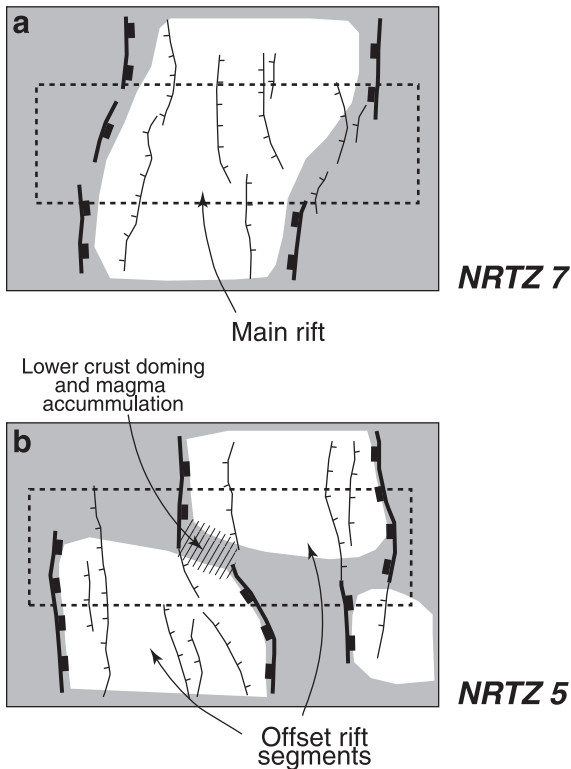Fig. 33. Interpretation of surface deformation for models with $\phi = 25°$ (a) and $\phi = 90°$ (b). Note the development of a single depression in (a) that can be interpreted as a the main rift zone. Conversely, two offset rifts develop in (b) separated by a transfer zone characterised by curved normal faults, prominent ductile doming and magma accumulation.

tono-magmatic evolution of the Main Ethiopian Rift, which represents a clear example of the application of analogue modelling results to the understanding of the relations between deformation and magmatism during continental extension.

5.1. Implications of current models for the mode of continental extension

Integration of current models with previous experiments may offer insights into the classification of the different modes of continental extension also accounting for the role of an underplated magma in controlling the distribution of surface deformation.

All the different studies have shown that the strength of the lithosphere represents one of the main parameters controlling the mode of extension. Other parameters, however, play a significant role in controlling the transition between the different styles of continental extension. These parameters are summarised in Fig. 36 and discussed below in relation to the resistance of the continental lithosphere.

5.1.1. High lithospheric strength

There is a general agreement between the different studies in highlighting that high upper crust thickness or a four-layer lithosphere characterised by a brittle upper mantle favours a narrow rifting mode of extension. This confirms that the increase of the lithosphere strength, which dominates during the extension process over gravitational forces, favours a concentrated deformation (Benes and Davy, 1996; Brun, 1999). However, the presence of magma has a significant influence on the spatial distribution of deformation (Fig. 36). Current experiments suggest that two grabens form beside the reservoir when the magma is present at depth, indicating that the presence of an underplated magma may represent an additional factor, together with the strain rate (Michon and Merle, 2000), in controlling the number of surface grabens. Additionally, in the case of a four-layer lithosphere, experiments by Callot et al. (2001, 2002) suggested that magmatic bodies strongly influence the mode of deformation when they are localised within the brittle upper mantle. In this situation, the lithospheric strength is strongly reduced, causing a strain localisation above the low-viscosity body; in terms of surface deformation, this leads to a strong narrowing of the deformed zone.

A reduction of the lithospheric strength increases the importance of ductile flow, resulting in a wider deformed zone where extension can be accommodated through wide rifting or core complex modes. However, different studies have shown that transition between these two extensional mechanisms may be controlled by some parameters, such as the brittle/ductile thickness ratio (investigated in the current experiments), the viscosity of the lower crust that can be interpreted in terms of thermal gradient (Benes and Davy, 1996), the presence of magmatic bodies introducing rheological heterogeneities (Brun et al., 1994; Brun, 1999; current experiments; Fig. 36) and the strain rate (see below).

5.1.2. Low lithospheric strength

For low resistance of the continental lithosphere (brittle/ductile thickness ratio of ~1:1), the wide
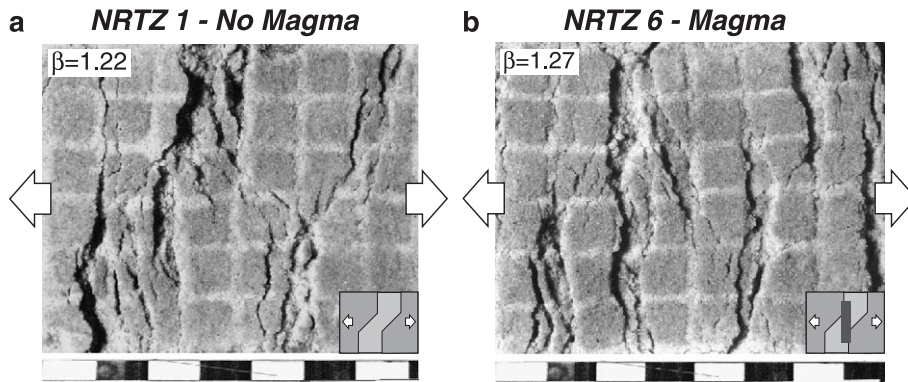
Fig. 34. Comparison between models performed with magma (a) and models without an initial magma reservoir (b). The rulers are in centimeters. See text for details.

rifting mode of extension is expected (Benes and Davy, 1996; Fig. 36). However, there are at least two parameters that may be able to promote a transition from wide rifting to core complex mode: the presence of magmatic bodies and the viscosity of the lower crust (Fig. 36).

5.1.2.1. Presence of magmatic bodies. Our three-layer Magm experiments suggest that the magma is able to localise or distribute deformation depending on its geometry at depth (Fig. 17). In case of both extensive and limited (narrow) underplating, the presence of the low-viscosity body favours a core complex-like extensional style, with deformation concentrated in few zones within which exhumation of the lower crust in the domes' regions occurs (see also Benes and Davy, 1996). Particularly, diffused deformation occurs in the presence of a wide magma reservoir decoupling the lower crust from the mantle; this deformation is accommodated by the development
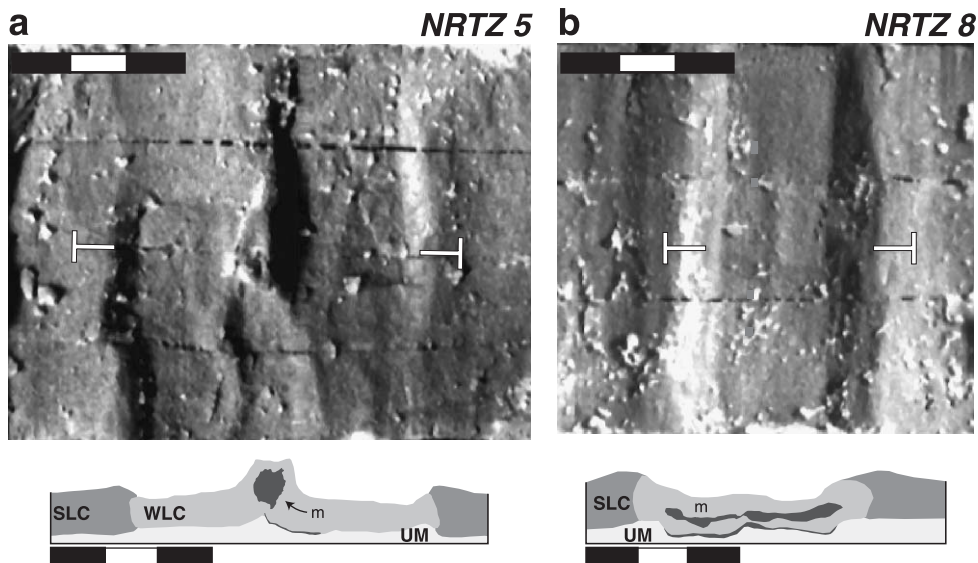
Fig. 35. End-member patterns of magma emplacement recognised in the experiments as dependence on the geometry of the weak lower crust. (a) Accumulation of magma within the transfer zone in model NRTZ5 with $\phi = 90°$. (b) Lateral transfer and off-axis emplacement of magma in model NTRZ8 with $\phi = 0°$. The rulers are in centimeters.
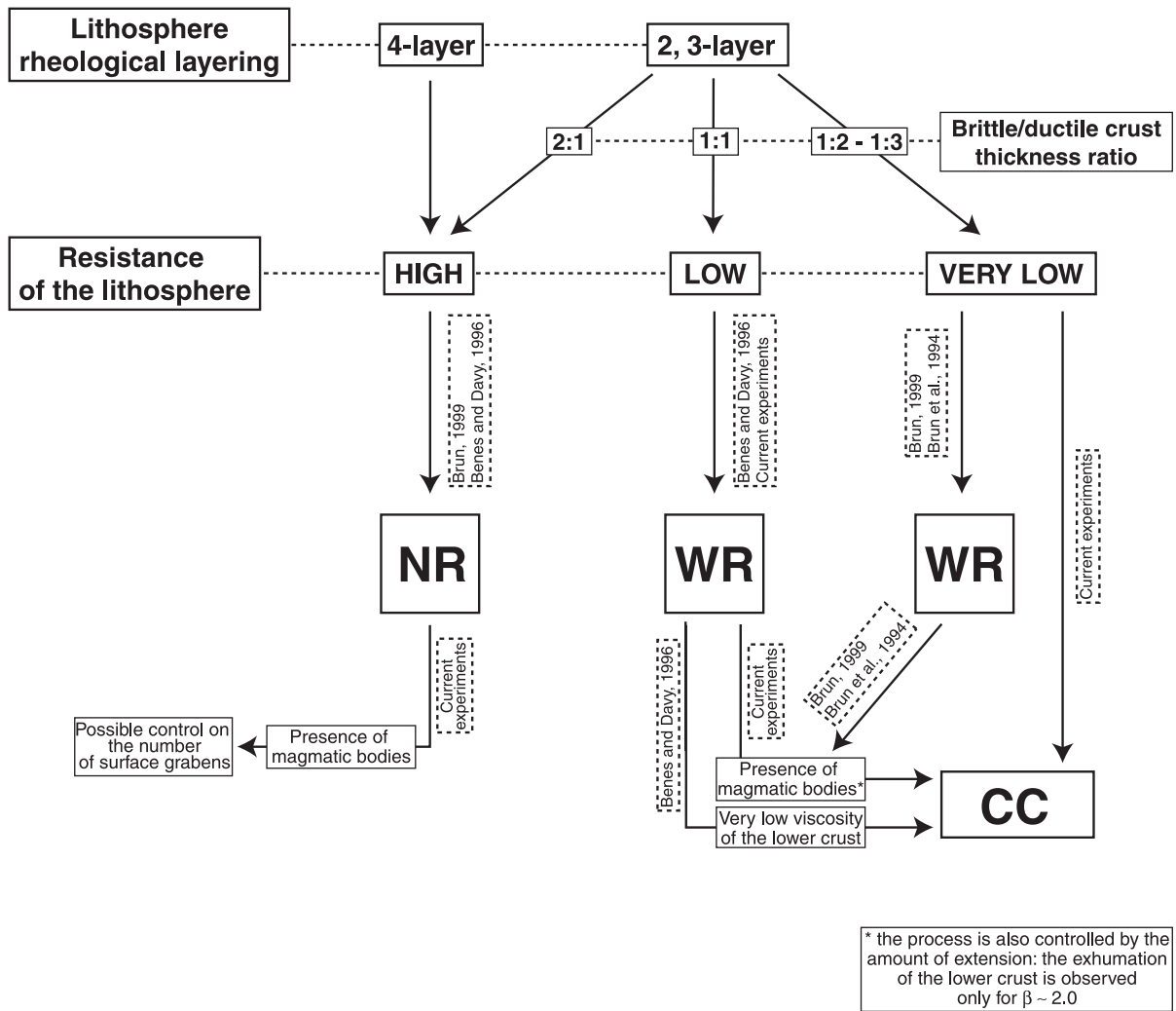
Fig. 36. Block diagram showing the main parameters (for a given strain rate) controlling the transitions between the different modes of extension. NR: narrow rifting mode; WR: wide rifting mode; CC: core complex mode of extension.

of regularly spaced ductile domes (Fig. 17e). Conversely, limited (narrow) underplating localises deformation beside the initial reservoir, giving rise to prominent core complex-like structures (Figs. 17c and 20). The influence of a localised rheological heterogeneity in favouring the core complex mode of extension is clearly exemplified by high strain rate (Type 1) series Magm models (Fig. 37). In these models, the lower crust was upwarped beside the initial reservoir by two domes that we interpret as core complex-like structures; away from the domes region, high-angle normal faults accommodated the deformation in the
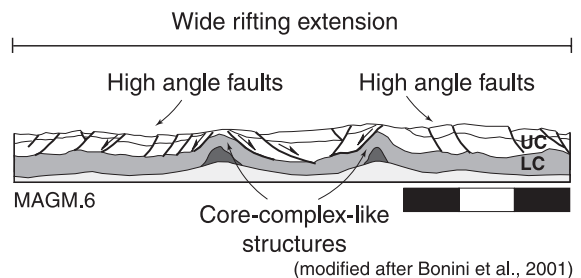
Fig. 37. Magma-induced strain localisation triggers core complex formation beside the initial reservoir, superimposed on a Basin and Range-like high-angle normal faulting.
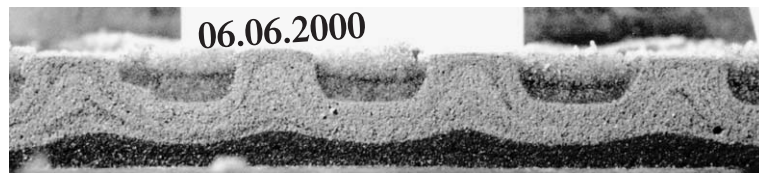
Fig. 38. Regularly spaced symmetric doming and core complex-like style of extension in model Magm25.

upper crust in a Basin and Range-like style of extension. This also suggests that core complex formation and wide rifting style of faulting may coexist together during high strain rate extension in the presence of a localised magmatic body, as suggested for some regions undergoing wide extension (e.g., Gulf of Corinth; Chéry, 2001).

5.1.2.2. Ductile crust viscosity. Warm lithospheres, characterised by a low viscosity of the lower crust, favour the transition from the wide rifting to core complex mode of extension (Benes and Davy, 1996).

5.1.3. Very low lithospheric strength

Centrifuge experiments of the series Magm suggest that a further decrease in the brittle/ductile crust thickness ratios (with values on the order of $\approx 1:2-1:3$) favours the dominance of ductile flow on the extension process, promoting a core complex-like mode of extension (Benes and Davy, 1996; Figs. 17i–m and 38). In this case, at the onset of extension, the deformation is distributed over the whole model surface, but soon, it became localised within narrow depressions intruded by the lower crust resulting in regularly spaced symmetric domes (Fig. 38; see also Benes

Table 2
Summary of experimental results and natural examples

Rift kinematics	Orthogonal extension	Oblique extension	Polyphase extension (first orthogonal–second oblique)
Structural pattern	Extension-orthogonal normal faults and grabens	Oblique and en echelon faults; strain partitioning between pure normal and oblique–slip structures. Deformation strongly controlled by the angle of obliquity and by the presence of magma	Extension-orthogonal normal faults and grabens in the orthogonal phase. In the oblique phase, the transcurrent component is accommodated by reactivation of the master faults (for low obliquity) or by newly formed oblique faults (for high obliquity)
Pattern of magma emplacement	Rift-parallel accumulation toward the rift shoulders and below the footwall of major normal faults (off-axis emplacement)	Rift-oblique (possibly en echelon) arrangement of magmatic bodies. Accumulation occurs within the main rift depression in correspondence to oblique en echelon faults	Transition from orthogonal extension-related off-axis emplacement to oblique en echelon emplacement
Natural examples	Spatial and temporal association of magmatism and deformation in core complexes: • Basin and Range region of the USA Off-axis volcanism in continental rifts • Main Ethiopian Rift • Kenya Rift • Red Sea • Limagne graben in the Cenozoic European Rift system	Oblique en echelon fault and volcanic belts: • Quaternary Wonji Fault Belt in the Main Ethiopian Rift • Reykjanes, Mohns and Gulf of Aden ridges	Two-phase evolution. Off-axis development during the first phase; oblique (and en echelon) volcanic and fault belts within the rift during the second phase: • Plio-Quaternary tectonomagmatic evolution of the Main Ethiopian Rift

and Davy, 1996). Notably, ductile domes developed independently from the presence of magma, which only influenced domes spacing (see Section 4.2.3). However, gravity spreading experiments by Brun et al. (1994) suggest different conclusions, showing that in case of a two-layer lithosphere with a thick lower crust (as occurs in the processes of post-orogenic collapse), the brittle upper crust is pervasively faulted and characterised by the development of tilted blocks in a wide rifting mode of extension (see also Brun, 1999). In agreement with experiments of the series Magm, the presence of a local rheological heterogeneity (i.e., partially molten bodies) is able to influence the mode of deformation, favouring strain localisation and the transition from wide rifting to core complex of modes of extension (Brun et al., 1994; Brun, 1999).

The above considerations, as well as the drawing of Fig. 36, are mainly based on experimental results not taking into account the influence of the applied strain rate. However, this parameter controls the coupling between brittle and ductile layers and is able to localise or distribute surface deformation and thus to exert an important influence on the mode of extension (see also Brun, 1999). For a given brittle/ductile thickness ratio ($\sim$ 1:1), an increase in strain rate favours a diffused deformation consisting of tilted blocks similar to highly extended areas, such as the Basin and Range (i.e., a WR mode of extension; Figs. 17a, b and 37). In this case, as stated above, the presence of a narrow magma reservoir may trigger the formation of core complex-like structures beside the initial chamber (Fig. 37). Conversely, experiments deformed with a relatively low strain rate (Type 2 models) promoted localised deformation, enhancing ductile doming and lower crust exhumation (Bonini et al., 2001).

We also note that the geometry of extension is able to influence the extension process: particularly, asymmetric extension favoured a narrowing of the deformed region, giving rise to discrete rifts (see model Magm15; Fig. 17d). In addition, the geometry of ductile domes displayed a dependence upon the geometry of extension: in case of symmetric extension, ductile domes exhibited a rather symmetric geometry, while an asymmetric extension promoted more asymmetric ductile domes (Fig. 17).

The above analysis, based on the results of analogue modelling studies, is in agreement with Buck's

(1991) modes of extension, since the initial conditions play a major role in controlling the mode of deformation. In experiments, the style of extension was mainly controlled (for a given strain rate) by the lithospheric rheology, in terms of proportion of brittle and ductile layering, viscosity, presence of magmatic bodies that can be considered in nature a function of the heat flow, crustal age and crustal thickness (see also Brune and Ellis, 1997). Modelling results suggest that old, thick and cold crusts are expected to yield narrow rifts, consistent with the observations in the East African, northern Red Sea and Baikal rifts (e.g., Fadaie and Ranalli, 1990; Buck, 1991; Ruppel, 1995; Prodehl et al., 1997). Conversely, younger, thinner and warmer lithospheres undergoing extension are expected to give wider extensional zones, where core complex-like structures may also develop. This is consistent with observations from the Aegean Sea and Basin and Range regions (e.g., Buck, 1991; Sokoutis et al., 1993; Jackson, 1994; Parsons, 1995; Ruppel, 1995; Gautier et al., 1999 and reference therein).

Finally, we stress here that core complex-like deformation, characterised by lateral flow and associated doming of the lower crust, represented a major process accommodating the extension of the models.
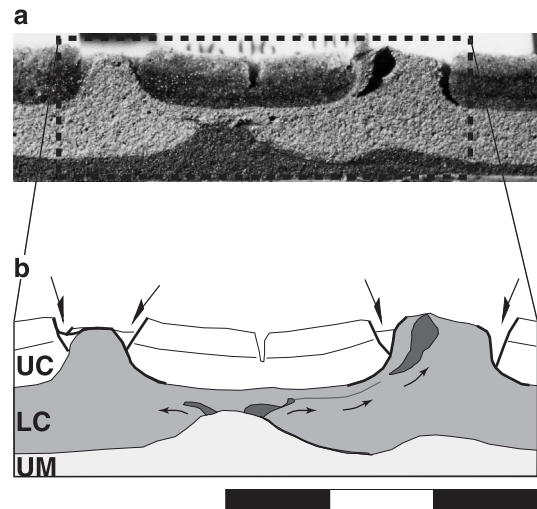
Fig. 39. Lateral magma transfer and emplacement at core regions during core complex development in model Magm24: (a) photo of the model cross-section and (b) line drawing. The small arrows in (b) schematically indicate the trajectories of magma transfer towards the cores of lower crust domes.
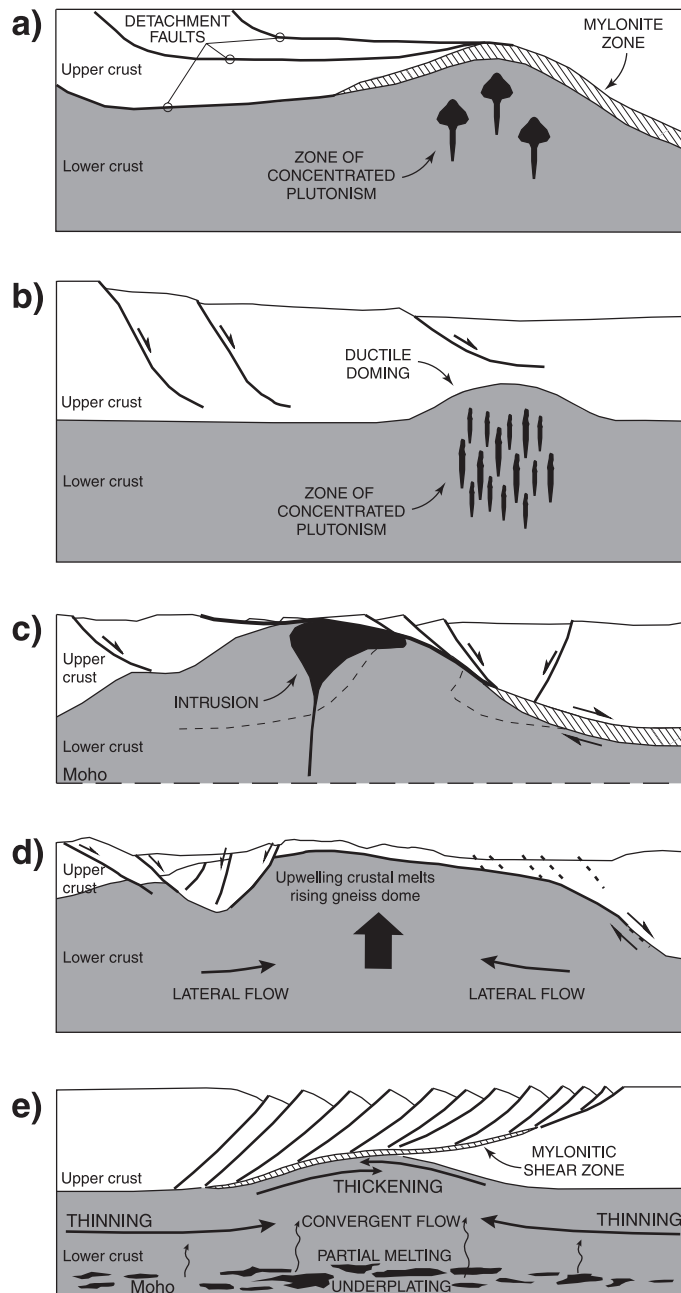
Fig. 40. Cartoon showing typical characteristics of core complex structures evidenced in the Basin and Range and the Aegean region, such as (a–c) ductile doming and accumulation of magma at the domes' core (redrawn after Lister and Baldwin, 1993; Parsons and Thompson, 1993; Gautier et al., 1993) and (d–e) the convergent lateral flow and thickening in the ductile domes' regions (redrawn after MacCready et al., 1997; Miller et al., 1999). Note that these characteristics are consistent with the experimental results.

We have noted above that this may be due to the chosen boundary conditions, in particular, the high thermal gradient preventing the presence of a brittle upper mantle and thus, the development of necking processes within this layer (Buck, 1991; Brun, 1999). The introduction of a mechanical VD at the base of the ductile upper mantle favoured, indeed, a narrow rifting-like deformation (e.g., models ObR9, PR1 and PR2; see Sections 4.2.4 and 4.2.5). However, the importance of lower crust flow is also highlighted in narrow rifting models (BC/DC = 2:1) showing lateral flow and ductile doming in the footwall of major normal faults. It is also interesting to note that although the connection between doming and magmatism was firstly evidenced in the classical post-orogenic core complex models (e.g. Coney, 1980; Crittenden et al., 1980; Lister and Davis, 1989; King and Ellis, 1990; Lister and Baldwin, 1993; Brun et al., 1994), recently, core complex-like structures have also been recognised in other extensional settings, such as the East African Rift System (e.g. Talbot and Ghebreab, 1997; Morley, 1999d; Ghebreab and Talbot, 2000) and even in oceanic crust (Blackman et al., 1998; Ranero and Reston, 1999). The above considerations raise the possibility that different extensional settings, which depend on the initial conditions of the system, may reflect a basically similar extension process in which lateral flow of viscous layers plays a major role (Bonini et al., 2001).

5.2. Natural examples

In the following sections we discuss the comparison of the experimental results with natural examples, taking into account both (1) the observed structural pattern and (2) the spatial distribution of magmatic products (see also Table 2).

5.2.1. Orthogonal extension
As evidenced in Section 4.2.3, series Magm models are characterised by a lateral squeezing of magma that tends to emplace in correspondence to the domes' core forming in the lower crust. This evolution is exemplified by the trajectories of magma transfer in Fig. 39, showing a subhorizontal lateral migration of magma from the axial zone and a rising into the domes' core below the main detachment fault, giving rise to a significant emplacement of igneous bodies.

We suggest that the pattern of deformation and magma emplacement displayed by series Magm models may account for the widespread magmatism localised in an external position (on the footwall) to the listric faults bounding the zones of localised uplift, such as the ductile domes characteristically associated with core complex structures (e.g., King and Ellis, 1990; Gautier et al., 1993; Lister and Baldwin, 1993; Parsons and Thompson, 1993; Brun and Van Den Driessche, 1994; Quirk et al., 1998; Gautier et al., 1999). Indeed, the magma in the models moves predominantly toward the dome cores where the exhumation of the lower crust occurs and the magmatic activity would manifest (compare the patterns of magma uprising within the crust in Fig. 39 with those in Fig. 40a and b). This lateral transfer of magma is driven by the lateral flow of the ductile lower crust, similarly to the flow trajectories converging towards the relatively thickened domes' regions hypothesized for the core complexes in the Basin and Range (Block and Royden, 1990; MacCready et al., 1997; Chéry, 2001; Fig. 40c and d). Notably, models characterised by low brittle/ductile thickness ratio (BC/DC = 1:2 – 1:3) were characterised by an immediate upraise of the
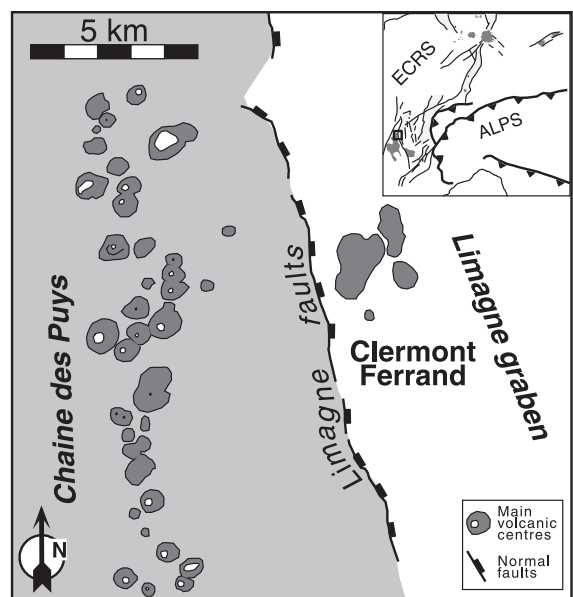

Fig. 41. Main volcanic centres in the Chaine des Puys (Massif Central, France). Note the off-axis positions of the volcanoes that grew on the footwall of the Limagne faults in an external position to the Limagne graben. ECRS: European Cenozoic Rift System.

underplated magma, with extrusion occurring even for low amount of bulk extension ($\beta \approx 1.25$). This evolution may account for the strong adiabatic decompression hypothesised for natural core complex structures on the basis of closely spaced isograds resulting in an anomalously high apparent thermal gradient (e.g., Brun and Van Den Driessche, 1994; Brun et al., 1994).

When a narrow rifting style of deformation occurs (e.g., models Magm20–21, ObR9, PR1, PR2, NRTZ5), magma is transferred laterally towards the rift shoulders, below which it accumulates (see Section 4.2.3). This pattern of magma transfer and emplacement may offer a model for the development of the so-called off-axis or flank volcanoes (see the following section).

5.2.1.1. The off-axis volcanism. Flank (or off-axis) volcanism refers to the emplacement of magmas and development of volcanism in an external position to the rift depression in continental rifts (e.g., Bosworth, 1987; Ellis and King, 1991). Flank volcanism is a typical feature of many regions undergoing extension, such as the East African Rift System (EARS), the Red Sea, the Basin and Range and the European Cenozoic Rift System (e.g., Bosworth, 1987; Ellis and King, 1991). In this latter rift system, well-preserved volcanic edifices characterise the Chaine des Puys in the Massif Central; these volcanoes developed on the footwall of the Limagne faults bordering the western margin of the Limagne graben (Ellis and King, 1991; Michon and Merle, 2001; Fig. 41). In the EARS, flank volcanism has been recognised in both the Kenya Rift
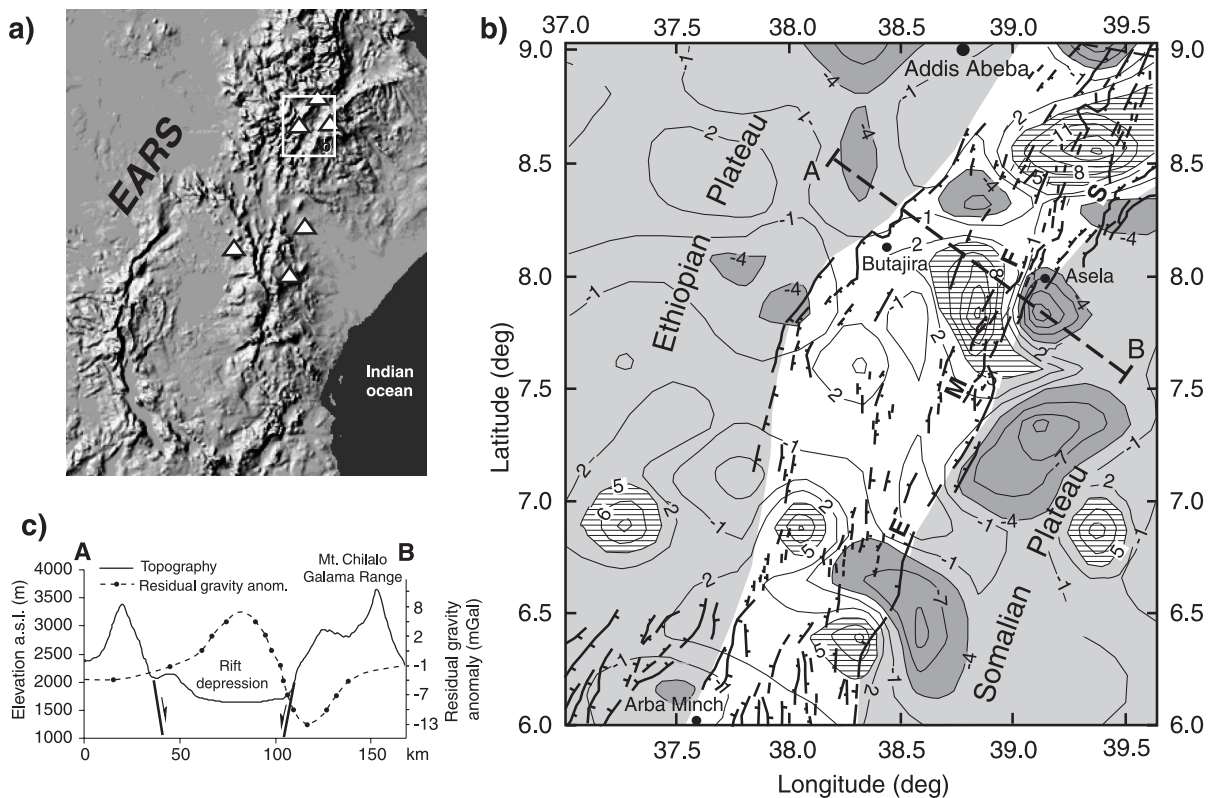
Fig. 42. (a) Digital elevation model of the East African Rift System with the main off-axis volcanoes (triangles). (b) Simplified MER fault pattern (modified after Boccaletti et al., 1998) superposed onto the residual anomaly gravity map (after Mahatsente et al., 1999). Negative anomalies lower than −4 mGal and positive anomaly larger than +5 mGal are indicated in dark grey and horizontal hutching, respectively; in light grey are indicated the plateau flanking the rift depression (in white). (c) Residual gravity anomalies (after Mahatsente et al., 1999) and topographic profiles crossing the rift and the shield volcanoes on the uplifted Somalian Plateau (location in b).
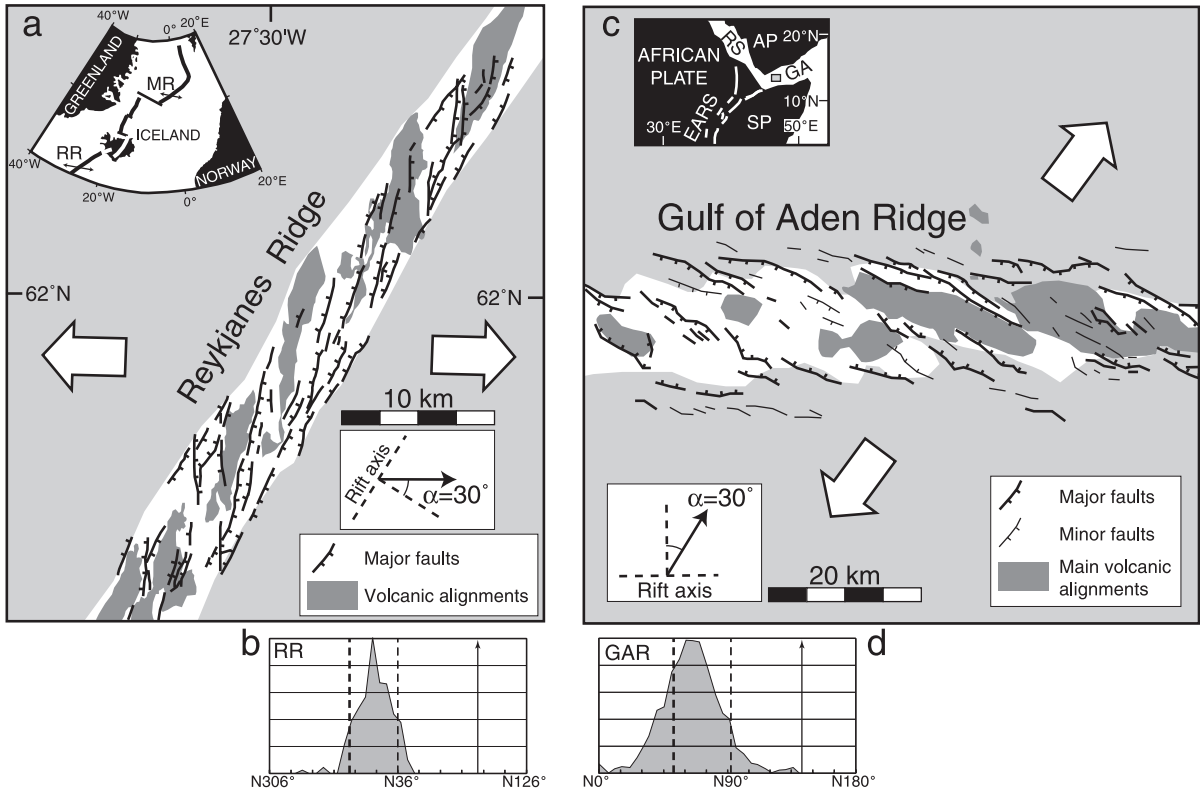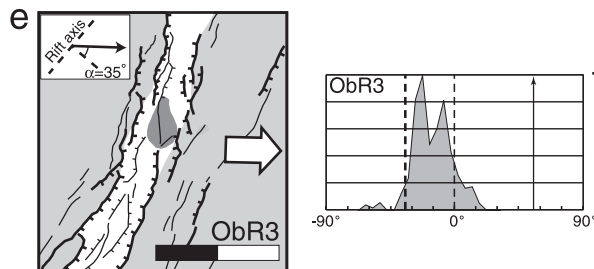
Fig. 43. Comparison of oblique rifting model results with the fault and volcanic patterns in the Reykjanes, Gulf of Aden and Mohns Ridges (RR, GAR and MR, respectively). (a) Structural pattern in the RR (after Murton and Parson, 1993). Note the oblique en echelon arrangement of the volcanic alignments. Inset shows the location of the MR and RR in the North Atlantic Ocean; thick lines represent the Mid-Atlantic Ridge, whereas lines with arrows indicate the spreading direction. (b) Histogram of fault distribution for the RR (after Murton and Parson, 1993). (c) Structural pattern in the GAR (after Dauteuil et al., 2001). Inset shows the location of the GAR; AP: Arabian Plate, EARS: East African Rift System, GA: Gulf of Aden, RS: Red Sea, SP: Somalian Plate. (d) Histogram of fault distribution for the GAR (after Dauteuil et al., 2001). Note that the fault pattern distribution of the dextral oblique-spreading GAR has been mirrored to match the analogue modelling performed with a sinistral oblique rifting kinematics. (e) Final top view line drawing of model ObR3 and (f) correspondent histogram of fault distribution (after Corti et al., 2001). (g) Structural pattern in the MR and (h) correspondent histogram of fault distribution (after Dauteuil and Brun, 1996). (i) Top view line drawing of model ObR4 and (m) histogram of fault distribution (after Corti et al., 2001). Note the coincidence between major and minor peaks in the fault distribution histograms of models (f, m) and the three natural examples (b, d and h).
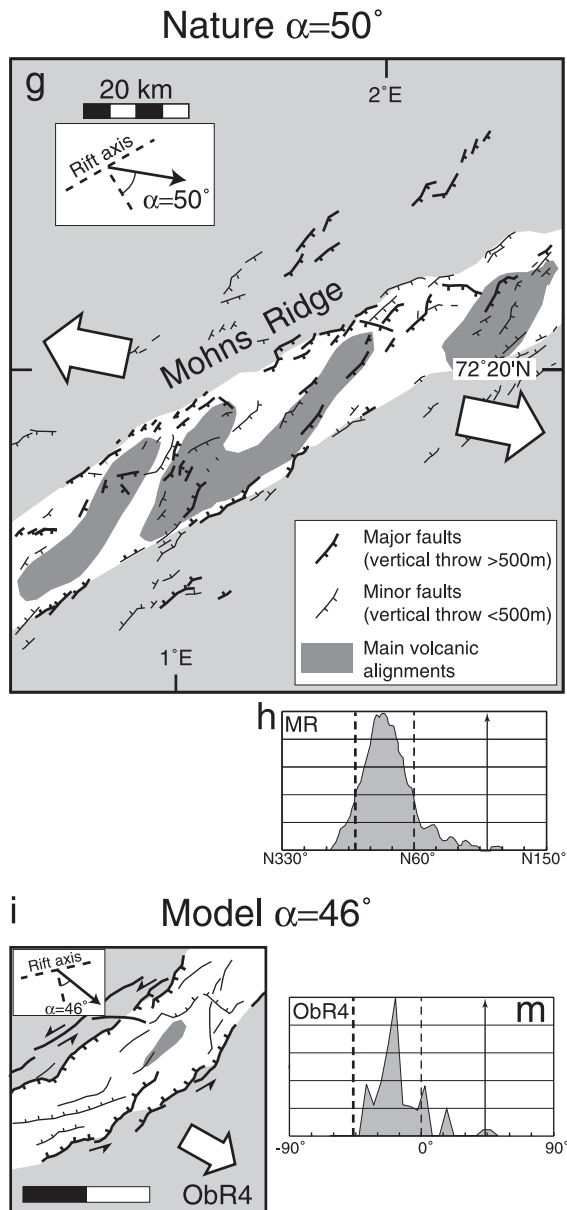
Nature α=50°

Model α=46°

Fig. 43 (*continued*).

Previous studies have explained the development of flank volcanoes in the Kenya rift as due to the interaction of extensional detachment faults with the asthenosphere (Bosworth, 1987). In the MER, flank volcanoes have been related to various mechanisms, such as (1) reactivation of a Precambrian structural weakness zone (Mohr and Potter, 1976), (2) reactivation of old boundary faults in case of a riftward migration of the rift margins (WoldeGabriel et al., 1999), (3) the outward flow of basaltic melts from magma chambers below the subsiding rift (Kazmin et al., 1980). An important model for flank volcanism development was presented by Ellis and King (1991). These authors proposed that during extension, a dilatational strain field develops in the footwall of normal faults. Provided a major magma source at the base of the crust, the presence of such strain field may favour a strong magma uprising that may feed flank volcanoes. However, their model requires a magma source be present at the base of the crust in order to develop the off-axis volcanoes. Applying the lessons of the modelling, we suggest that the formation of important magmatic reservoirs feeding flank volcanism is related to the lateral migration of an initially underplated magma, accompanying the lateral flow and doming of the ductile crust (Bonini et al., 2001). In this process, which is substantially similar to that proposed by Kazmin et al. (1980), major magma reservoirs may form into the footwall of developing major boundary faults (off-axis emplacement), providing the melt source required by the Ellis and King's (1991) model. The hypothesis that such voluminous volcanic products are associated with magmatic chambers below the rift shoulders is also supported by residual gravity anomaly maps obtained through 3D modelling of gravity data in the Main Ethiopian Rift (Mahatsente et al., 1999; Fig. 42). These data outline the occurrence of important relative minimum anomalies coinciding with the volcanoes on the Somalian Plateau, a fact that we consider as indicative of magma still localised below these volcanic centres (Fig. 42). Outward lateral flow and doming of ductile crust as well as magma emplacement below the rift shoulders might be also consistent with the enigmatic marked increase in crustal thickness (as much as ~ 45 km) toward the western MER margin as imaged a single seismic-refraction profile across the Ethiopian Plateau (Berckhemer et al., 1975).

(e.g., Bosworth, 1987) and in the Main Ethiopian Rift (e.g., Bonini et al., 2001; Fig. 42), where several central volcanoes built up on the eastern rift shoulders (Somalian Plateau) in an external position to the border faults (Eastern Margin Fault System) flanking the rift depression (see also Section 5.2.3 and Fig. 44).

In the light of the analogue modelling results, we suggest that the lateral (extension-parallel) migration of magma in continental rifts may be inhibited if:

1. a transfer zone develops between two offset rift segments; in this case, the pattern of migration is perturbed and magma moves predominantly in an extension-orthogonal rather than extension-parallel direction (see results of series NRTZ experiments, Section 4.2.6);
2. a stress field reorientation takes place, causing oblique rifting with magma emplacement occurring within the rift depression (see results of series ObR and PR experiments, Sections 4.2.4 and 4.2.5);

3. riftward flow of ductile materials is produced in case of episodic rifting during stages of tectonic inactivity or strongly reduced activity (Mulugeta and Ghebreab, 2001). In this case, a convergent flow of magma toward the rift axis is expected.

5.2.2. Oblique extension

Oblique extension models outlined a linkage among surface oblique en echelon faulting within the main rift, lower crust doming and accumulation of magma. An example of the spatial association between magmatism and oblique structures is found again in the Main Ethiopian Rift (MER), where an oblique rifting Quaternary phase produced the development of oblique
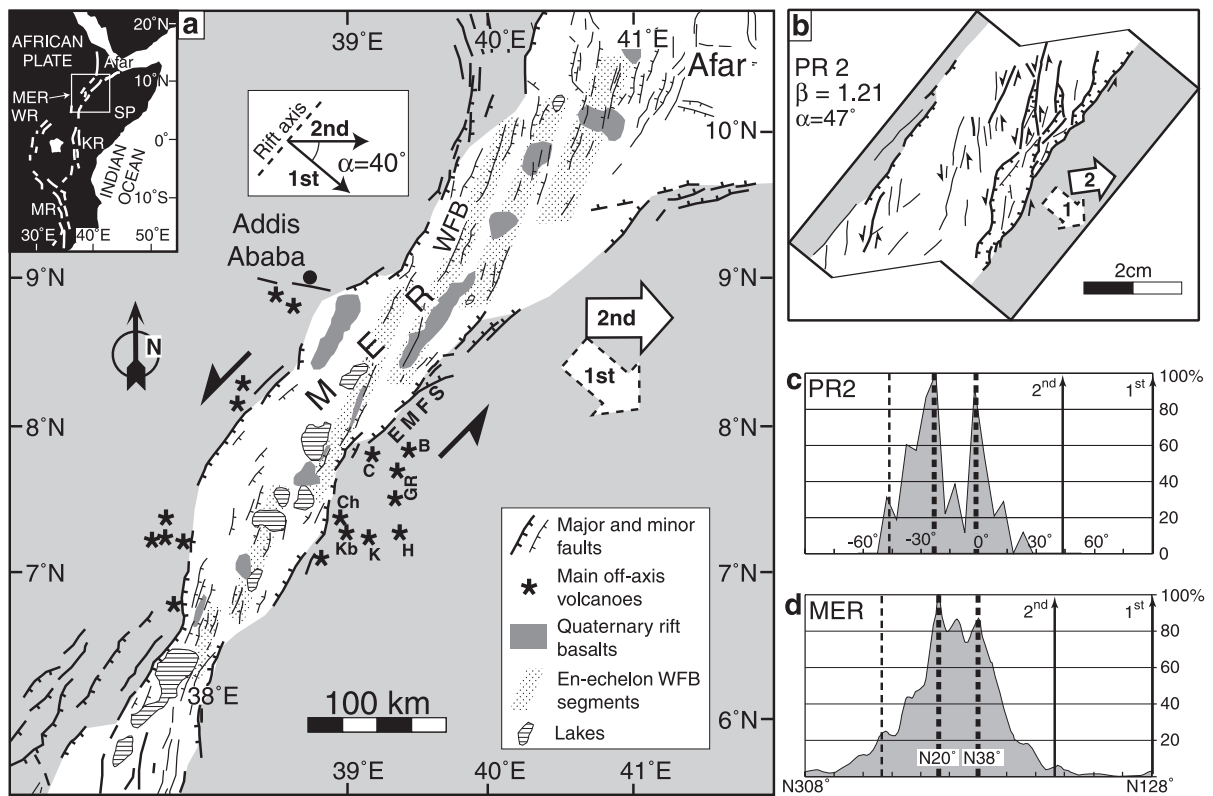
Fig. 44. Comparison of models PR with the structural and volcanic pattern of the Main Ethiopian Rift (MER). Inset shows the location of the MER; KR: Kenya Rift, MR: Malawi Rift, SP: Somalian Plate, WR: Western Rift. (a) Schematic structural map of the MER (after Hayward and Ebinger, 1996; Boccaletti et al., 1999). Note the location of off-axis volcanoes and the coincidence of Quaternary rift basalts with the en echelon fault system of the WFB. B: Badda, C: Chilalo, Ch: Chike, GR: Galama Volcanic Range, H: Hunkuolo, K: Kaka, Kb: Kubsa; EMFS: Eastern Margin Fault System. (b) Top view line drawing of model PR2. (c) Histogram of fault distribution of model PR2 and correspondent histogram (d) for the MER (after Bonini et al., 1997). Arrows indicate the direction of extension during the different rifting phases. Thin dashed lines represent the normal to the extension vector, thick dashed lines indicate the main peaks of fault distribution. Note the coincidence between the two peaks in the histograms.

fault belts (the so-called Wonji Fault Belt; Mohr, 1967) that is associated with a magmatic activity concentrated within the main rift (e.g., Mohr and Wood, 1976; see following Section 5.2.3). However, since oblique rifting in the MER follows a previous Mio-Pliocene orthogonal rifting phase, we will discuss in detail this natural example in the following section dedicated to polyphase extension.

Similar examples of oblique rifting controlling magmatic and volcanic patterns characterise some oceanic ridges, such as the Reykjanes Ridge (RR), south of Iceland, the Mohns Ridge (MR), in the Norwegian–Greenland Sea, and the Gulf of Aden ridge (GAR; e.g., Searle and Laughton, 1981; Dauteuil and Brun, 1993, 1996; Parson et al., 1993; Appelgate and Shor, 1994; McAllister et al., 1995; Dauteuil et al., 2001; Fig. 43). The RR and the MR formed during an orthogonal rifting phase, followed by a reorientation of the stress field that determined the spreading vector to be oblique to the rift trend (e.g., Dauteuil and Brun, 1993, 1996). Conversely, obliquity of spreading in the GAR results from a local configuration of the ridge that displays a regional bending towards the Afar Triple Junction (Dauteuil et al., 2001). In all these three examples, the deformation pattern is characterised by en echelon

faults oblique to the axial valley trend (Fig. 43). The good correspondence between experiments and the natural examples is documented by the very similar orientation of the main peaks in the histograms of fault distribution corresponding to structures oblique to the stretching vector and to the axial valley trend (Fig. 43). In addition, similar to the experimental results, the structural pattern in the RR, MR and GAR is accompanied by the development of en echelon volcanic alignments, preferentially located along oblique structures (e.g., Murton and Parson, 1993; Appelgate and Shor, 1994; Dauteuil and Brun, 1996; Tuckwell et al., 1998; Dauteuil et al., 2001; Fig. 43a and e).

5.2.3. Polyphase extension: the tectono-magmatic evolution of the Main Ethiopian Rift

The Main Ethiopian Rift (MER) is characterised by a fault pattern composed of a NE–SW border fault system and a N–S to N20°E-trending system, composed of en echelon right-stepping faults, obliquely affecting the rift floor, commonly referred to as Wonji Fault Belt (WFB; Mohr, 1962, 1967, 1987; Gibson, 1969; Meyer et al., 1975; Mohr and Wood, 1976; Kazmin, 1980; Chorowicz et al., 1994;
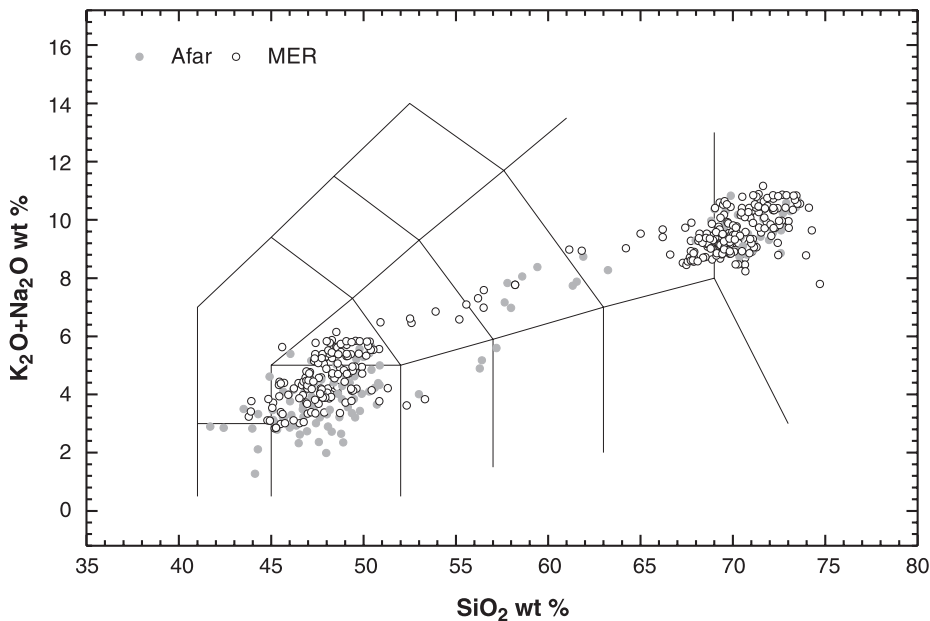
Fig. 45. Total alkali silica diagram (Le Maitre, 1989) for volcanic products from the MER and Afar.

Fig. 44a). This structural pattern has been interpreted as resulting from a two-phase rifting evolution characterised by a first (Mio-Pliocene) phase of orthogonal rifting followed by a later (Quaternary) stage of oblique extension (Bonini et al., 1997; Boccaletti et al., 1998; Fig. 44a). According to this evolution, the WFB developed at about 1.8–1.6 Ma ago (Meyer et al., 1975) to accommodate the strong sinistral component of motion along the rift axis (e.g. Boccaletti et al., 1998).

The MER tectonic evolution is matched by an intense volcanic activity up to historical times. After a prerift phase of widespread flood basalt and subordinate felsic volcanism, the synrift magmatic products in the MER are characterised by a typical bimodal character (Fig. 45). During orthogonal rifting, the volcanic activity encompassed the full width of the rift, and volcanic products are widespread from the Ethiopian shoulder (western margin) to the Somalian shoulder (eastern margin). The style of volcanic activity is markedly different, passing from the rift depression to the shoulders, being essentially fissural on the rift floor and central on the rift shoulders, where important Middle–Late
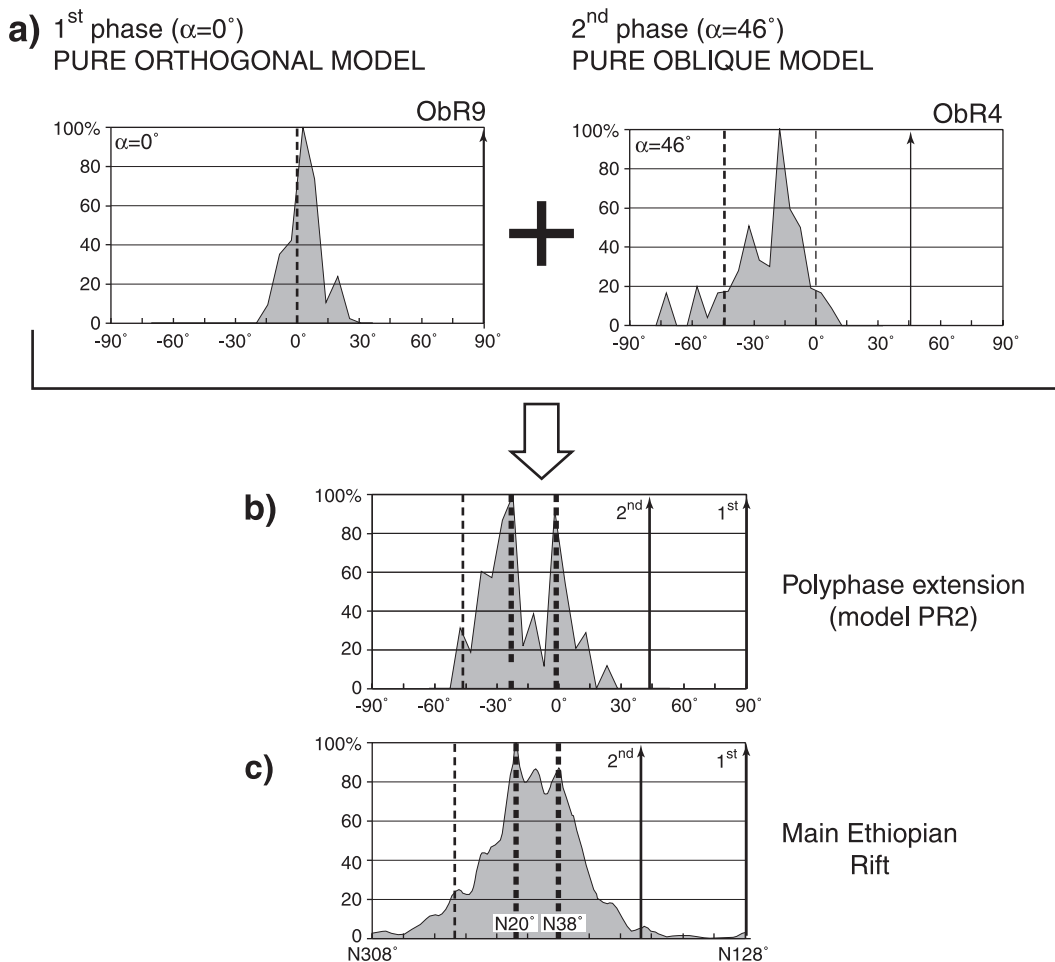
Fig. 46. Evolution of fault orientation during a two-phase extension and comparison with the MER fault pattern. (a) Fault orientation graphs of pure orthogonal and pure oblique rifting models. (b) Fault orientation of model PR2 (polypahse rifting) that can be considered as resulting from the sum of the faults developed during the two rifting phases. (c) MER fault pattern (after Bonini et al., 1997).

Pliocene off-axis (flank) volcanoes develop. These volcanic centres are mainly of basaltic and trachytic composition on the eastern (Somalian) shoulder, whereas on the Ethiopian shoulder, more differentiated products (trachytic–rhyolitic composition) are dominant (Kunz et al., 1975; Mohr and Potter, 1976; WoldeGabriel et al., 1990; Fig. 44a). However, the major basaltic shield volcanoes (Chilalo, Badda, Hunkuolo, Kaka and the Galama Volcanic Range) developed on the Eastern Margin Fault System on the Somalian Plateau, which is moving relatively to the African plate (e.g. Chase, 1978; Jestin et al., 1994; Fig. 44a).

At 1.8–1.6 Ma, volcanic activity became confined to the rift floor (e.g., Mohr, 1967; Di Paola, 1972; Mohr and Wood, 1976; WoldeGabriel et al., 1990, 1999) and was characterised by central activity with development of large caldera structures and summit calderas, volcanic fields with monogenetic basaltic cones and flows and acid domes generally associated with the Wonji faults (e.g., WoldeGabriel et al., 1990; Boccaletti et al., 1999; Fig. 44).

Results of series polyphase rifting (PR) models provides useful insights into the complex relations between deformation and magmatic evolution (Corti et al., submitted for publication). In particular, the experimental results corroborate the hypothesis by Bonini et al. (1997) and Boccaletti et al. (1998) of a two-stage (first orthogonal–second oblique) evolution for the MER (Fig. 46). This consideration arises from the striking similarity in the structural pattern of model PR2 and the MER, being the main peaks in the fault distribution histograms coinciding in both cases (Figs. 44c, d and 46). Notably, although a dextral component of displacement has been described along some WFB faults (Chorowicz et al., 1994; Acocella and Korme, 2002), this kinematics does not contradict a Quaternary regional E–W-trending extension. Dextral faulting along some of the WFB faults can be indeed explained as resulting from a counterclockwise rotation of major crustal blocks within the deforming region that developed in response to the sinistral oblique rifting phase. The occurrence of oblique faults showing some component of dextral motion in experiments characterised by sinistral oblique rifting (Corti et al., 2001, submitted for publication) supports this view.

The analysis of the dynamic relations between continental rifting and the magmatic evolution in
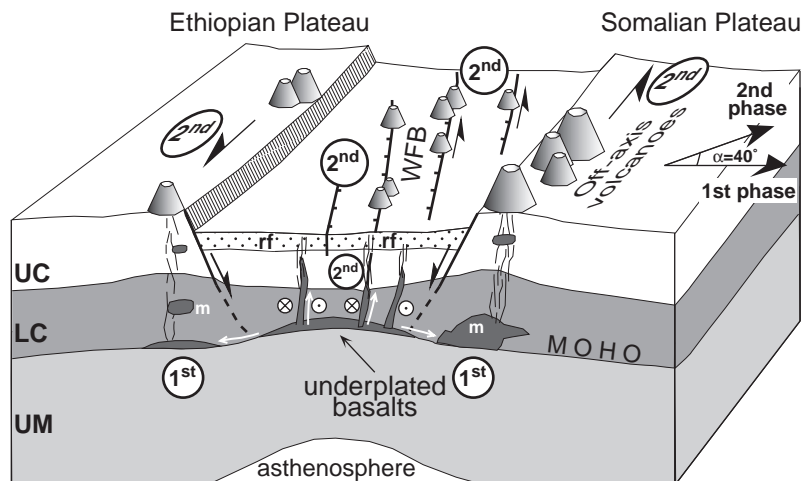
Fig. 47. Interpretative schematic 3D block diagram of the MER evolution based on the modelling results, relating (1) off-axis volcanism to lateral flow of the lower crust and magma during the first orthogonal rifting phase (denoted by 1st) and (2) oblique WFB faulting and magmatism to the second oblique rifting phase (denoted by 2nd). Note that this interpretation includes both the effect of isostatic compensation provided by the asthenosphere and the thermal thinning of the crust, which were not considered in the current models. UC: upper crust; LC: lower crust; m: magma; rf: rift fill.

the MER should also take into account (1) the occurrence of off-axis volcanoes during the orthogonal rifting phase and (2) the in-rift concentration of faulting and magmatism during the oblique phase generating Quaternary volcanic products along the en echelon WFB faults (Fig. 44a). Results of models of the series PR well accord with this evolution. In particular, the occurrence of off-axis volcanoes during the orthogonal phase could indicate a process similar to that observed in analogue models, where lateral transfer of melt toward the border faults footwall allows the development of important magma chambers below the rift shoulders (Section 5.2.1.1; Fig. 47). The stress field reorientation at the beginning of the Quaternary may have caused the off-axis volcanoes activity to be strongly reduced by inhibiting the lateral transfer of magma, although some melt is probably

still present at depth as suggested by gravity data (see above Section 5.2.1.1). During the second oblique phase, newly formed en echelon oblique and strike−slip faults accommodated the sinistral component of motion, promoting an oblique and en echelon uprising of melts within the main rift depression and favouring the volcanic activity to be concentrated along the en echelon WFB segments (Fig. 47). In this scenario, the basalts erupting along the WFB should be characterised by a lower probability to develop AFC processes (fractional crystallisation plus crustal assimilation) with respect to the magma collecting in the reservoirs below the rift shoulders that would tend to be isolated from the principal magma feeding system. This hypothesis is supported by the Sr isotopic data determined in lavas of the off-axis Mt. Chilalo volcano which exhibit a comparatively higher degree
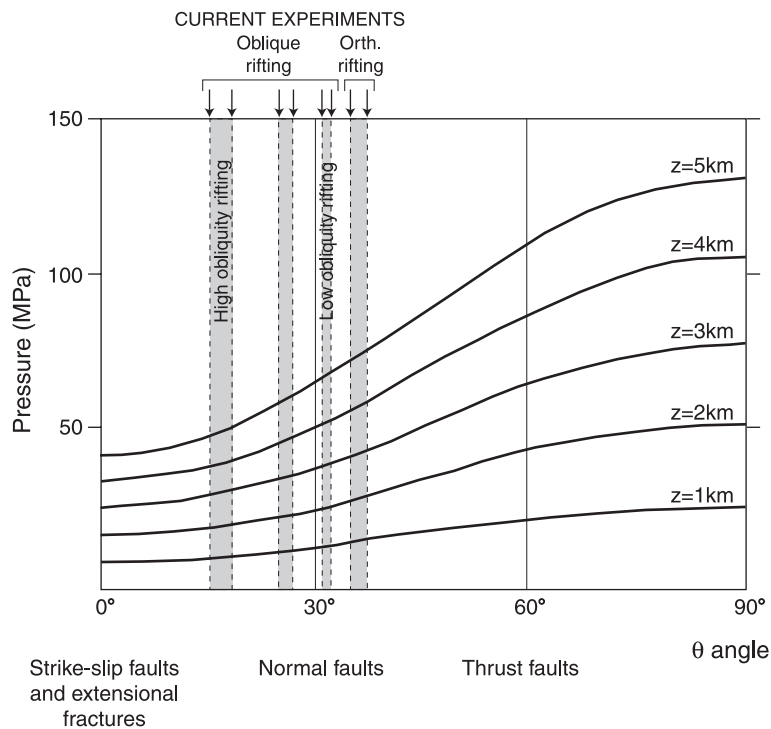
Fig. 48. Graph showing the values of the pressure P necessary to penetrate a preexisting fracture as a function of the angle θ (complementary to the dip of the fractures or faults) for various depths (represented by different curves). Arrows on the top of the graph and shaded regions represent the dip of oblique and orthogonal rifting-related structures, as measured from models' cross-sections. Note that oblique rifting-related faults (characterised by high dips and low θ values) require lower values of pressure to be penetrated than orthogonal rifting-related faults. Modified after Acocella et al. (1999b).

of crustal contamination with respect to the Quaternary basaltic spatter cones and basaltic flows exposed along the MER rift floor (Trua et al., 1999). More primitive products during the oblique rifting phase should also be favoured by the development of a higher density of faults and fractures in the main rift zone and by the higher dip of oblique–slip faults with respect to pure dip–slip (normal) faults developing in orthogonal models. Indeed, the pressure required to penetrate fractures is (for a given depth) a function of the angle θ that represents the complementary to the fracture dip (Acocella et al., 1999b; Fig. 48). As a consequence, faults characterised by high dips (such as oblique–slip faults developing during oblique rifting) require the lowermost values of pressure to be penetrated, thus representing a preferential pathway for magmas to ascend (Acocella et al., 1999b; Fig. 48).

5.2.4. Magma emplacement at transfer zones

As discussed in Section 2.3.1, concentration of magmatic processes at transfer zones has been observed in many regions undergoing extension. In the Western Branch of the East African Rift System, for example, the four volcanic provinces are located in correspondence to major transfer zones (e.g., Ebinger, 1989b; Fig. 49). Detailed analysis of the fault pattern characterising these transfer zones highlight a close similarity with structures formed in series NRTZ models (Fig. 49a). In particular, in the Kivu transfer zone, two offset rift segments are linked by a structurally complex area of mechanical interaction characterised by bending and linking of major boundary faults with opposite polarity (Fig. 49). This pattern shows a remarkable similarity with model results (compare Fig. 49a with Fig. 49b). The curved faults, propagating from en echelon depressions, are observed
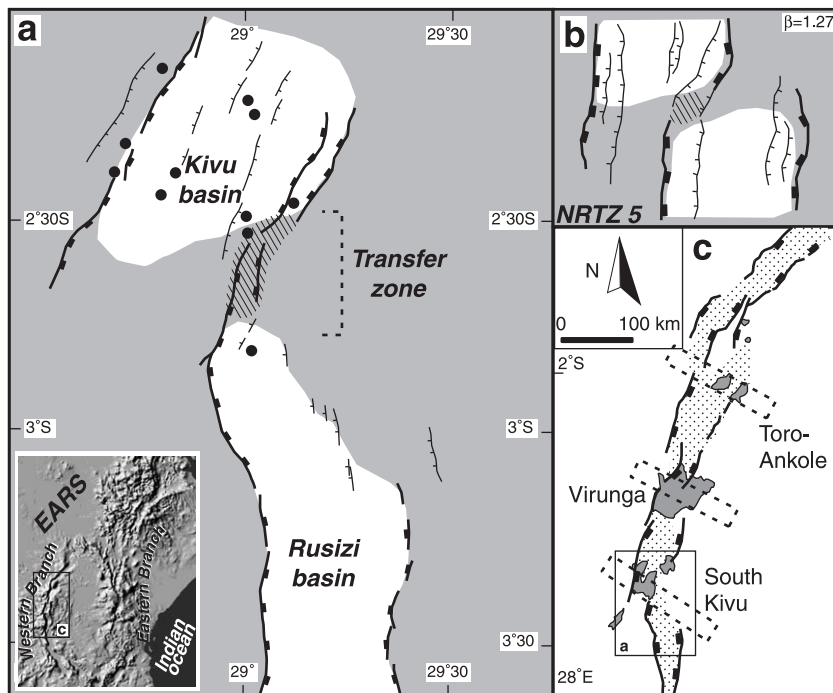
Fig. 49. Comparison of model NRTZ5 results with nature. (a) Structural pattern of the South Kivu volcanic province (after Ebinger, 1989b). Dots indicate the main volcanic centres; dashed pattern indicates the transfer zone between the two offset rift segments. Inset show the location of the Western Branch of the East African Rift System. (b) Structural pattern of model NRTZ5 for $\beta = 1.27$. Note the close similarity between structures in model (b) and (a) nature. (c) Concentration of volcanic activity at transfer zones in the Western Branch (after Rosendahl, 1987; Ebinger, 1989a).

in several transfer zones worldwide (e.g., Nelson et al., 1992 and references therein; see also Acocella et al., 1999a). Applying the lessons of our models to natural transfer zones, we suggest that the interaction between magmatic and deformational processes plays a major role in controlling the volcanic and fault patterns in these regions (see Section 4.2.6). Particularly, we suggest that concentration of volcanic activity at transfer zones may be favoured by an along-axis (extension-orthogonal) migration of magma, driven by the pressure decrease associated with the development of oblique faults (or pull-apart-like structures) in the transfer zone.

6. Summary and conclusions

In this review paper, we focused on the processes of extension of the lithosphere and continental breakup, which are of a paramount importance in the earth sciences, since they precede the development of passive margins and new oceanic basins. Structural analysis of regions undergoing extension suggest that continental extension may occur in two major different modes (England, 1983; Buck, 1991): narrow rifting, when extension occurs in narrow regions (generally < 100 km wide) of localised deformation, and wide rifting, when extensional strain affects regions as wide as 1000 km. An additional structural style, the core complex, characterised by concentrated deformation in the upper crust coupled to a diffuse flow in the lower crust, has been considered either a distinct mode of extension or a local anomaly within wide rifts. Both numerical and analogue models have investigated the structural pattern resulting from extension of a rheologically layered lithosphere and the main parameters controlling the mode of extension. These experimental works highlighted that the process of lithospheric extension may be influenced by the strain rate, the initial conditions (in terms of initial thermal profiles and crustal thickness) and the mechanical instability caused by extension of the rheologically layered lithosphere. Numerical and analogue approaches have suggested that magmatic bodies eventually present within the continental lithosphere are able to significantly affect the process of extension. In particular, both the thermal and mechanical effects

related to the presence of magma strongly weaken the lithosphere-enhancing deformation and strain; deformation, in turn, is able to affect the modality of magma ascent and emplacement, possibly leading to a feedback process between magmatism and deformation. To better constrain these dynamic relations, in this paper, we have reviewed experimental data derived from centrifuge models performed, taking into account the presence of an initially underplated magmatic reservoir. These models have provided useful insights for the understanding of the relations between the presence of magma and deformation during continental extension, which can be summarised as follows.

(1) During orthogonal rifting, magma as well as lower crust are passively squeezed from an axial position towards the footwall of the major normal faults, resulting in major magma accumulations occurring in a lateral position (off-axis emplacement) with a rift-parallel trend. This process, that may involve feedback relations, causing the further collection of large volumes of magma into the footwall, is able to account for the close association between magma emplacement and the development of core complex-like structures, such as in the Basin and Range Province of the United States. Lateral transfer and off-axis emplacement of magma are also able to provide an explanation for the occurrence of flank or off-axis volcanoes in continental rifts, such as the Main Ethiopian and Kenya rifts in the East African Rift System, the Limagne Graben in the Cenozoic European Rift System, the Red Sea.

(2) During oblique rifting, the occurrence of magma at depth influence the fault pattern, localising strain in the overlying crust. In turn, deformation favours magma to emplace within the main rift depression, giving rise to elongated intrusions with an oblique, and in some cases, en echelon pattern. In nature, this pattern may be representative of the en echelon faults and volcanic alignments, oblique to the axial valley trend, characterising continental rifts such as the Main Ethiopian Rift and also some oceanic ridges, such as the Reykjanes, Mohns and Gulf of Aden ridges.

(3) During a polyphase rifting history (first orthogonal–second oblique), the rift kinematics strongly

affects the modalities of magma emplacement: during the orthogonal rifting, magma is squeezed laterally, causing an off-axis emplacement, whereas during the successive oblique rifting phase emplacement occurs in oblique (or en echelon) intrusions. This evolution matches the tectono-magmatic history of the Main Ethiopian Rift where important off-axis volcanoes formed on the rift shoulders during the Miocene–Pliocene orthogonal rifting. A second Quaternary oblique rifting phase concentrated magmatism within the rift depression, along the oblique en echelon segments of the Wonji Fault Belt.

(4) Within narrow rift-related transfer zones, the presence of the underplated magma localises again strain in the overlying crust, thus influencing the surface fault pattern; on the other hand, localised deformation causes magma to accumulate in correspondence to the transfer zone, with a main flow pattern that is perpendicular to the extension direction. The resulting patterns of magma emplacement and deformation may offer insights for explaining the correspondence to the volcanic provinces with major transfer zones in the Western Branch of the East African Rift System.

Concerning the mode of continental extension, experiments suggest an active role played by the magma in controlling the extension process, as it can be able to control the spatial distribution of deformation and the mode of extension, favouring the transition from the wide rifting mode to a local core complex style. Similar to natural examples, model core complexes and wide rifting style of faulting may coexist together during high strain rate extension in the presence of a localised magmatic body. We suggest that core complex-like deformation, characterised by lateral flow and associated doming of the lower crust, may represent a major process accommodating the extensional deformation. This is in nature documented by the common recognition of core complex-like structures in extensional settings, such as the classical post-orogenic settings, narrow rifts and even in oceanic crust.

In conclusion, analysis of new data provided by centrifuge analogue models suggests that deformation and magma emplacement in the continental crust are intimately related, and their interactions constitute a key factor in deciphering the evolution of both continental and oceanic rifts.

Appendix A. The scaling procedure

An analogue model is representative of a particular natural process if it is geometrically, dynamically, cinematically and rheologically similar to its natural prototype (e.g., Hubbert, 1937; Ramberg, 1981; Weijermars and Schmeling, 1986; Brun, 1999). Such conditions require that the model must represent a reduced geometric replica of the prototype, with proportional correspondent lengths and equal correspondent angles (geometrical similarity), and that the force field (thus, rheology) and boundary conditions must be properly scaled. The scaling of the quantities controlling the force field requires that the model to prototype ratios for forces and stresses (including gravitational, inertial, viscous, elastic and frictional forces) must be constant (dynamic similarity). This will ensure a similarity in terms of stress magnitudes and trajectories. Geometrical and dynamic similarity, in turn, will provide a fulfilled kinematical similarity, hence, a similar evolution of the model and the natural prototype, although the model has a smaller geometric scale and is performed at a faster time-scale. Finally,

rheological similarity is fulfilled if the materials used in analogue experiments are characterised by a similar rheological behaviour with respect to the natural prototype (Weijermars and Schmeling, 1986). For viscous materials, this conditions requires that the analogue and prototype flow (stress–strain) curves must exhibit identical shapes and slopes (Weijermars and Schmeling, 1986; Fig. A1).

Hubbert (1937) showed that the scaling ratio of a particular parameter in the model and in the natural prototype is given by the ratio of the dimensional

equations of this parameter in the original and in the model. This implies that dimensionless quantities must be equal in the model and in the prototypes.

In the following sections, the basic scaling principles for brittle and ductile deformation, as well as the calculations of dimensionless ratios of forces used to test dynamic similarity, are briefly illustrated. For more detailed discussions about scaling principles, see Hubbert (1937), Ramberg (1981), Weijermars and Schemling (1986), Davy and Cobbold, 1991; Weijermars et al. (1993).
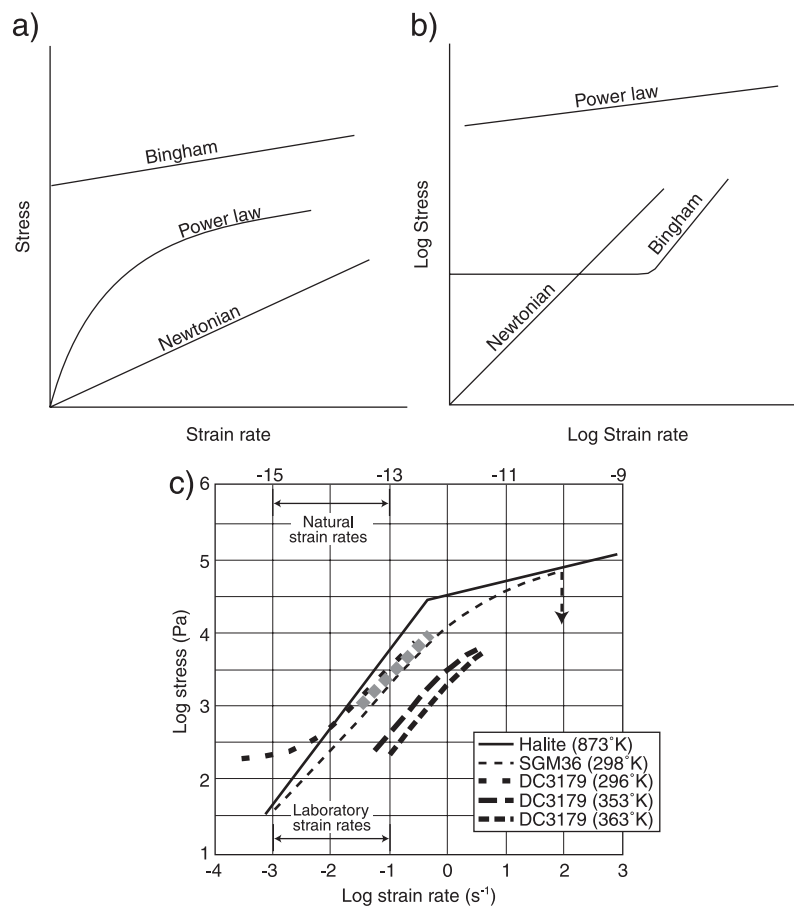
Fig. A1. Newtonian, Bingham and power-law flow behaviour plotted on linear (a) and logarithmic (b) axes. (c) Flow curves (on a log–log graph) for halite (1 cm grain diameter deforming at 200 MPa confining pressure and natural strain rates of $10^{-13}-10^{-15}$ s^{-1}) and different experimental materials. Rheological similarity is fulfilled if the shape and the slope of the rock and model material flow curves are similar. The dashed grey line indicates the sand–silicone mixture used in the experiments of the series Magm to simulate the lower crust. Note that at room temperatures ($\approx$ 298 K), the flow curve of SGM36 is geometrically similar to that of halite, ensuring a rheological similarity at this deforming conditions. No geometrical (and thus, rheological) similarity is observed for the bouncing putty DC3179; similarity is achieved deforming this material at higher temperatures. Modified after Weijermars and Schmeling (1986) and Hailemariam and Mulugeta (1998).

A.1. Brittle behaviour

Brittle failure can be expressed by a frictional shear failure criterion in the form (e.g., Weijermars, 1997):

$$(\sigma_1 - \sigma_3) = \frac{2[c_0 + \mu\rho gz(1 - \lambda)]}{(\mu^2 + 1)^{1/2} - \mu} \quad \text{[compression]} \tag{A1}$$

$$(\sigma_1 - \sigma_3) = \frac{-2[c_0 + \mu\rho gz(1 - \lambda)]}{(\mu^2 + 1)^{1/2} + \mu} \quad \text{[extension]} \tag{A2}$$

$$(\sigma_1 - \sigma_3) = \frac{2[c_0 + \mu\rho gz(1 - \lambda)]}{(\mu^2 + 1)^{1/2}} \quad \text{[strike − slip]} \tag{A3}$$

where $\sigma_1 - \sigma_3$ is the critical stress difference, c_0 the cohesion, μ the internal friction, ρ the density of the overlying material at depth z, g the acceleration due to gravity and λ the Hubbert–Rubey coefficient of fluid pressure (ratio of water pressure to overburden pressure). However, in natural rocks, the stress required to activate fault slip is largely insensitive to the rock composition (Byerlee, 1978). In particular, Byerlee's data fit a Mohr–Coulomb criterion with constants $c = 0$ MPa and $\mu = 0.85$ for shallow crustal depth (< 10 km) and $c = 60$ MPa and $\mu = 0.6$ for deeper crust (>10 km). Thus, starting from the Mohr–Coulomb law

$$\tau = c + \mu\sigma \tag{A4}$$

(where τ and σ are the shear and normal stresses acting on the fault plane), Byerlee's criterion can be expressed as:

$$\tau = 0.85\sigma \quad (z < 10 \text{ km}) \tag{A5}$$

$$\tau = 60 \text{ MPa} + 0.6\sigma \quad (z > 10 \text{ km}). \tag{A6}$$

Scaling of the brittle behaviour in the experiments is normally obtained starting from Eq. (A4). Following Hubbert (1937) and Ramberg (1981), ratios of stresses (τ^* and σ^*) can be obtained from the equation:

$$\sigma^* = \rho^* h^* g^* \tag{A7}$$

where ρ^* (ρ_m/ρ_n), h^* (h_m/h_n) and g^* (g_m/g_n) represent density, length and gravity model to nature ratios. For normal gravity experiments $g_m = g_n$ and $g^* = 1$, whereas in centrifuge experiments, the centrifugal force induced by artificial gravity field needs to be scaled down. Considering ρ^* (which is imposed by the materials used in the experiments), by arbitrary fixing h^*, from Eq. (A7), we can directly obtain the stress scaling ratio. Note that by having the same dimensions of stress (Pa), the cohesion must have a similar scaling ratio ($c^* = c_m/c_n = \sigma^*$).

Similarly, the coefficient of internal friction $\mu = \tan\phi$ (Eq. (A4)), an adimensional quantity, must share similar values both in the model and in the prototype. In nature, μ varies between 0.6 and 0.85 (Byerlee, 1978; Brace and Kohlstedt, 1980). This requirement is met by the quartz sand commonly used in the experiments exhibiting μ values ranging about from 0.4 up to 1, dependent on the physical handling technique (Krantz, 1991; Faccenna et al., 1995; Cobbold and Castro, 1999), such that $\mu_m \approx \mu_n$.

A.2. Ductile behaviour

For high temperatures and low strain rates, a ductile response is expected, with a deformation law expressed by a ductile power-law creep equation (e.g., Goetze and Evans, 1979):

$$\dot{\varepsilon} = a_0 \exp(-Q/RT)(\sigma_1 - \sigma_3)^n, \tag{A8}$$

where $\dot{\varepsilon}$ is the strain rate, T the absolute temperature (in Kelvin), R the universal gas constant (8.13 kJ mol^{-1} K^{-1}) and a_0 (the frequency factor, Pa^{-n} s^{-1}), n (the stress sensitivity of the strain rate, dimensionless) and Q (activation energy, kJ mol^{-1}) are material parameters that are either independent or only weakly dependent on temperature and pressure.

Modelling of ductile flow requires, for dynamic similarity to be maintained, the condition of rheological similarity to be fulfilled: the shape and slopes of flow curves of rocks and model materials should be similar, and each flow should operate on similar parts of their respective flow curves (Weijermars and Schmeling, 1986). Materials normally used in analogue experiments show three different behaviours: Bingham, Newtonian and power-law flow (e.g., Weijermars and Schmeling, 1986; Hai-

lemariam and Mulugeta, 1998; Fig. A1). Bingham flow is unusual in solid rocks, and analogue materials presenting such a rheological behaviour in many cases do not fulfill rheological similarity (Fig. A1).

For scaling of the ductile behaviour, Eq. (A8) can be rewritten and simplified in:

$$\dot{\varepsilon} = A(\sigma_1 - \sigma_3)^n. \tag{A9}$$

When $n = 1$ the flow is Newtonian, and Eq. (A3) assumes the simplified form:

$$\dot{\varepsilon} = (\sigma_1 - \sigma_3)/\eta, \tag{A10}$$

where η represents the viscosity.

In case of Newtonian flow, Weijermars and Schmeling (1986) demonstrated that geometrical similarity and similar boundary conditions are sufficient to achieve dynamic similarity, provided that inertia is insignificant in solid rock flow. In such conditions, some basic equations are used to scale down model velocity and viscosities:

$$\varepsilon^* = \sigma^*/\eta^* \tag{A11}$$

$$\varepsilon^* = V^*/h^* \tag{A12}$$

where $\varepsilon^* = (\varepsilon_m/\varepsilon_n)$, $\eta^* = (\eta_m/\eta_n)$ and $V^* = (V_m/V_n)$ represent the scaling ratios of the strain rate, viscosity and velocity, respectively.

From these equations we can either (1) fix the viscosity ratio (by assuming a particular lower crust viscosity) in Eq. (A11) and calculate the scaled natural velocity from Eq. (A12) or (2) assume a natural velocity in Eq. (A12) and scale down the natural viscosity from Eq. (A11).

The scaling ratio of time can be directly achieved once resolved Eqs. (A11) and (A12) by considering:

$$\varepsilon^* = 1/T^*. \tag{A13}$$

For low-inertia flow in non-Newtonian continua, dynamic similarity is fulfilled only if the flow curve of a model material is geometrically similar to one assumed or measured for the natural prototype (rheological similarity; Weijermars and Schmeling, 1986). If such similitude conditions are fulfilled,

then natural and model quantities scaling rules can be obtained directly from Eq. (A9):

$$\dot{\varepsilon}^* = A^* \frac{(\sigma_m)^{n_m}}{(\sigma_n)^{n_n}}, \tag{A14}$$

where A^* (A_m/A_n) represents the scaling ratio of the constant A. Because n represents the slope of the flow curve in a log–log graph, in the condition of rheological similarity $n_m = n_n$ ($= n$), and Eq. (A14) can be simplified in the form:

$$\dot{\varepsilon}^* = A^*(\sigma^*)^n. \tag{A15}$$

For the analogue materials, the two parameters A and n can be determined directly from the stress–strain laboratory tests: in a log–log graph, by applying the simplified flow Eq. (A9) in the logarithmic form ($\log = \log A + n \log \sigma$), n and A represent the slope of the curve and the intercept with the stress axes, respectively. Similarly, as suggested by Weijermars and Schmeling (1986), characteristic values for the natural A and n constants can be determined from empirical data reported in log–log graphs (such as Fig. 3 of Weijermars and Schmeling, 1986) by applying the simplified flow Eq. (A9).

A.3. Test of dynamic similarity through the use of dimensionless ratios of forces

Ramberg (1981) showed that the evaluation of the conditions of dynamic similarity and the scaling of the models can also be obtained through the comparison of a set of dimensionless numbers or ratios of characteristic forces between models and nature. For viscous deformation, one of the most frequently used dimensionless ratio is the Ramberg number (R_m, named by Weijermars and Schmeling, 1986) which represents the ratio of gravitational to viscous forces:

$$R_m = \frac{\rho_d g h_d}{\eta \varepsilon} = \frac{\rho_d g h_d}{\eta (V/h_d)} = \frac{\rho_d g h_d^2}{\eta V} \tag{A16}$$

where ρ_d and h_d are the density and the thickness of the ductile layer, g is the gravitational acceleration, η is the viscosity and ε is the strain rate and V is the velocity. For the brittle behaviour, dynamic similarity

can be tested through the comparison of the ratio of gravitational to frictional forces which can be considered analogous to the Smoluchowsky number (S_m) defined by Ramberg (1981):

$$S_m = \frac{\rho_b g h_b}{c + \mu_c \rho_b g h_b} \qquad (A17)$$

where ρ_b and h_b are the density and the thickness of the brittle layer, g is the gravitational acceleration, c is the cohesion and μ_c the internal friction coefficient. A similar dimensionless number that can be used to test the dynamic similarity in the brittle regime is the ratio between the gravitational forces and the cohesive strength (see appendix 4 in Mulugeta, 1988).

Since dynamic similarity requires the ratio between forces in experiments and in the prototype to be constant if compared kind for kind, the ratio between two dissimilar forces in the model must assume the same value as the ratio between the same forces in nature. Thus, experimental R_m and S_m numbers must share similar values with respect to nature, and this similarity can be used to scale down the models (see Sokoutis et al., 2000).

Appendix B. Experimental materials and scaling of series Magm, ObR, PR, TrZn and NRTZ

The complex rheological layering of the continental lithosphere can be simplified in laboratory experiments by selecting opportune materials whose characteristic may reproduce the rheological behaviour of natural rocks. In analogue experiments, the rheological layering of the lithosphere is simplified by assuming that the material properties of each layer are invariant with depth (e.g., Davy and Cobbold, 1991). As a result of this assumption, model strength profiles consist of straight segments, sloping downwards for brittle layers (considering constant cohesion and angle of internal friction with depth) and vertical for ductile layers (for which we neglect the temperature dependence of material properties and assume that viscosity is constant throughout each layer; Fig. A2). Particularly, several analogue works have demonstrated that the brittle behaviour of the upper crust can be successfully reproduced by using quartz sand (see Brun, 1999 and references therein). This material has a Coulomb behaviour (such that the strength increases linearly with depth) and is able to develop discrete faults (with associated stress drop). In addition, sand is correctly scaled in terms of cohesive strength and can be easily sedimented or eroded. According to Mulugeta (1988), sand can be considered a useful analogue of the upper crust even in centrifuge experiments (see following section). Clay is another experimental material that is commonly used to reproduce the brittle behaviour of the upper crust and the sedimentary cover (e.g., Koyi, 1997 and references therein; Clifton et al., 2000; Clifton and Schlische, 2001).

Newtonian silicone putties with different characteristics in terms of viscosities and densities, such as the
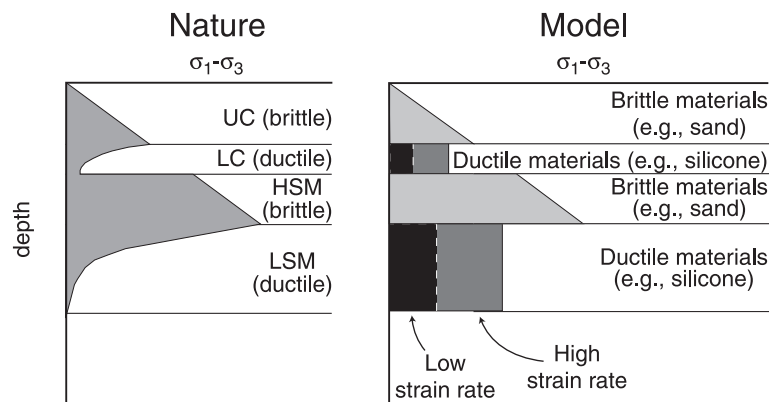

Fig. A2. Comparison between a four-layer strength profile in nature and in models. Note the dependence of strength of ductile materials on the applied strain rate, which allows to simulate different strength profiles in laboratory models (after Brun, 1999). UC: upper crust; LC: lower crust; HSM: high strength mantle; LSM: low strength mantle.

polydimethylsiloxane (PDMS), have commonly used to model ductile rocks in normal gravity or centrifuge experiments (e.g., Weijermars, 1986; Weijermars et al., 1993; Koyi, 1997; Brun, 1999). At a lithospheric scale, these materials have been used to reproduce the behaviour of the lower crust and lower lithospheric mantle (e.g., Vendeville et al., 1987; Davy and Cobbold, 1991; Brun, 1999 and references therein). For a given relative thicknesses of brittle and ductile layers, because of the strain rate dependence of strengths of ductile materials, a wide range of strength profiles can be simulated for different applied strain rates (Fig. A2).

Two different analogue materials have been widely used to reproduce the asthenosphere: honey and glycerol. Honey is characterised by a Newtonian behaviour with low viscosity (e.g., Vendeville et al., 1987; Faccenna et al., 1996, 1999) whereas glycerol can be mixed with barite or gypsum to obtain a proper density able to reproduce the asthenosphere (e.g., Sokoutis et al., 2000).

Low-viscosity silicone putties have been used in normal gravity experiments to reproduce magmatic bodies (e.g., Brun et al., 1994; Román-Berdiel et al., 1995, 1997; Benn et al., 1998, 2000; Román-Berdiel, 1999; Callot et al., 2001). Similarly, magmas have been simulated in centrifuge experiments using glycerol, a low-viscosity (1 Pa s) Newtonian material (Cruden et al., 1995; see following section).

Silicone putties, painter's putties, modelling clay, paraffin and stitching wax, among others, are materials widely used in centrifuge experiments to simulate lithospheric rheologies (e.g., Ramberg, 1963, 1971, 1981; Dixon and Summers, 1985; Mulugeta, 1985; Dixon and Simpson, 1987; Koyi, 1997; Koyi and Skelton, 2001).

B.1. Experimental materials of series Magm, ObR, PR, TrZn and NRTZ

During each experimental series, the upper continental crust was simulated with quartz sand which was soaked with paraffin oil to enhance the cohesion, since models were introduced vertically in the centrifuge apparatus. Following the procedure outlined in Mulugeta (1988), the cohesion of sand has been determined at ≈ 400 Pa in the centrifuge force field (Bonini et al., 2001; Corti et al., 2001, 2002, submitted for publication). Coloured sand layers were

introduced in the model as passive markers to visualise the faults' offset. The underlying ductile crust was simulated by a near-Newtonian layer produced by mixtures of Rhodorsil Gomme 70009 (manufactured by Rhone Poulenc, France) and quartz–sand in different proportions. This layer had a density ρ_d which varied in the different experiments between 1410 and 1550 kg m^{-3} and a viscosity of $\eta \approx 6 \times 10^4$–$3 \times 10^5$ Pa s at the experimental strain rate of $\approx 10^{-3}$ s^{-1} (Bonini et al., 2001; Corti et al., 2001, 2002). Magma was simulated using glycerol, a low-viscosity (1 Pa s) Newtonian material with a density of $\rho_v = 1260$ kg m^{-3} (Cruden et al., 1995). This material was mixed with a red pigment to enhance the colour contrast.

A 4-mm-thick layer simulating the uppermost portion of the mantle, composed of a mixture of silicone and sand with a density of 1500–1600 kg m^{-3} and a viscosity of 10^5–5×10^5 Pa s, was placed below the crust, surrounding the magma chamber. To account for the density contrast in nature, the density and the viscosity of the analogue upper mantle were maintained higher than the corresponding values of the lower crust.

B.2. Scaling of series Magm, ObR, PR, TrZn and NRTZ

During our experiments, we have assumed an initial thickness of the crust of about 35–40 km, such that the model ratio of length h^* model/nature is $\approx 4.5 \times 10^{-7}$. To compare the experimental results, all models were deformed in an artificial gravity field of 200g, such that $g^* = g_m/g_n = 200$. The model/nature ratios of length, gravity and density ($\rho^* \approx 0.5$) impose a ratio of normal stress of $\sigma^* = \rho^* g^* h^* \approx 4.5 \times 10^{-5}$ (see Appendix A). Viscosity ratio η^* ranges from 10^{-15} up to 10^{-19}, considering $\eta_m \approx 10^5$ Pa s and prototype viscosity values η_n for the lower continental crust in the range 10^{20}–10^{24} Pa s (e.g., Buck, 1991; Weijermars, 1997). The ratio of normal stress σ^* and the viscosity ratio η^* imposes a strain rate ratio ($\varepsilon^* = \sigma^*/\eta^*$, see Appendix A) ranging from $\approx 4.5 \times 10^{10}$ to $\approx 4.5 \times 10^{14}$. Considering that the horizontal displacement rate $V^* = V_m/V_n$ is given by the product of ε^* and h^* (see Appendix A), a mean experimental extension rate of 2×10^{-4} m s^{-1} scales down to ≈ 3 mm year^{-1} in nature (considering a natural average

Table A2.1
Scaling parameters for series Magm models and natural examples

Lower crust density ρ_{lc} (kg m^{-3})	Upper crust density ρ_{uc} (kg m^{-3})	Gravitational acceleration g (m s^{-2})	Lower crust thickness h_{lc} (m)	Upper crust thickness h_{uc} (m)	Viscosity η (Pa s)	Extension rate V (m s^{-1})	Cohesive strength c_0 (Pa)	R_m	R_s
Series Magm 1300 1410	1962	8×10^{-3}	7×10^{-3}	10^5	2×10^{-4}	400	9	45
Nature 2900	2700	9.81	1.8×10^4	1.8×10^4	10^{22}	9×10^{-11}	10^7	10	48

Scaling parameters refer to the onset of deformation. Natural brittle parameters computed according to the Byerlee's criterion.

viscosity of 10^{22} Pa s), which is a good approximation for an average extension rate in continental rift systems (e.g., 3–8 mm year^{-1} in the Main Ethiopian Rift; e.g., Hayward and Ebinger, 1996).

Similarity in the brittle layer can be tested comparing the brittle parameters of the analogue materials. Since the cohesion-scaling ratio must be similar to the stress-scaling ratio (see Appendix A), we have:

$$c^* \approx 5 \times 10^{-5}.$$

Assuming a mean cohesion for the upper crust in the order of 10^7 Pa implies that cohesion of sand used in our centrifuge experiments should be in the order of 500 Pa, a value that is rather similar to those obtained in laboratory tests (≈ 400 Pa). Similarity of the coefficient of internal friction is ensured in the current experiments by the use of sand with $\mu \approx 0.6$. Examples of calculations of dimensionless ratios for testing

of dynamic–cinematic similarity (see Appendix A) are reported in Table A2.1. A very close similarity between nature and experiments indicates that models are dynamically and cinematically scaled.

Appendix C. The centrifuge technique and experimental setup of series Magm, ObR, PR, TrZn and NRTZ

All the experiments of the series Magm, ObR, PR, TrZn and NRTZ were performed at the Hans Ramberg Tectonic Laboratory of Uppsala University (Sweden) by using the large capacity centrifuge (Ramberg, 1981). The use of the centrifuge technique to deform models is based on the principle that centrifugal forces play the same role of gravity in nature. Enhancing the gravity field, this technique is excellently suited for the study of tectonic phenomena where the pull of gravity play a significant role (gravity sliding, diapirism,

Table A3.1
Parameters of models deformation for experiments of the series Magm

Model	Geometry of extension	Average velocity of extension (mm/s)	BC/DC	Magma chamber geometry	Amount of extension (β)
MAGM.6	symmetric rifting	6.6×10^{-1} (TYPE 1)	0.9:1	orthogonal (5×1 cm)	2.1
MAGM.7	symmetric rifting	6.6×10^{-1} (TYPE 1)	0.9:1	orthogonal (5×1 cm)	1.77
MAGM.11	asymmetric rifting	3.3×10^{-1} (TYPE 1)	0.9:1	orthogonal (5×1 cm)	1.38
MAGM.13	symmetric rifting	2.0×10^{-1} (TYPE 2)	0.9:1	orthogonal (5×1 cm)	2
MAGM.15	asymmetric rifting	1.0×10^{-1} (TYPE 2)	0.9:1	orthogonal (5×1 cm)	1.35
MAGM.16	symmetric rifting	2.0×10^{-1} (TYPE 2)	0.9:1	no magma	1.7
MAGM.19	symmetric rifting	2.0×10^{-1} (TYPE 2)	0.9:1	wide magma chamber (5×5 cm)	1.7
MAGM.20	symmetric rifting	2.0×10^{-1} (TYPE 2)	2:1	orthogonal (5×1 cm)	1.62
MAGM.21	symmetric rifting	2.0×10^{-1} (TYPE 2)	2:1	no magma	1.75
MAGM.22	symmetric rifting	2.0×10^{-1} (TYPE 2)	1:3	orthogonal (5×1 cm)	1.8
MAGM.23	symmetric rifting	2.0×10^{-1} (TYPE 2)	1:3	no magma	1.95
MAGM.24	symmetric rifting	2.0×10^{-1} (TYPE 2)	1:2	orthogonal (5×1 cm)	1.55
MAGM.25	symmetric rifting	2.0×10^{-1} (TYPE 2)	1:2	no magma	1.7

Table A3.2
Parameters of models deformation for experiments of the series ObR and PR

Model	Geometry of extension	Average velocity of extension (mm/s)	BC/DC	Magma chamber geometry	Amount of extension (β)
ObR2	oblique extension $\alpha = 13°$	2.2×10^{-1}	1:1	orthogonal (2.5×0.7 cm)	1.43
ObR3	oblique extension $\alpha = 35°$	1.3×10^{-1}	1:1	orthogonal (2.5×0.7 cm)	1.42
ObR4	oblique extension $\alpha = 46°$	1.8×10^{-1}	1:1	orthogonal (2.5×0.7 cm)	1.56
ObR5	oblique extension $\alpha = 57°$	1.3×10^{-1}	1:1	orthogonal (2.5×0.7 cm)	1.48
ObR6	oblique extension $\alpha = 45°$	1.7×10^{-1}	1:1	no magma	1.58
ObR7	oblique extension $\alpha = 30°$	2.6×10^{-1}	1:1	no magma	1.56
ObR8	oblique extension $\alpha = 20°$	1.6×10^{-1}	1:1	no magma	1.45
ObR9	orthogonal extension $\alpha = 0°$	1.0×10^{-1}	1:1	orthogonal (2.5×0.7 cm)	1.36
ObR10	orthogonal extension $\alpha = 0°$	1.1×10^{-1}	1:1	no magma	1.36

magma ascent and emplacement, etc.). Indeed, in the terrestrial gravity field (normal-gravity experiments), only very weak materials are able to achieve spontaneous collapse and sensibly rapid flow driven by unstable mass distribution. This, on one hand, limits the choice of suitable materials (e.g., asphalt, heavy oil, soft wax, wet clay, etc.). On the other hand, because of the softness of the materials, neither the construction of the initial model nor a detailed study of the final pattern is possible in many instances. These inconveniences are avoided by running the models in the centrifuge. Indeed, the centrifugal force may be several thousand times stronger than the gravity force field, allowing the use of materials that are several thousand times stronger and correspondingly more viscous than materials usable in non-centrifuged (normal-gravity) models of the same size (e.g., Ramberg, 1981; Dixon and Summers, 1985). This represent one of the major advantages related to the use of the centrifuge technique in the study of gravity-driven geologic processes.

In all the experiments, models where built inside Plexiglas boxes with different dimensions for each series (see the following sections); these boxes (and

hence, the models) were subjected to centrifugal forces of 200*g*. During each experimental series, the models were deformed under different boundary conditions (see the following sections). Top view photos of the models were taken at various stages. After a successful experiment, the models were frozen before taking a number of cross-sections to study their 3D internal geometry.

C.1. Experimental setup and procedure

C.1.1. Series Magm
The series Magm was performed to analyse the emplacement of a magma initially underplated at the base of the crust and its interactions with deformation in the case of symmetric and asymmetric continental extension (see also section 4.2.3; Bonini et al., 2001).

The models, with dimension of $9 \times 7.5 \times 1.9$ cm, were built inside a Plexiglas box with internal dimension of $19 \times 7.5 \times 10$ cm (Fig. 16a). During the experiments, a rectangular magma chamber (0.2 cm thick, 1 cm wide and 5.5 cm long) was placed in the middle part of the model, below the analogue lower crust (Fig. 16a; Table A3.1).

Table A3.3
Parameters of models deformation for experiments of the series PR

Model	Geometry of extension	Average velocity of extension (mm/s)	BC/DC	Magma chamber geometry	Amount of extension (β)
PR1	polyphase extension	2.0×10^{-1}	1:1	orthogonal (2.5×0.7 cm)	
	first phase: $\alpha = 0°$				1.2
	second phase: $\alpha = 15°$				1.35
PR2	polyphase extension	2.0×10^{-1}	1:1	orthogonal (2.5×0.7 cm)	
	first phase: $\alpha = 0°$				1.12
	second phase: $\alpha = 47°$				1.21

Table A3.4
Parameters of models deformation for experiments of the series ObR and PR

Model	Geometry of extension	Average velocity of extension (mm/s) (°)	BC/DC	Magma chamber geometry	Amount of extension (β) (°)
TrZn2	transfer zone	1.2×10^{-1}	1:1	wide squared magma reservoir (WSMR)	1.20
TrZn3	transfer zone°	1.2×10^{-1}	1:1	narrow rectangular magma reservoir (NRMR)	1.18

(°): both the extension rate and the final amount of extension (β) represent an average value measured considering a single extending half of the model.

Models were thinned vertically and expanded laterally in response to the centrifugal body force field simulating gravity in nature; to control the amount and the rate of extension, rectangular blocks of Plasticine, placed at the rear and front end of the models, were sequentially removed before running the model for 30 s in the centrifuge. In the symmetric models, extension was allowed at both sides, whereas in asymmetric models, extension was allowed at one side only. The bottom and the side walls of the box were lubricated with liquid soap to avoid boundary friction. We allowed the models to stretch laterally at increments of 1 cm (Type 1 models) and 0.3 cm (Type 2 models) for each extremity during 30-s intervals. This implies that symmetric rifting models were deformed at extension rates of 0.66 (Type 1) and 0.2 mm s^{-1} (Type 2), while asymmetric rifting models were deformed at extension rates of 0.33 (Type 1) and 0.10 mm s^{-1} (Type 2; Table A3.1). These model extension rates scale down to natural values of $v_n \approx 10$ mm year^{-1} (Type 1) and $v_n \approx 3$ mm year^{-1} (Type 2) for symmetric rifting models and to $v_n \approx 5$ mm year^{-1} (Type 1) $v_n \approx 1.5$ mm year^{-1} (Type 2) for asymmetric rifting models.

C.1.2. Series ObR and PR

The experiments of the ObR and PR series were designed to investigate the relations between structural evolution and magma emplacement during oblique and polyphase continental extension, respectively (see also Sections 4.2.4 and 4.2.5; Corti et al., submitted for publication).

The models were built in an aluminium box with dimension $6.6 \times 6.5 \times 12$ cm, surrounded by Plasticine placed inside a wider Plexiglas box of dimension $19 \times 19 \times 15$ cm (Fig. 16b and c). The aluminium box was divided into two halves, one of which was allowed to move during successive runs in the centrifuge (Fig. 16b and c). The other half was stationary. A thin acetate sheet was fixed to the base of a moving part of the aluminium box, allowing half of the model to move solidly with the box. This setup created a velocity discontinuity (VD) in the central part of the model, parallel to the main rift trend (e.g., Allemand et al., 1989; Tron and Brun, 1991; Román-Berdiel et al., 2000). To minimise boundary friction, the bottom and the side walls of the moving half of the box were lubricated either with liquid soap or Vaseline oil.

Similarly to the series Magm experiments, oblique rifting was obtained and controlled by removing slices of Plasticine at the two extremities of the moving half of the model during successive runs in the centrifuge (Fig. 16b and c). In response to the centrifugal body force field, vertical collapse and lateral expansion of the model took place in a direction perpendicular to the VD (Fig. 16b and c).

Table A3.5
Parameters of models deformation for experiments of the series NRTZ

Model	ϕ angle* (°)	Average velocity of extension (mm/s)	BC/DC	Magma chamber geometry	Amount of extension (β)
NRTZ1	45	2.1×10^{-1}	1:1	no magma	1.50
NRTZ5	90	2.7×10^{-1}	1:1	orthogonal (5×1 cm)	1.45
NRTZ6	45	2.5×10^{-1}	1:1	orthogonal (5×1 cm)	1.51
NRTZ7	25	2.4×10^{-1}	1:1	orthogonal (5×1 cm)	1.53
NRTZ8	0	2.1×10^{-1}	1:1	orthogonal (5×1 cm)	1.50

*Angle between the direction of the rheological discontinuity in the transfer zone and the perpendicular to the direction of extension.

This movement was partly accompanied by the lateral expansion of a piece of silicone putty at one end of the aluminium box, which generated a vector parallel to the VD (Fig. 16b and c). The sum of the two vectors resulted in a mean displacement vector oblique to the central VD with an obliquity angle (α) controlled by the amount of Plasticine removed (Fig. 16b and c). In order to investigate the influence of the angle of obliquity (for a given brittle/ductile crust thickness ratio and a given strain rate) on the fault pattern, α was varied during the experiments from $0°$ to about $60°$ (see Table A3.2); in all models, the displacement along the central VD was left-lateral. A squared magma chamber with dimension of 2.5 cm $\times$ 0.7 cm $\times$ 0.2 mm was placed at the base of the model continental crust (Fig. 16b and c; Table A3.2). To compare results, corresponding models were also performed without introducing the magma chambers (see Table A3.2).

The same experimental setup was adopted for models of the series PR investigating polyphase rifting. In this case, a first phase of orthogonal rifting was followed by a second phase of oblique rifting characterised by high and low obliquity angles (Table A3.3).

C.1.3. Series TrZn

In this experimental series, we investigated the relations between deformation and magma emplacement during the development of a transfer zone progressively propagating across an underplated magma (Corti et al., 2002). Analogously to previous experiments (e.g., Serra and Nelson, 1988), we reproduced a transfer zone in the central part of the model by extending two halves of the models in opposite directions (Fig. 16d). This setup simulated an along-strike change of polarity between different rift segments.

During the experiments, we allowed the models to stretch laterally at increments of about 3.5 mm during 30-s intervals, which correspond to model extension rates of $\approx 1.2 \times 10^{-1}$ mm s^{-1} (Table A3.4). In all models the brittle layer was extended up to about 20% bulk extension (Table A3.4).

In order to model the influence on deformation of the underplated magma body, different model setups were investigated changing the dimensions of the initial magma reservoir (Table A3.4). In particular, we simulated the occurrence of a narrow rectangular magma reservoir (NRMR, $1 \times 5 \times 0.2$ cm, model Tr Zn3) and a wide squared magma reservoir (WSMR, $5 \times 5 \times 0.2$ cm, model TrZn2).

C.1.4. Series NRTZ

The experiments of the series NRTZ were performed to investigate the emplacement of an underplated magma within narrow rift-related transfer zones (see Section 4.2.6). To this purpose, during the experiments, we have reproduced a zone of weakness within the lower crust characterised by a viscosity that is about one order of magnitude lower than the surrounding crust (Table A3.5; Fig. 16e). During extension, deformation in the upper crust is localised above the zone of weakness and, in order to reproduce two interacting offset rift segments, we varied the geometry of the weak lower crust. Particularly, following Acocella et al. (1999a), we changed the overlap (L) between the offset segments to reproduce different angles (ϕ) between the direction of the rheological discontinuity in the transfer zone and the rift trend (Fig. 16e; Table 1). In all the experiments, the overstep (S) between the offset segments was kept constant.

Deformation of the models resulted in the development of a transfer zone connecting the rift segments, with an architecture that was mainly controlled by the angle ϕ (see Section 4.2.6).

References

Achauer, U., and the KRISP Working Group, 1994. A three-dimensional image of the upper mantle beneath the central Kenya rift from teleseismic investigations. In: Prodehl, C., Keller, G.R., Khan, M.A. (Eds.), Crustal and Upper Mantle Structure of the Kenya Rift. Tectonophysics, vol. 236, pp. 305–329.

Acocella, V., Korme, T., 2002. Holocene extension direction along the Main Ethiopian Rift, East Africa. Terra Nova 14, 191–197.

Acocella, V., Faccenna, C., Funiciello, R., Rossetti, F., 1999a. Sand-box modelling of basement-controlled transfer zones in extensional domains. Terra Nova 11, 149–156.

Acocella, V., Salvini, F., Funiciello, R., Faccenna, C., 1999b. The role of transfer structures on volcanic activity at Campi Flegrei (Southern Italy). Journal of Volcanology and Geothermal Research 91, 123–139.

Acocella, V., Faccenna, C., Funiciello, R., Rossetti, F., 2000. Analogue modelling of extensional transfer zones. Bolletino della Società Geologica Italiana 119, 85–96.

Allemand, P., Brun, J.-P., 1991. Width of continental rifts and rheological layering of the lithosphere. Tectonophysics 188, 63–69.

Allemand, P., Brun, J.-P., Davy, P., Van Den Driessche, J., 1989.

Symétrie et asymétrie des rifts et mécanismes d'amincissement de la lithospère. Bulletin de la Société Géologique de France 8, 445–451.

Appelgate, B., Shor, A.N., 1994. The northern Mid-Atlantic and Reykjanes Ridges: spreading centre morphology between 55°50′N and 63°00′N. Journal of Geophysical Research 99, 17935–17956.

Armijo, R., Tapponnier, P., Mercier, J., 1986. Quaternary extension in southern Tibet: field observations and tectonic implications. Journal of Geophysical Research 91, 13803–13872.

Artemjev, M.E., Artyushkov, E.V., 1971. Structure and isostasy of the Baikal rift and the mechanism of rifting. Journal of Geophysical Research 78, 7675–7708.

Arzi, A.A., 1978. Critical phenomena in the rheology of partially melted rocks. Tectonophysics 44, 173–184.

Axen, G.J., 1995. Extensional segmentation of the Main Gulf Escarpment, Mexico and United States. Geology 23, 515–518.

Axen, G.J., Taylor, W.J., Bartley, J.M., 1993. Space-time patterns and tectonic controls of Tertiary extension and magmatism in the Great Basin of the western United States. Geological Society of America Bulletin 195, 56–76.

Baker, B.H., Morgan, P., 1981. Continental rifting: progress and outlook. Eos, Transactions of the American Geophysical Union 62, 585–586.

Baker, B.H., Mohr, P.A., Williams, L.A.J., 1972. Geology of the Eastern Rift System of Africa. Geological Society of America Special Paper, vol. 136, 67 pp., Boulder, CO.

Bartley, J.M., Glazner, A.F., 1985. Hydrothermal systems and Tertiary low-angle normal faulting in the southwestern United States. Geology 13, 562–564.

Basile, C., Brun, J.P., 1999. Transtensional faulting patterns ranging from pull-apart basins to transform continental margins: an experimental investigation. Journal of Structural Geology 21, 23–37.

Bassi, G., 1991. Factors controlling the style of continental rifting: insights from numerical modelling. Earth and Planetary Science Letters 105, 430–452.

Bassi, G., 1995. Relative importance of strain rate and rheology for the mode of continental extension. Geophysical Journal International 122, 195–210.

Bassi, G., Keen, C.E., Potter, P., 1993. Contrasting styles of rifting: models and examples from the Eastern Canadian margin. Tectonics 12, 639–655.

Behrendt, J.C., LeMasurier, W.E., Cooper, A.K., Tessensohn, F., Tréhu, A., Damaske, D., 1991. Geophysical studies of the West Antarctic Rift System. Tectonics 10, 1257–1273.

Benes, V., Davy, P., 1996. Modes of continental lithospheric extension: experimental verification of strain localization processes. Tectonophysics 254, 69–87.

Benn, K., Odonne, F., de Saint-Blanquat, M., 1998. Pluton emplacement during transpression in brittle crust: new views from analog experiments. Geology 26, 1079–1082.

Benn, K., Odonne, F., Lee, S.K.Y., Darcovich, K., 2000. Analogue models of pluton emplacement during transpression in brittle and ductile crust. Transactions of the Royal Society of Edinburgh: Earth Sciences 91, 111–121 (Hutton IV special issue).

Berckhemer, H., Baier, B., Bartelsen, H., Behle, A., Burckhardt, H., Gebrande, H., Makris, J., Menzel, H., Miller, H., Vees, R., 1975. Deep seismic soundings in the Afar region and on the highland of Ethiopia. In: Pilger, A., Rosler, A. (Eds.), Afar Depression of Ethiopia. Schweizerbart, Stuttgart, pp. 89–107.

Bergantz, G.W., 1989. Underplating and partial melting: implications for melt generation and extraction. Science 245, 1093–1095.

Beslier, M.O., 1991. Formation des marges passives et remontée du manteau: modélisation expérimentale et exemple de la marge de la Galice. Mémoires des Geosciences Rennes 45 (199 pp.).

Blackman, D.K., Cann, J.R., Janssen, B., Smith, D.K., 1998. Origin of extensional core complexes: evidence from the Mid-Atlantic Ridge at Atlantis Fracture Zone. Journal of Geophysical Research 103, 21315–21333.

Block, L., Royden, L., 1990. Core complex geometries and regional scale flow inn the lower crust. Tectonics 9, 557–567.

Boccaletti, M., Bonini, M., Mazzuoli, R., Abebe, B., Piccardi, L., Tortorici, L., 1998. Quaternary oblique extensional tectonics in the Ethiopian Rift (Horn of Africa). Tectonophysics 287, 97–116.

Boccaletti, M., Mazzuoli, R., Bonini, M., Trua, T., Abebe, B., 1999. Plio-Quaternary volcano-tectonic activity in the northern sector of the Main Ethiopian Rift (MER): relationships with oblique rifting. Journal of African Earth Sciences 29, 679–698.

Bohlen, S.R., Mezger, K., 1989. Origin of granulite terranes and the formation of the lowermost continental crust. Science 244, 326–329.

Bonatti, E., 1985. Punctiform initiation of seafloor spreading in the Red Sea during transition from a continental to an oceanic rift. Nature 316, 33–37.

Bonini, M., Souriot, T., Boccaletti, M., Brun, J.P., 1997. Successive orthogonal and oblique extension episodes in a rift zone: laboratory experiments with application to the Ethiopian Rift. Tectonics 16, 347–362.

Bonini, M., Sokoutis, D., Mulugeta, G., Boccaletti, M., Corti, G., Innocenti, F., Manetti, P., Mazzarini, F., 2001. Dynamics of magma emplacement in centrifuge models of continental extension with implications for flank volcanism. Tectonics 20, 1053–1065.

Bosworth, W., 1987. Off-axis volcanism in the Gregory rift, east Africa: implications for models of continental rifting. Geology 15, 397–400.

Bosworth, W., Strecker, M.R., Blisniuk, P.M., 1992. Integration of East African paleostress and present-day stress data: implications for Continental Stress Field Dynamics. Journal of Geophysical Research 97, 11851–11865.

Bott, M.H.P., 1992. Modeling the loading stresses associated with active continental rift systems. Tectonophysics 36, 77–86.

Bott, M.H.P., 1995. Mechanisms of rifting: geodynamic modeling of continental rift systems. In: Olsen, K.H. (Ed.), Continental Rifts: Evolution, Structure, Tectonics. Developments in Geotectonics, vol. 25, pp. 27–43.

Boudreau, A.E., 1999. PELE—a version of the MELTS software program for the PC platform. Computers and Geosciences 25, 21–203.

Brace, W.F., Kohlstedt, D.L., 1980. Limits on lithospheric stress

imposed by laboratory experiments. Journal of Geophysical Research 85, 6248–6252.

Braile, L.W., Keller, G.R., Wendlandt, R.F., Morgan, P., Khan, M.A., 1995. The East African Rift System. In: Olsen, K.H. (Ed.), Continental Rifts: Evolution, Structure, Tectonics. Developments in Geotectonics, vol. 25, pp. 213–231.

Braun, J., Beaumont, C., 1987. Styles of continental rifting: results from dynamic models of lithospheric extension. Memoir—Canadian Society of Petroleum Geologists 12, 241–258.

Brown, M., Solar, G.S., 1998. Shear-zone systems and melts: feedback relations and self-organization in orogenic belts. Journal of Structural Geology 20, 211–227.

Brun, J.-P., 1999. Narrow rifts versus wide rifts: inferences for the mechanics of rifting from laboratory experiments. Philosophical Transactions of the Royal Society of London, Series A 357, 695–712.

Brun, J.-P., Beslier, M.O., 1996. Mantle exhumation at passive margins. Earth and Planetary Science Letters 142, 161–173.

Brun, J.-P., Tron, V., 1993. Development of the North Viking Graben: inferences from laboratory modelling. Sedimentary Geology 86, 31–51.

Brun, J.-P., Van Den Driessche, J., 1994. Extensional gneiss domes and detachment fault systems: structure and kinematics. Bulletin de la Société Géologique de France 165, 519–530.

Brun, J.-P., Choukroune, P., Faugères, E., 1985. Les discontinuities significatives de l'amincissement crustal: application aux marges passives. Bulletin de la Société Géologique de France 8, 139–144.

Brun, J.-P., Sokoutis, D., Van Den Driessche, J., 1994. Analogue modeling of detachment fault systems and core complexes. Geology 22, 319–322.

Brune, J.N., Ellis, M.A., 1997. Structural features in a brittle–ductile wax model of continental extension. Nature 387, 67–70.

Buck, W.R., 1988. Flexural rotation of normal faults. Tectonics 7, 959–973.

Buck, W.R., 1991. Modes of continental lithospheric extension. Journal of Geophysical Research 96, 20161–20178.

Burke, K., Dewey, J.F., 1973. Plume-generated triple junctions: key indicators in applying plate tectonics of old rocks. Journal of Geology 81, 406–433.

Burov, E., Cloetingh, S., 1997. Erosion and rift dynamics: new thermomechanical aspects of post-rift evolution of extensional basins. Earth and Planetary Science Letters 150, 7–26.

Byerlee, J.D., 1978. Friction of rocks. Pure Applied Geophysics 116, 615–626.

Callot, J.P., Grigne, C., Geoffroy, L., Brun, J.-P., 2001. Development of volcanic margins: two-dimensional laboratory models. Tectonics 20, 148–159.

Callot, J.P., Geoffroy, L., Brun, J.-P., 2002. Development of volcanic margins: three-dimensional laboratory models. Tectonics 21 (6), 1052 (doi: 10.1029/2001TC901019).

Carter, N.L., Tsenn, M.C., 1987. Flow properties of continental lithosphere. Tectonophysics 136, 27–63.

Chapin, C.E., 1989. Volcanism along the Socorro accommodation zone, Rio Grande rift, New Mexico. In: Chapin, C.E., Zidek, J. (Eds.), Field excursions to volcanic terranes in the western United States. Volume I: Southern Rocky Mountain region, New Mexico Bureau of Mines and Mineral Resources Memoir, vol. 46, pp. 46–57.

Chapin, C.E., Chater, S.M., 1994. Tectonic setting of the axial basins of the northern and central Rio Grande rift. In: Keller, G.R., Chater, S.M. (Eds.), Basins of the Rio Grande Rift: Structure, Stratigraphy, and Tectonic Setting. Geological Society of America Special Paper, vol. 291, pp. 5–25.

Chase, C.G., 1978. Plate kinematics: the Americas, East Africa and the rest of the world. Earth Planetary Science Letters 37, 355–368.

Chéry, J., 2001. Core complex mechanics: from the Gulf of Corinth to the Snake Range. Geology 29, 439–442.

Chèry, J., Daignières, M., Lucazeau, F., Vilotte, J.-P., 1989. Strain localization in rift zones (case of thermally softened lithosphere): a finite element approach. Bulletin de la Société Géologique de France 8, 437–443.

Chorowicz, J., Collet, B., Bonavia, F., Korme, T., 1994. Northwest to North-Northwest extension direction in the Ethiopian rift deduced from the orientation of extension structures and fault–slip analysis. Geological Society of America Bulletin 105, 1560–1570.

Christensen, U.R., 1992. An Eulerian technique for thermomechanical modelling of lithospheric extension. Journal of Geophysical Research 97, 2015–2036.

Clifton, A.E., Schlische, R.W., 2001. Nucleation, growth, and linkage of faults in oblique rift zones: results from experimental clay models and implications for maximum fault size. Geology 29, 455–458.

Clifton, A.E., Schlische, R.W., Withjack, M.O., Ackermann, R.V., 2000. Influence of rift obliquity on fault-population systematics: results of experimental clay models. Journal of Structural Geology 22, 1491–1509.

Cobbold, P.R., Castro, L., 1999. Fluid pressure and effective stress in sandbox models. Tectonophysics 301, 1–19.

Coney, P.J., 1980. Cordilleran metamorphic core complexes: an overview. In: Crittenden, M.D., Coney, P.J., Davis, G.H. (Eds.), Cordilleran Metamorphic Core Complexes. Geological Society of America Memoir, vol. 153, pp. 7–31.

Corti, G., Bonini, M., Innocenti, F., Manetti, P., Mulugeta, G., 2001. Centrifuge models simulating magma emplacement during oblique rifting. Journal of Geodynamics 31, 557–576.

Corti, G., Bonini, M., Mazzarini, F., Boccaletti, M., Innocenti, F., Manetti, P., Mulugeta, G., Sokoutis, D., 2002. Magma-induced strain localization in centrifuge models of transfer zones. Tectonophysics 348, 205–218.

Corti, G., Bonini, M., Innocenti, F., Manetti, P., Abebe, T., submitted for publication. Magma emplacement during polyphase rifting: insights from analogue centrifuge models and application to the Main Ethiopian Rift. Journal of African Science.

Courtillot, V., Tapponnier, P., Varet, J., 1974. Surface features associated with transform faults: a comparison between observed examples and an experimental model. Tectonophysics 24, 317–329.

Crittenden, M.D., Coney, P.J., Davis, G.H. (Eds.), 1980. Cordilleran metamorphic core complexes. Geological Society of America Memoir, vol. 153, 490 pp.

Crough, S.T., 1983. Rifts and swells: geophysical constraints on causality. Tectonophysics 94, 23–37.

Cruden, A.R., Koyi, H., Schmeling, H., 1995. Diapiric basal entrainment of mafic into felsic magma. Earth and Planetary Science Letters 131, 321–340.

Dauteuil, O., Brun, J.P., 1993. Oblique rifting in a low spreading ridge. Nature 361, 145–148.

Dauteuil, O., Brun, J.P., 1996. Deformation partitioning in a slow spreading ridge undergoing oblique extension: Mohns Ridge, Norwegian Sea. Tectonics 15, 870–884.

Dauteuil, O., Huchon, P., Quemeneur, F., Souriot, T., 2001. Propagation of an oblique spreading centre: the western Gulf of Aden. Tectonophysics 332, 423–442.

Davy, P., 1986. Modélisation thermo-mécanique de la collision continentale. Thèse d'Université, Univ. Rennes I, Rennes, France.

Davy, P., Cobbold, P.R., 1991. Experiments on shortening of 4-layer model of the continental lithosphere. In: Cobbold, P.R. (Ed.), Experimental and Numerical Modelling of Continental Deformation. Tectonophysics, vol. 188, pp. 1–25.

Di Paola, G.M., 1972. The Ethiopian Rift Valley (between 7° and 8°40′ lat. North). Bulletin of Volcanology 36, 517–560.

Dixon, J.M., Simpson, D.G., 1987. Centrifuge modelling of laccolith intrusion. Journal of Structural Geology 7, 87–103.

Dixon, J.M., Summers, J.M., 1985. Recent developments in centrifuge modelling of tectonic processes: equipment, model construction techniques and rheology of model materials. Journal of Structural Geology 7, 83–102.

Ebinger, C.J., 1989a. Tectonic development of the western branch of the East African Rift System. Geological Society of America Bulletin 101, 885–903.

Ebinger, C.J., 1989b. Geometric and kinematic development of border faults and accommodation zones, Kivu-Rusizi rift, Africa. Tectonics 8, 117–133.

Ebinger, C.J., Casey, M., 2001. Continental breakup in magmatic provinces: an Ethiopian example. Geology 29, 527–530.

Ebinger, C.J., Deino, A.L., Drake, R.E., Tesha, A.L., 1989. Chronology of volcanism and rift basin propagation: Rungwe Volcanic Province, East Africa. Journal of Geophysical Research 94, 15785–15803.

Ellis, M., King, G., 1991. Structural control of flank volcanism in continental rifts. Science 254, 839–842.

Elmohandes, S.-E., 1981. The central European graben system: rifting imitated by clay modelling. Tectonophysics 73, 69–78.

England, P.C., 1983. Constraints on extension of continental lithosphere. Journal of Geophysical Research 88, 1145–1152.

Faccenna, C., Nalpas, T., Brun, J.-P., Davy, P., 1995. The influence of pre-existing thrust faults on normal fault geometry in nature and in experiments. Journal of Structural Geology 17, 1139–1149.

Faccenna, C., Davy, P., Brun, J.-P., Funiciello, R., Giardini, D., Mattei, M., Nalpas, T., 1996. The dynamics of back-arc extensions: a experimental approach to the opening of the Tyrrhenian sea. Geophysical Journal International 126, 781–795.

Faccenna, C., Giardini, D., Davy, P., Argentieri, A., 1999. Initiation of subduction at Atlantic-type margins: insights from laboratory experiments. Journal of Geophysical Research 104, 2749–2766.

Fadaie, K., Ranalli, G., 1990. Rheology of the lithosphere in the East African Rift System. Geophysical Journal International 102, 445–453.

Faugère, E., Brun, J.P., 1984. Modélisation expérimentale de la distension continentale. Comptes Rendus de l'Academie des Sciences Paris, Serie II 299, 365–370.

Faulds, J.E., Varga, R.J., 1998. The role of accommodation zones and transfer zones in the regional segmentation of extended terranes. In: Faulds, J.E., Stewart, J.H. (Eds.), Accommodation Zones and Transfer Zones: the Regional Segmentation of the Basin and Range Provinces. Geological Society of America Special Paper, vol. 323, pp. 1–45.

Fletcher, R.C., Hallet, B., 1983. Unstable extension of the lithosphere: a mechanical model for Basin-and-Range structure. Journal of Geophysical Research 88, 7457–7466.

Furlong, K.P., Fountain, D.M., 1986. Continental crustal underplating: thermal considerations and seismic–petrologic consequences. Journal of Geophysical Research 91, 8285–8294.

Fyfe, W.S., 1992. Magma underplating of continental crust. Journal of Volcanology and Geothermal Research 50, 33–40.

Gans, P.B., 1987. An open-system, two-layer crustal stretching model for the eastern Great Basin. Tectonics 6, 1–12.

Gans, P.B., 1997. Large-magnitude Oligo-Miocene extension in the southern Sonora: implications for the tectonic evolution of northwest Mexico. Tectonics 16, 388–408.

Gans, P.B., Bohrson, W.A., 1998. Suppression of volcanism during rapid extension in the Basin and Range Province, United States. Science 279, 66–68.

Gans, P.B., Mahood, G.A., Scherner, E., 1989. Synextensional magmatism in the Basin and Range province: a case study from the Eastern Great Basin. Geological Society of America Special Paper 233 (53 pp.).

Gartrell, A.P., 1997. Evolution of rift basins and low-angle detachments in multilayer analog models. Geology 25, 616–618.

Gartrell, A.P., 2001. Crustal rheology and its effect on rift basin styles. In: Koyi, H.A., Mancktelow, N.S. (Eds.), Tectonic Modeling; a Volume in Honor of Hans Ramberg. Memoir—Geological Society of America, vol. 193, pp. 221–233.

Gautier, P., Ballèvre, M., Brun, J.-P., Jolivet, L., 1990. Cinématique de l'extension ductile à Naxos et Paros (Cyclades). Comptes Rendus de l'Académie des Sciences Paris, Serie II 310, 147–153.

Gautier, P., Brun, J.-P., Jolivet, L., 1993. Structure and kinematics of Upper Cenozoic extensional detachment on Naxos and Paros (Cyclades islands, Greece). Tectonics 12, 1180–1194.

Gautier, P., Brun, J.-P., Moriceau, R., Sokoutis, D., Martinod, J., Jolivet, L., 1999. Timing, kinematics and cause of Aegean extension: a scenario based on a comparison with simple analogue experiments. Tectonophysics 315, 31–72.

Geoffroy, L., 1998. Diapirism and intraplate extension—cause or consequence. Comptes Rendus de l'Academie des Sciences, Serie II: Sciences de la Terre et des Planets 326, 267–273.

Geoffroy, L., 2001. The structure of volcanic margins: some problematics from the North Atlantic/Labrador-Baffin System. Marine and Petroleum Geology 18, 463–469.

Ghebreab, W., Talbot, C.J., 2000. Red Sea extension influenced by Pan-African tectonic grain in eastern Eritrea. Journal of Structural Geology 22, 931–946.

Gibson, I.L., 1969. The structure and volcanic geology of an axial portion of the Main Ethiopian Rift. Tectonophysics 8, 561–565.

Girdler, R.W., 1983. Processes of rifting and break up of Africa. In: Morgan, P., Baker, B.H. (Eds.), Processes of Continental Rifting. Tectonophysics, vol. 94, pp. 241–252.

Glazner, A.F., Bartley, J.M., 1984. Timing and tectonic setting of the Tertiary low-angle normal faulting and associated magmatism in the southwestern United States. Tectonics 3, 385–396.

Goetze, C., Evans, B., 1979. Stress and temperature in the bending lithosphere as constrained by experimental rock mechanics. Geophysical Journal of the Royal Astronomical Society 59, 463–478.

Hailemariam, H., Mulugeta, G., 1998. Temperature-dependent rheology of bouncing putties used as rock analogs. Tectonophysics 294, 131–141.

Hamilton, W., 1987. Crustal extension in the Basin and Range Province, southwestern United States. In: Coward, M.P., Dewey, J.F., Hancock, P.L. (Eds.), Continental Extensional Tectonics. Geological Society Special Publications, vol. 28, pp. 155–176.

Hamilton, W., Myers, W.B., 1966. Cenozoic tectonics of the western United States. Reviews of Geophysics 4, 509–549.

Hauser, E., Potter, C., Hauge, T., Burgess, S., Burtch, S., Mutschler, R., Allmendinger, R., Brown, L., Kaufman, S., Olivier, J., 1987. Crustal structure of eastern Nevada from COCORP deep seismic reflection data. Geological Society of America Bulletin 99, 833–844.

Hayward, N.J., Ebinger, C.J., 1996. Variations in the along-axis segmentation of the Afar Rift system. Tectonics 15, 244–257.

Hill, E.J., Baldwin, S.L., Lister, G.S., 1992. Unroofing of active metamorphic core complexes in the D'Entrecasteaux Islands, Papua New Guinea. Geology 20, 907–910.

Hill, E.J., Baldwin, S.L., Lister, G.S., 1995. Magmatism as an essential driving force for formation of active metamorphic core complexes in eastern Papua New Guinea. Journal of Geophysical Research 100, 10441–10451.

Hollister, L.S., Crawford, M.L., 1986. Melt-enhanced deformation—a major tectonic process. Geology 14, 558–561.

Hopper, J.R., Buck, R.W., 1996. The effect of lower crust flow on continental extension and passive margin formation. Journal of Geophysical Research 101, 20175–20194.

Houseman, G., England, P., 1986. A dynamic model of lithosphere extension and sedimentary basin formation. Journal of Geophysical Research 91, 719–729.

Hubbert, M.K., 1937. Theory of scaled models as applied to the study of geological structures. Geological Society of America Bulletin 48, 1459–1520.

Huismans, R.S., Podladchikov, Y.Y., Cloetingh, S., 2001. Transition from passive to active rifting: relative importance of asthenospheric doming and passive extension of the lithosphere. Journal of Geophysical Research 106, 11271–11291.

Illies, J.H., Greiner, G., 1978. Rhinegraben and the Alpine system. Geological Society of America Bulletin 89, 770–782.

Jackson, J.A., 1994. The Aegean deformation. Annual Review of Geophysics 22, 239–272.

Jackson, M.P.A., Vendeville, B., 1994. Regional extension as a geologic trigger for diapirism. Geological Society of America Bulletin 106, 57–73.

Jestin, F., Huchon, P., Gaulier, M., 1994. The Somalia plate and the East African Rift System: present-day kinematics. Geophysical Journal International 116, 637–654.

Kazmin, V., 1980. Transform faults in the East African Rift System. Geodynamic Evolution of the Afro-Arabian Rift System. Accademia Nazionale dei Lincei, Atti dei Convegni Lincei, vol. 47, pp. 65–73.

Kazmin, V., Seife, M.B., Nicoletti, M., Petrucciani, C., 1980. Evolution of the northern part of the Ethiopian Rift. Geodynamic Evolution of the Afro-Arabian Rift System. Accademia Nazionale dei Lincei, Atti dei Convegni Lincei, vol. 47, pp. 275–292.

Keen, C.E., 1985. The dynamics of rifting: deformation of the lithosphere by active and passive driving mechanisms. Geophysical Journal of the Royal Astronomical Society 80, 95–120.

Keep, M., McKlay, K., 1997. Analogue modelling of multiphase rift systems. Tectonophysics 273, 239–270.

King, G., Ellis, M., 1990. The origin of large local uplift in extensional regions. Nature 348, 689–693.

Kirby, S.H., 1983. Rheology of the lithosphere. Reviews of Geophysics 21, 1458–1487.

Kirby, S.H., Kronenberg, A.K., 1987. Rheology of the lithosphere: selected topics. Reviews of Geophysics 25, 1219–1244.

Koyi, H., 1997. Analogue modelling; from a qualitative to a quantitative technique, a historical outline. Journal of Petroleum Geology 20, 233–238.

Koyi, H.A., Skelton, A., 2001. Centrifuge modelling of the evolution of low-angle detachment faults from high-angle normal faults. Journal of Structural Geology 23, 1179–1185.

Krantz, R.W., 1991. Measurements of friction coefficients and cohesion for faulting and fault reactivation in laboratory models using sand and sand mixture. Tectonophysics 188, 203–207.

Kunz, K., Kreuzer, H., Muller, P., 1975. K/Ar determination of the trap basalts of the southeastern part of the Afar Rift. In: Pilger, A., Rosler, A. (Eds.), Afar Depression of Ethiopia. Schweizerbart, Stuttgart, pp. 370–374.

Kuznir, N.J., Park, R.G., 1987. The extensional strength of the continental lithosphere: its dependence on geothermal gradient, and crustal composition and thickness. In: Coward, M.P., Dewey, J.F., Hancock, P.L. (Eds.), Continental Extensional Tectonics. Geological Society Special Publications, vol. 28, pp. 35–52.

Le Maitre, R.W. (Ed.), 1989. A Classification of Igneous Rocks and Glossary of Terms Blackwell, Oxford, UK.

Lesne, O., Calais, E., Deverchere, J., 1998. Finite-element modeling of crustal deformation in the Baikal rift zone—new insights into the active–passive rifting debate. Tectonophysics 289, 327–340.

Lister, G.S., Baldwin, S.L., 1993. Plutonism and the origin of metamorphic core complexes. Geology 21, 607–610.

Lister, G.S., Davis, G.A., 1989. Models for the formation of metamorphic core complexes and mylonitic detachment terranes. Journal of Structural Geology 11, 65–94.

Lynch, H.D., Morgan, P., 1987. The tensile strength of the lithosphere and the localisation of extension. In: Coward, M.P., Dewey, J.F., Hancock, P.L. (Eds.), Continental Extension-

al Tectonics. Geological Society Special Publications, vol. 28, pp. 53–65.

MacCready, T., Snoke, A.W., Wrigth, J.E., Howard, K., 1997. Mid-crustal flow during Tertiary extension in the Ruby Mountains core complex, Nevada. Geological Society of America Bulletin 109, 1576–1594.

Maggi, A., Jackson, J.A., McKenzie, D., Priestley, K., 2000a. Earthquake focal depths, effective elastic thickness, and the strength of the continental lithosphere. Geology 28, 495–498.

Maggi, A., Jackson, J.A., McKenzie, D., Priestley, K., 2000b. A re-assessment of focal depth distribution in southern Iran, the Tien Shan and northern India: do occur in the continental mantle? Geophysical Journal International 143, 629–661.

Mahatsente, R., Jentzsch, G., Jahr, T., 1999. Crustal structure of the Main Ethiopian Rift from gravity data: 3-dimensional modeling. Tectonophysics 313, 363–382.

Mart, Y., Dauteuil, O., 2000. Analogue experiments of propagation of oblique rifts. Tectonophysics 316, 121–132.

Martinod, J., Davy, P., 1992. Periodic instabilities during compression or extension of the lithosphere: 1. Deformation modes from an analytical perturbation method. Journal of Geophysical Research 97, 1999–2014.

Matthews, D., Cheadle, M., 1986. Deep reflections from the Caledonides and Variscides west of Britain, and comparisons with the Himalayas. In: Baranzagi, M., Brown, L. (Eds.), Reflection Seismology: A Global Perspective. Geodynamics Series, vol. 13. AGU, Washington, DC, pp. 5–19.

Mauduit, T., Dauteuil, O., 1996. Small-scale models of oceanic transform faults. Journal of Geophysical Research 101, 20195–20209.

McAllister, E.J., Cann, J., Spencer, S., 1995. The evolution of crustal deformation in an oceanic extensional environment. Journal of Structural Geology 17, 183–199.

McCaffrey, K.J.W., Miller, C.F., Karlstrom, K.E., Simpson, C., 1999. Synmagmatic deformation patterns in the Old Woman Mountains, SE California. Journal of Structural Geology 21, 335–349.

McClay, K.R., White, M.J., 1995. Analogue modelling of orthogonal and oblique rifting. Marine and Petroleum Geology 12, 137–151.

Merle, O., Michon, L., 2001. The formation of the West European rift: a new model as exemplified by the Massif Central area. Bulletin de la Société Géologique de France 172 (2), 213–221.

Meyer, W., Pilger, A., Rosler, A., Stets, J., 1975. Tectonic evolution of the northern part of the Main Ethiopian Rift in Southern Ethiopia. In: Pilger, A., Rosler, A. (Eds.), Afar Depression of Ethiopia. Schweizerbart, Stuttgart, pp. 352–362.

Michon, L., Merle, O., 2000. Crustal structures of the Rhinegraben and the Massif Central grabens: an experimental approach. Tectonics 19, 896–904.

Michon, L., Merle, O., 2001. The evolution of the Massif Central rift: spatio-temporal distribution of the volcanism. Bulletin de la Société Géologique de France 172 (2), 201–211.

Miller, E.L., Gans, P.B., Garing, J., 1983. The Snake Range decollement: an exhumed mid-Tertiary ductile–brittle transition. Tectonics 2, 239–263.

Miller, E.L., Dumitru, T.A., Brown, R.W., Gans, P.B., 1999. Rapid Miocene slip on the Snake Range–Deep Creek Range fault system, east-central Nevada. Geological Society of America Bulletin 111, 886–905.

Mohr, P., 1962. The Ethiopian Rift System. Bulletin of the Geophysical Observatory of Addis Ababa 5, 33–62.

Mohr, P., 1967. The Ethiopian Rift System. Bulletin of the Geophysical Observatory of Addis Ababa 11, 1–65.

Mohr, P., 1987. Patterns of faulting in the Ethiopian Rift Valley. Tectonophysics 143, 169–179.

Mohr, P.A., Potter, E.C., 1976. The Sagatu Ridge dike swarms, Ethiopian rift margin. Journal of Volcanology and Geothermal Research 1, 55–71.

Mohr, P.A., Wood, C.A., 1976. Volcano spacing and lithospheric attenuation in the Eastern Rift of Africa. Earth and Planetary Science Letters 33, 126–144.

Morgan, P., Baker, B.H. (Eds.), 1983. Processes of Continental Rifting. Tectonophysics, vol. 94, 680 pp.

Morgan, P., Seager, W.R., Golombek, M.P., 1986. Cenozoic mechanical and tectonics evolution of the Rio Grande Rift. Journal of Geophysical Research 91, 6263–6276.

Morley, C.K., 1988. Variable extension in Lake Tanganyika. Tectonics 7, 785–802.

Morley, C.K., 1994. Interaction of deep and shallow processes in the evolution of the Kenya Rift. Tectonophysics 236, 81–91.

Morley, C.K., 1999a. Aspects of transfer zone geometry and evolution in East African Rifts. In: Morley, C.K. (Ed.), Geoscience of Rift Systems—Evolution of East Africa. American Association of Petroleum Geologists Studies in Geology, vol. 44, pp. 161–171.

Morley, C.K., 1999b. Marked along-strike variations in dip of normal faults—the Lokichar fault, N. Kenya rift: a possible cause for metamorphic core complexes. Journal of Structural Geology 21, 479–492.

Morley, C.K., 1999c. Basin evolution trends in East Africa. In: Morley, C.K. (Ed.), Geoscience of Rift Systems—Evolution of East Africa. American Association of Petroleum Geologists Studies in Geology, vol. 44, pp. 131–150.

Morley, C.K., 1999d. Tectonic evolution of the East African Rift System and the modifying influence of magmatism: a review. Acta Vulcanologica 11, 1–19.

Morley, C.K., 1999e. How successful are analogue models in addressing the influence of pre-existing fabrics on rift structures? Journal of Structural Geology 21, 1267–1274.

Morley, C.K., 1999f. Influence of preexisting fabrics on rift structure. In: Morley, C.K. (Ed.), Geoscience of Rift Systems—Evolution of East Africa. American Association of Petroleum Geologists Studies in Geology, vol. 44, pp. 151–160.

Morley, C.K., Nelson, R.A., Patton, T.L., Munn, S.G., 1990. Transfer zones in the East African Rift System and their relevance to hydrocarbon exploration in rifts. American Association of Petroleum Geologists Bulletin 74, 1234–1253.

Morley, C.K., Woganan, N., Sankumarn, N., Hoon, T.B., Alief, A., Simmons, M., 2001. Late Oligocene–Recent stress evolution in rift basins of northern and central Thailand: implications for escape tectonics. Tectonophysics 334, 115–150.

Mulugeta, G., 1985. Dynamic models of continental rift valley systems. Tectonophysics 113, 49–73.

Mulugeta, G., 1988. Squeeze-box in the centrifuge. Tectonophysics 148, 323–335.

Mulugeta, G., Ghebreab, W., 2001. Modeling heterogenous stretching during episodic or steady rifting of the continental lithosphere. Geology 29, 895–898.

Murton, B.J., Parson, L.M., 1993. Segmentation, volcanism and deformation of oblique spreading centers—a quantitative study of the Reykjanes Ridge. Tectonophysics 222, 237–257.

Naylor, M.A., Larroque, J.M., Gauthier, B.D.M., 1994. Understanding extensional tectonics: insights from sand-box models. In: Roure, F., et al., (Eds.), Geodynamic Evolution of Sedimentary Basins, International Symposium, Moscow. Editions Technip, Paris, pp. 69–83.

Nelson, R.A., Patton, T.L., Morley, C.K., 1992. Rift-segment interaction and its relation to hydrocarbon exploration in continental rift systems. American Association of Petroleum Geologists Bulletin 76, 1153–1169.

Neumann, E.-R., Ramberg, I.B. (Eds.), 1978. Petrology and Geochemistry of Continental Rifts. Reidel, Dordrecht, 296 pp.

Neves, S.P., Vauchez, A., Archanjo, C.J., 1996. Shear zone-controlled magma emplacement or magma-assisted nucleation of shear zones? Insights from northeast Brazil. Tectonophysics 262, 349–364.

Olsen, K.H., Morgan, P., 1995. Introduction: progress in understanding continental rifts. In: Olsen, K.H. (Ed.), Continental Rifts: Evolution, Structure, Tectonics. Developments in Geotectonics, vol. 25, pp. 3–26.

Parson, L.M., et al., 1993. En echelon axial volcanic ridges at the Reykjanes Ridge: a life cycle of volcanism and tectonics. Earth and Planetary Science Letters 117, 73–87.

Parsons, T., 1995. The Basin and Range Province. In: Olsen, K.H. (Ed.), Continental Rifts: Evolution, Structure, Tectonics. Developments in Geotectonics, vol. 25, pp. 277–324.

Parsons, T., Thompson, G.A., 1991. The role of magma overpressure in suppressing earthquakes and topography: worldwide examples. Science 253, 1399–1402.

Parsons, T., Thompson, G.A., 1993. Does magmatism influence low-angle normal faulting? Geology 21, 247–250.

Parsons, T., Howie, J.M., Thompson, G.A., 1992. Seismic constraints on the nature of lower crustal reflectors beneath the extending southern transition zone of the Colorado Plateau, Arizona. Journal of Geophysical Research 97, 12391–12407.

Parsons, T., Thompson, G.A., Smith, R.P., 1998. More than one way to stretch: a tectonic model for extension along the plume track of the Yellowstone hotspot and adjacent Basin and Range Province. Tectonics 17, 221–234.

Petford, N., Cruden, A.R., McCaffrey, K.J.W., Vigneresse, J.-L., 2000. Granite magma formation, transport and emplacement in the Earth's crust. Nature 408, 669–673.

Prodehl, C., Fuchs, K., Mechie, J., 1997. Seismic-refraction studies of the Afro-Arabian rift system—a brief review. Tectonophysics 278, 1–13.

Quirk, D.G., D'Lemos, R.S., Mulligan, S., Rabti, M.R., 1998. Insights into the collection and emplacement of granitic magma based on 3D seismic images of normal fault-related salt structures. Terra Nova 10, 268–273.

Ramberg, H., 1963. Experimental study of gravity tectonics by means of centrifuged models. Bulletin of the Geological Institutions of the University of Uppsala 42, 1–97.

Ramberg, H., 1971. Dynamic models simulating rift valleys and continental drift. Lithos 4, 259–276.

Ramberg, H., 1981. Gravity, Deformation and the Earth's Crust Academic Press, London. 452 pp.

Ramberg, I.B., Morgan, P., 1984. Physical characteristics and evolutionary trends of continental rifts. Proceedings of the 27th International Geology Congress, vol. 7. VHU Science Press, Amsterdam, pp. 165–216.

Ranalli, G., 1995. Rheology of the Earth, 2nd ed. Chapman & Hall, London. 413 pp.

Ranalli, G., Murphy, D.C., 1987. Rheological stratification of the lithosphere. Tectonophysics 132, 281–296.

Ranero, C.R., Reston, T.J., 1999. Detachment faulting at ocean core complexes. Geology 27, 983–986.

Richard, Y., Froidevaux, C., 1986. Stretching instabilities and lithospheric boudinage. Journal of Geophysical Research 91, 8314–8324.

Ring, U., Betzler, C., Delvaux, D., 1992. Normal versus strike–slip faulting during rift development in East Africa. Geology 20, 1015–1018.

Román-Berdiel, T., 1999. Geometry of granite emplacement in the upper crust: contributions of analogue modelling. In: Castro, A., Fernandez, C., Vigneresse, J.L. (Eds.), Understanding Granites: Integrating New and Classical Techniques. Geological Society Special Publications, vol. 168, pp. 77–94.

Román-Berdiel, T., Gapais, D., Brun, J.-P., 1995. Analogue models of laccolith formation. Journal of Structural Geology 17, 1337–1346.

Román-Berdiel, T., Gapais, D., Brun, J.-P., 1997. Granite intrusion along strike–slip zones in experiment and nature. American Journal of Science 297, 651–678.

Román-Berdiel, T., Aranguren, A., Cuevas, J., Tubía, J.M., Gapais, D., Brun, J.P., 2000. Experiments on granite intrusions in transtension. In: Vigneresse, J.L., Mart, Y., Vendeville, B. (Eds.), Salt, Shale and Igneous Diapirs in and Around Europe. Geological Society, London, Special Publications, vol. 174, pp. 21–42.

Rosendahl, B.L., 1987. Architecture of continental rifts with special reference to east Africa. Annual Reviews of Earth and Planetary Sciences 15, 445–503.

Ruppel, C., 1995. Extensional processes in continental lithosphere. Journal of Geophysical Research 100, 24187–24215.

Sawyer, D.S., 1985. Brittle failure in the upper mantle during extension of continental lithosphere. Journal of Geophysical Research 90, 3021–3026.

Scott, S.D., Benes, V., 1996. Oblique rifting in the Havre Trough and its propagation into the continental margin of New Zealand: comparison with analogue experiments. Marine Geophysical Researches 18, 189–201.

Searle, R.C., Laughton, A.S., 1981. Fine-scale sonar study of tectonics and volcanism on the Reykjanes ridge. Oceanologica Acta 4, 5–13.

Sengör, A.M.C., Burke, K., 1978. Relative timing of rifting and volcanism on Earth and its tectonic implications. Geophysical Research Letters 5, 419–421.

Serra, S., Nelson, R.A., 1988. Clay modelling of rift asymmetry and associated structures. Tectonophysics 153, 307–312.

Simpson, C., 1999. Introduction: The influence of granite emplacement on tectonics. In: Simpson, C. (Ed.), The Influence of Granite Emplacement on Tectonics. Tectonophysics, vol. 312, pp. vii–vii.

Smith, R.B., 1977. Formation of folds, boudinage and mullions in non-Newtonian materials. Geological Society of America Bulletin 88, 312–320.

Sokoutis, D., Brun, J.-P., Van Den Driessche, J., Pavlides, S., 1993. A major Oligo-Miocene detachment in southern Rhodope controlling north Aegean extension. Geological Society of London Journal 150, 243–246.

Sokoutis, S., Bonini, M., Medvedev, S., Boccaletti, M., Talbot, C.J., Koyi, H., 2000. Indentation of a continent with a built-in thickness change: experiment and nature. Tectonophysics 320, 243–270.

Sonder, L.J., England, P.C., 1989. Effects of temperature-dependent rheology on large-scale continental extension. Journal of Geophysical Research 94, 7603–7619.

Sonder, L.J., England, P.C., Wernicke, B.P., Christiansen, R.L., 1987. A physical model for Cenozoic extension of western North America. In: Coward, M.P., Dewey, J.F., Hancock, P.L. (Eds.), Continental Extional Tectonics. Geological Society Special Publications, vol. 28, pp. 187–201.

Steckler, M.S., Berthelot, F., Lybris, N., LePichon, X., 1988. Subsidence of the Gulf of Suez: implications for rifting and plate kinematics. Tectonophysics 153, 249–270.

Strecker, M.R., Blisniuk, P.M., Eisbacher, G.H., 1990. Rotation of extension direction in the central Kenya rift. Geology 18, 299–302.

Talbot, C.J., Ghebreab, W., 1997. Red Sea detachment and basement core complexes in Eritrea. Geology 25, 655–658.

Teyssier, C., Vaderhaeghe, O. (Eds.), 2001. Partial Melting of Crust and Flow of Orogens. Tectonophysics, vol. 342, 474 pp.

Tommasi, A., Vauchez, A., 2001. Continental rifting parallel to ancient collisional belts: an effect of the mechanical anisotropy of the lithospheric mantle. Earth and Planetary Science Letters 185, 199–210.

Tommasi, A., Vauchez, A., Fernandes, L.A.D., Porcher, C.C., 1994. Magma assisted strain localization in an orogen-parallel transcurrent shear zone of southern Brazil. Tectonics 13, 421–437.

Tron, V., Brun, J.P., 1991. Experiments on oblique rifting in brittle–ductile systems. Tectonophysics 188, 71–84.

Trua, T., Deniel, C., Mazzuoli, R., 1999. Crustal control in the genesis of Plio-Quaternary bimodal magmatism of the Main Ethiopian Rift (MER): geochemical and isotopic (Sr, Nd and Pb) evidence. Chemical Geology 155, 201–231.

Tuckwell, G.W., Bull, J.M., Sanderson, D.J., 1998. Numerical models of faulting of oblique spreading centers. Journal of Geophysical Research 103, 15473–15482.

Turcotte, D.L., Emermen, S.H., 1983. Mechanisms of active and passive rifting. Tectonophysics 94, 39–50.

Vauchez, A., Neves, S.P., Tommasi, A., 1997. Transcurrent shear zone and magma emplacement in Neoproterozoic belts of Brazil. In: Bouchez, J.L., Hutton, D., Stephens, V. (Eds.), Granite: from Melt Segregation to Emplacement Fabrics. Kluwer Academic Publishing, Dordrecht, pp. 275–293.

Vendeville, B., Cobbold, P., Davy, P., Brun, J.-P., Choukroune, P., 1987. Physical models of extensional tectonics at various scales. In: Coward, M.P., Dewey, J.F., Hancock, P.L. (Eds.), Continental Extensional Tectonics. Geological Society, London, Special Publication, vol. 28, pp. 95–107.

Ward, P., 1991. On plate tectonics and the geologic evolution of southwestern North America. Journal of Geophysical Research 96, 12479–12496.

Weijermars, R., 1986. Flow behaviour and physical chemistry of bouncing putties and related polymers in view of tectonic laboratory applications. Tectonophysics 124, 325–358.

Weijermars, R., 1997. Principles of Rock Mechanics Alboran Science Publishing, Amsterdam, 359 pp.

Weijermars, R., Schmeling, H., 1986. Scaling of Newtonian and non-Newtonian fluid dynamics without inertia for quantitative modelling of rock flow due to gravity (including the concept of rheological similarity). Physics of the Earth and Planetary Interiors 43, 316–330.

Weijermars, R., Jackson, M.P.A., Vendeville, B., 1993. Rheological and tectonic modelling of salt province. Tectonophysics 217, 143–174.

Wernicke, B., 1992. Cenozoic extensional tectonics of the U.S. Cordillera. In: Burchfield, B.C., Lipman, P.W., Zoback, M.L. (Eds.), The Cordilleran Orogen; Conterminous U.S. The Geology of North America, vol. G-3. Geol. Soc. Am., Boulder, CO, pp. 553–581.

Wernicke, B., Spencer, J.E., Burchfield, B.C., Guth, P.L., 1982. Magnitude of crustal extension in the southern Great Basin. Geology 10, 499–502.

White, R.S., 1992. Magmatism during and after continental break-up. In: Storey, B.C., Alabaster, T., Pankhurst, R.J. (Eds.), Magmatism and the Causes of Continental Break-up. Geological Society, London, Special Publications, vol. 68, pp. 1–16.

White, R.S., McKenzie, D., 1989. Magmatism at rift zones: the generation of volcanic continental margins and flood basalts. Journal of Geophysical Research 94, 7685–7729.

Wilshire, H.G., 1990. Lithology and evolution of the crust–mantle boundary region in the southwestern Basin and Range province. Journal of Geophysical Research 95, 649–665.

Wilson, M., 1993. Magmatism and the geodynamics of basin formation. Sedimentary Geology 86, 5–29.

Withjack, M.O., Jamison, W.R., 1986. Deformation produced by oblique rifting. Tectonophysics 126, 99–124.

WoldeGabriel, G., Aronson, J.L., Walter, R.C., 1990. Geology, geochronology, and rift basin development in the central sector of the Main Ethiopia Rift. Geological Society of America Bulletin 102, 439–458.

WoldeGabriel, G., Walter, R.C., Hart, W.K., Mertzman, S.A., Aronson, J.L., 1999. Temporal relations and geochemical features of felsic volcanism in the central sector of the Main Ethiopian Rift. Acta Vulcanologica 11, 53–67.

Yin, A., 1989. Origin of regional, rooted low-angle normal faults: a mechanical model and its tectonic implications. Tectonics 8, 469–482.

Zeyen, H., Negredo, A., Fernandez, M., 1996. Extension with lateral material accommodation—"active" vs. "passive" rifting. Tectonophysics 266, 121–137.

Ziegler, P.A., 1995. Cenozoic rift system of western and Central Europe: an overview. Geologie en Mijnbouw 73, 99–127.

Ziegler, P., Cloetingh, S., 2003. Dynamic processess controlling evolution of rifted basins. Earth Sci. Rev., in press.

Zoback, M.L., Anderson, R.E., Thompson, G.A., 1981. Cenozoic evolution of the state of stress and style of tectonism of the Basin and Range province of the western United States. Philosophical Transactions of the Royal Society of London A 300, 407–434.

Zuber, M.T., Parmentier, E.M., 1986. Lithospheric necking: a dynamic model for rift morphology. Earth and Planetary Science Letters 77, 373–383.

Zuber, M.T., Parmentier, E.M., Fletcher, R.C., 1986. Extension of the continental lithosphere: a model for two scales of Basin and Range deformation. Journal of Geophysical Research 91, 4826–4838.

Giacomo Corti received degree in geology at the University of Florence and a PhD at the University of Pisa. His research has been mainly focused on the dynamics of magma migration and emplacement during continental extension, through integration of field geological–structural studies, analogue modelling and geophysical data. His research interests also include the analysis of active tectonics in the Northern Apennines, the Quaternary magmatism of the Tuscan Magmatic Province and the extensional tectonics in the East African Rift System.

Marco Bonini is a Researcher at the Institute of Geosciences and Earth Resources (IGG) of the National Research Council (CNR) of Italy. He received his PhD at Firenze University, Italy in Tectonics and Structural Geology. His main research interests integrate field geological–structural studies, analogue modelling and geophysical data for investigating the dynamics of tectonic deformation processes. His research includes basin analysis, thrust and active tectonics in the Apennines and extensional tectonics in the Ethiopian Rift. At present, he is mainly involved in analogue modelling studies addressing the role of ductile layers during continental collision, thrust tectonics and continental extension.

Sandro Conticelli received a "Laurea" in Geological Sciences and a PhD in Mineralogy and Petrology from Università degli Studi di Firenze. He has worked as NATO fellow for the Max Planck Institut für Chemie of Mainz (Germany), as postdoctoral fellow for the Italian CNR and as Research fellow for the Department of Earth Sciences of Florence. He has been appointed as Associate Professor of Igneous and Metamorphic Petrology at the Università degli Studi della Basilicata from 1998 to 2001. He is presently Full Professor of Igneous and Metamorphic Petrology at the Università degli Studi di Firenze. His major research interests lie in petrological aspects of magmatic rocks, studying the genesis and evolution of volcanic and intrusive associations from different geotectonic settings.

Fabrizio Innocenti, after receiving a degree in geology at University of Pisa, became assistant professor and, from 1975, Full Professor in Petrography. His research interests focus on petrology of magmatic rocks and on the relationships between magmatism and geodynamics. Currently, he works on the Tertiary and Quaternary magmatism of the Tuscan Magmatic Province, Southern Italy, Ethiopian Rift, Anatolia and southern south America.

Piero Manetti is Full Professor of Petrology at the Department of Earth Sciences of University of Florence. He is currently the director of the Institute of Geosciences and Earth Resources of the National Council of Italy. He is the author of several publications concerning sedimentary and magmatic petrology. He research focused on the relations between magmatic processes and geodynamics in the central and eastern Mediterranean, Black Sea, Ethiopia and Yemen. He is currently working on the magmatism of Mexican Volcanic Belt and the basaltic volcanism of the Argentinean and Chilean Patagonia.

Dimitrios Sokoutis is a Senior Researcher and Manager of the Tectonic Lab at the Vrije Universiteit Amsterdam. He received his PhD (1988) at Uppsala University, Sweden, in Tectonics and Geodynamics. His research integrates field geological studies combined with physical analogue modelling. Currently, he works with lithospheric scale models in cooperation with numerical modelers addressing the role of rheology during continental–continental collision, rifting associated with and without magmatism, as well as the effects of erosion and sedimentation in orogenic belts.